UTILIZATION OF VARIOUS PROJECTILES TO MITIGATE FOULING IN TUBULAR HEAT EXCHANGERS

A dissertation accepted by the Faculty of
Energy-, Process- and Bio-Engineering of the
University of Stuttgart

in Partial Fulfillment of the Requirements
for the Degree of Doctor of Engineering Sciences (Dr.-Ing.)

by

Mohammad Reza Jalalirad, B.Sc., M.Sc.
born in Arak, Iran

Institute for Thermodynamics and Thermal Engineering
University of Stuttgart, Germany
Published 2016

Supervisor: Prof. Dr. Dr.-Ing. habil. H. Müller-Steinhagen
Co-Examiners: Prof. Dr. –Ing. Günter Scheffknecht
and
Prof. Dr. –Ing. Stephan Scholl

Date of Oral Examination:

21st December, 2015

ABSTRACT

Heat exchangers are the workhorse of most chemical, petrochemical, food processing and power generating processes. Of the many types of heat exchangers, approximately 60% of the market is still dominated by shell and tube heat exchangers. One major problem of heat exchangers and particularly the shell and tube type is directly related to the deposition of unwanted materials on the heat transfer surfaces. Fouling may cause one or more of several major operating problems: i) reduction of heat transfer, ii) under-deposit corrosion, iii) increased pressure loss and iv) flow mal-distribution.

There are many different mitigation techniques available in the market to maintain the surface of heat exchangers clean to some extent. Among them are projectiles of various shapes, materials and hardnesses which circulate via a separate loop through the exchanger. The advantages of this method include effective fouling mitigation and stable operating conditions. Having said that, there are nevertheless numerous unanswered questions such as optimum injection interval, minimum required shear force to remove fouling layers, applicability of projectiles at elevated temperatures, minimum required velocity of projectile propulsion, and the criterion for the selection of projectiles for any specific fouling process. The present study, as part of a European Project entitled Clean-Ex, endeavors to address some of these questions.

A test rig was designed and constructed to simulate conditions under which fouling occurs in water service processes. The rig includes an online cleaning device which enables introduction of projectiles for various operating scenarios including i) continuous or ii) at different time intervals. A comprehensive set of experimental runs was carried out for crystallization fouling of $CaSO_4$ solutions with and without projectiles. Due to laboratory restrictions, fouling runs were performed at accelerated conditions to rigorously characterize the impact of projectile cleaning in terms of injection intervals and various types of projectiles.

The experimental results showed that the projectiles are capable of removing parts of the fouling layer at the early stage of the fouling process. The cleaning efficiency decreases as the fouling layer builds up such that the projectile is not effective when the asymptotic fouling is approached. In addition, shorter injection intervals of the projectiles decrease the asymptotic fouling resistance. Sintering of the fouling layer which hinders the cleaning action of projectiles should be accounted for this phenomenon. Furthermore, all projectiles decreased the induction time of the fouling process. The asymptotic fouling resistance was also approached much quicker compared to the case of no injection.

The performance of any projectile lies in a trade-off between its size, texture and stiffness. Stiffness produces a shear force required to dislodge the deposit and size is required to maintain the contact area between projectile and the surface. Accordingly, a criterion was developed to determine the optimum projectile size and stiffness for best

cleaning performance. The criterion shows that bigger and softer projectiles cannot last for a long time injection processes. Given the importance of size and stiffness, the projectiles were subsequently divided into two groups of hard and soft due to the required stiffness and velocity to move the projectile within the tube. To discriminate between these two groups, a new term called contact stability factor or Z factor is proposed which is a function of stiffness and size.

A mechanistic model has also been developed to predict the asymptotic fouling resistance when projectiles are in operation, based on injection rate, fouling rate and removal rates. The model predicts the asymptotic fouling resistance with an accuracy of 69% based on $CaSO_4$ concentration, saturation concentration, injection interval, shear force and contact stability of the tube with the projectile.

KURZFASSUNG

Wärmeübertrager sind das Arbeitspferd der meisten chemischen, petrochemischen, Lebensmittel- und Energieerzeugungsprozesse. Es gibt viele verschiedene Typen von Wärmeübertragern, allerdings werden etwa 60% des Marktes durch den Rohrbündelwärmeübertrager dominiert. Ein Hauptproblem von Wärmeübertragern und insbesondere dem Rohrbündeltyp wird direkt auf die Ablagerung von unerwünschten Materialien auf den Wärmeübertragungsflächen zurückgeführt. Fouling kann ein oder mehrere große Betriebsprobleme verursachen: i) Reduzierung der Wärmeübertragung, ii) Korrosion unter der Ablagerung, iii) erhöhter Druckverlust und iv) Strömungsfehlverteilung.

Es gibt viele verschiedene Minderungstechniken auf dem Markt, um die Oberfläche der Wärmeübertrager zu einem gewissen Grad sauber zu halten. Unter ihnen sind Projektile verschiedener Formen, Materialien und Härte, die seit Jahrzehnten verwendet werden, um Ablagerung im Rohrbündelwärmeübertragern zu reduzieren, indem sie in einem separaten Kreislauf zirkulieren und bei Gebrauch zugeschaltet werden. Die Vorteile dieser Methode sind die wirksame Minderung des Foulings und stabile Betriebsbedingungen. Es gibt jedoch zahlreiche unbeantwortete Fragen, wie optimale Injektionsintervalle, die mindestens erforderliche Scherkraft, um die Foulingschicht zu beseitigen, die Anwendbarkeit der Projektile bei erhöhten Temperaturen, die erforderliche Mindestgeschwindigkeit des Projektils, und das Kriterium für die Auswahl der Projektile für eine bestimmte Foulingprozess. Die vorliegende Studie ist bestrebt, einige dieser Fragen im Rahmen eines europäischen Projekts, das den Titel Clean-Ex trägt, zu beantworten.

Dazu wurde eine Versuchsanlage entwickelt und aufgebaut, um Bedingungen, unter denen Fouling in Brauchwasserprozessen auftritt, zu simulieren. Die Anlage umfasst eine Online-Reinigungsvorrichtung für die Einbringung von Projektilen für verschiedene Betriebsszenarien, d.h. i) kontinuierlich oder ii) in unterschiedlichen Zeitintervallen. Eine umfassende Reihe von Versuchen wurde für das Kristallisationsfouling von $CaSO_4$-Lösungen mit und ohne Projektile durchgeführt. Aufgrund der Beschränkungen auf Laborbedingungen wurde die Ablagerungsbildung bei beschleunigten Bedingungen durchgeführt, um die Wirkung der Reinigung durch Projektile hinsichtlich der Injektionsfrequenzen und der verschiedenen Arten von Projektilen deutlich zu charakterisieren.

Die experimentellen Ergebnisse zeigten, dass die Projektile Teile der Foulingschicht im frühen Stadium des Foulingprozesses entfernen können. Die Reinigungseffizienz nimmt ab, wenn sich die Foulingschicht aufbaut, so dass das Projektil wirkungslos ist, wenn sich das Fouling dem asymptotischen Endwert annähert. Außerdem verringert eine hohe Injektionsgeschwindigkeit der Projektile den asymptotischen Foulingwiderstand. Die

Sinterung der Foulingschicht, die die Reinigungswirkung von Projektilen behindert, ist für dieses Phänomen verantwortlich. Alle Projektile verringern die Induktionszeit; diejenigen, die ausreichend Kontakt haben, um eine größere Scherkraft auf die Oberfläche auszuüben, verringern den asymptotischen Foulingwiderstand. Das asymptotische Fouling wird dadurch viel schneller erreicht als ohne Injektion.

Die Leistung eines jeden Projektils liegt in einem Kompromiss zwischen Größe, Textur und Steifigkeit. Steifigkeit produziert die erforderliche Scherkraft, um die Ablagerungen zu entfernen, und die Größe bestimmt den Kontakt zwischen Projektil und der Oberfläche. Dementsprechend wurde ein Kriterium entwickelt, um die optimale Größe und Steifigkeit des Projektils für die beste Reinigungsleistung zu erhalten. Das Kriterium zeigt auch, dass größere und weichere Projektile längere Injektionszeiten nicht aushalten können. Angesichts der Wichtigkeit von Größe und Steifigkeit wurden die Projektile anschließend in zwei Gruppen von harten und weichen Projektilen eingeteilt. Dies geschah aufgrund der Steifigkeit und der erforderlichen Geschwindigkeit, um das Projektil im Rohr zu bewegen. Um zwischen diesen beiden Gruppen zu unterscheiden, wurde ein neuer Begriff, Kontaktstabilitätsfaktor oder Z-Faktor, vorgeschlagen, der eine Funktion der Steifigkeit und Größe ist.

Weiterhin wurde ein mechanistisches Modell entwickelt, um den asymptotischen Foulingwiderstand im Falle injizierter Projektile, basierend auf Injektions-, Fouling- und Minderungsraten, vorherzusagen. Das Modell sagt den asymptotischen Foulingwiderstand mit einer Genauigkeit von 69% voraus, abhängig von der $CaSO_4$ Konzentration, der Sättigungskonzentration, dem Injektionsintervall und der Kontaktstabilität des Rohres mit Projektil.

ACKNOWLEDGEMENTS

First of all, I gratefully acknowledge the financial support of the European Commission for granting the Clean-Ex project (contract number 227462).

Also I gratefully acknowledge the help and support of the following people without whom I would have been unable to carry out this study.

First and foremost, I am grateful to my supervisor, Professor H. Müller-Steinhagen, for his invaluable comments, guidance and support throughout this study. Without his input, none of this work would have been possible.

Special thanks go to Dr. M.R. Malayeri, my co-supervisor and the head of fouling and cleaning in process industries at the Institute of Thermodynamics and Thermal Engineering (ITW), University of Stuttgart. His guidance, discussions whenever I needed, weekly meetings, and the encouragement throughout my doctoral research were outstanding.

I am also grateful to staff and technicians at ITW for their help and warm hospitality especially my close colleagues Dr. Al-Janabi, Dr. Essawy and the guest researcher Dr. Abd-Elhady.

I would like to express my sincere thanks and gratitude to the senior manager of "Azarab Industries Company", the company that I am employed, for the permission of a long term leave which allowed me to pursue my PhD.

Last but not least, I am especially thankful for the wonderful support from my family members specially my mother and father.

Table of Contents

NOMENCLATURE

$A1$	Area under the curve of fouling resistance vs. time with projectile, m^2
$A2$	Area under the curve of fouling resistance vs. time without projectile, m^2
A_c	Cross-sectional of tube, m^2
A_{dyn}	Contact area between tube and projectile at dynamic condition, Eq. 4.8, m^2
A_{hyd}	Contact area between tube and projectile at hydrodynamic condition Eq. 4.9, m^2
A_i	Inner surface area of the heated tube, m^2
B	Bias error
C	Uncertainty
C	Constant value in Eq. C.4,-
C_s	Saturation concentration, g/L
$C_{s,wo}$	Saturation concentration at surface of deposit without projectile, g/L
$C_{s,w}$	Saturation concentration at surface of deposit with projectile, g/L
C_b	Bulk concentration, g/L
C^*	Representative saturation concentration without projectile, g/L
C^{**}	Representative saturation concentration with projectile, g/L
c	Geometrical parameter indicating dimensions of projectile to tube, A_{dyn}/A_c
c_p	Specific heat capacity, J/kg·K
D_{tube}	Inner diameter of tube, mm
$D_{proj.}$	Diameter of projectile, mm
E	Activation energy, J/mol
f	Friction factor, -
f_k	Ball injection frequency in Eq. 2.1, balls/h
f_u	Average ball circulation time in Eq. 2.1, s
F_{dyn}	Dynamic force Eq. 4.8, N
F_{hyd}	Hydrodynamic force Eq. 4.9, N
i	Number of recorded data during experiment, -
k	Constant in Eq. 5.6, m^2/s
k_0	Pre-exponential factor (pre-factor) in Arrhenius equation, $m^4/kg{\cdot}s$
k_A	Arrhenius constant rate of reaction, $m^4/kg{\cdot}s$
k_2	Constant in Eq. 5.9, variable dimension
L	Overall length of tube in heated section, m
$\dot{m}$	Mass flux, $kg/m^2{\cdot}s$
n	Total number of logged experimental data, -
n	Number of observations Eq. 3.10, -
n	Injection rate, #/min
n	Ratio of ball charge to number of parallel tubes in Eq. 2.1, -
OE	Overall efficiency, -
P	Precision error

p	Pressure (absolute), Pa
p_g	Gage pressure, Pa
p	Injection interval factor, -
$\dot{Q}$	Rate of heat transfer across the heated tube, W
$\dot{q}$	Heat flux, W/m^2
r	Inner diameter of tube, Eq. 4.3, m
R_f	Fouling resistance, m^2·K/W
$\bar{R}$	Average thermal resistance, m^2·K/W,
R	The universal gas constant in Eq. 5.14, J/mol·K
R	Thermal resistance in Eq. 3.8, m^2·K/W
$\bar{R}$	Average thermal resistance in Eq. 3.10, m^2·K/W
R_f^*	Asymptotic fouling resistance, m^2·K/W
$R_{f,w}^*$	Asymptotic fouling resistance with projectile, m^2·K/W
$R_{f,wo}^*$	Asymptotic fouling resistance without projectile, m^2·K/W
$R_{f,w}$	Function of fouling resistance with projectile, m^2·K/W
$R_{f,wo}$	Function of fouling resistance without projectile, m^2·K/W
S	Distance between thermocouple and inner surface of tube, m
s	Standard deviation in stiffness test, N
T	Temperature, K
T_f	Temperature of furnace, K
T_b	Bulk temperature (the temperature of the circulating flow in the test rig), K
T_{bb}	Bulk temperature in heated section (Eq. 3.2), K
T_i	Inlet temperatures to the heated section, K
T_o	Outlet temperature from the heated section, K
T_s	Surface temperature, K
$T_{s,c}$	Surface temperature at clean condition, K
$T_{s,f,w}$	Surface temperature at fouling condition with projectile, K
$T_{s,f,wo}$	Surface temperature at fouling condition without projectile, K
T_w	Wall temperature, reported values by left and right thermocouples, K
t	time, s
U	Overall heat transfer coefficient, W/m^2.K
U_f	Overall heat transfer coefficient at fouling conditions, W/m^2·K
U_c	Overall heat transfer coefficient at clean conditions, W/m^2·K
v	Velocity, m/s
v	Variation coefficient in stiffness test, N
W_c	Weight of designed heat exchanger for clean condition, kg
W_f	Weight of heat exchanger designed with fouling resistance, kg
x	Average exerted force on the projectile, Eq. 4.13, N
x_d	Thickness of the deposit layer, m

Z	Contact stability factor

Greek Symbols

α	Convective heat transfer coefficient, W/m^2·K
α	Factor of force and deformation, N
δ	Thickness of fouling, m
ε	Deformation [%]
θ	Relaxation time, min^{-1}
λ	Thermal conductivity of tube, W/m·K
λ_d	Thermal conductivity of deposit, W/m·K
τ_s	Shear stress at the fluid-deposit interface, Pa
τ_{dyn}	Dynamic shear (momentary), Pa
τ_{hyd}	Hydrodynamic shear (momentary), Pa
$\tau_{c,hyd}$	Continuous hydrodynamic shear, Pa
ϕ_d	Mass deposition rate of fouling per unit area, kg/m^2·s
ϕ_r	Mass removal rate of fouling per unit area, kg/m^2·s
ϕ	Strength of deposit, N/m^2

Subscripts/Superscripts

b	bulk
c	clean
c	continuous
d	deposit
r	removal
dyn	dynamic condition, projectile under mechanical pushing
f	fouling, furnace
hyd	hydrodynamic condition, projectile under propulsion force of flow
i	inlet, inner
o	outlet
s	surface
w	with
wo	without

Abbreviations

EDTA	Ethylene-Diamine-Tetra-Acetic Acid
FL	Fouling Layer
HE	Heat Exchanger

IT	Induction Time
IKT	Institut für Kunststofftechnik (Institute of Polymer Technology)
inj	Injection
MST	Minimum Sintering Temperature
Proj	Projectile
2WV	Two Way Valve
3WV	Three Way Valve
$CaSO_4$	Calcium Sulfate anhydrite
$Ca(NO_3)_2.4H_2O$	Calcium Nitrate Tetrahydrate
Na_2SO_4	Sodium Sulphate
w/o	Without

1 INTRODUCTION

1.1 Tubular Heat Exchangers in Industry

Heat exchangers are devices for proper heat exchange between two media which are separated by a well-conductive wall, i.e. metal, to prevent mixing. Their utilization is widespread which includes space heating, refrigeration, air conditioning, power plants, chemical plants, petrochemical complexes, refineries, natural gas processing, and automobiles. Heat exchangers can be divided into structurally different types such as plate and frame, finned tube, double pipe, spiral tube, as well as shell and tube. Of many types of heat exchangers, approximately 60% of the market is still dominated by the shell and tube heat exchanger. It is largely favored due to its long performance history, relative simplicity, and its wide temperature and pressure design ranges (Chemical Engineering Resources, www.cheresources.com).

Shell and tube heat exchangers usually contain a number of tubes through which a fluid flows which must be either heated or cooled. The second fluid runs over the tubes within a larger container which is called shell. The set of tubes is called bundle and can be made up of several types and sizes of tubes: plain, longitudinally finned, spiral, and so forth. Shell and tube heat exchangers are typically used for high pressure/temperature applications. The American Society of Mechanical Engineers (ASME) has developed technical guides on how to optimally design and construct various components of shell and tube heat exchangers. Furthermore, there are many recommended types of shell and tube heat exchangers by the Tubular Exchanger Manufacturers Association (TEMA) for different operating conditions, properties of flow and costs for different applications.

1.2 Fouling of Heat Exchangers

The accumulation of unwanted deposits on the surface of heat exchangers is usually referred as fouling, though for crystallization type of fouling it is often called scaling. It is a highly undesirable occurrence and can consist of many different materials that stick onto the surface. In heat exchangers, fouling reduces the thermal efficiency since there is an additional resistance to heat transfer. The hydraulic performance of heat exchangers may also be affected as the local fluid velocity will rise because of a reduced diameter of the tube caused by the deposit layer. This results in a higher pressure drop so that the pumping power has to be increased. In the worst case, fouling can even totally clog the tubes. Fouling may also cause one or more of several major operating problems such as under-deposit corrosion and flow mal-distribution.

For all different types of heat exchangers, correlations exist for the design and operation of a new/clean heat exchanger. However, there remains one large element of

uncertainty due to the deposits that impede the optimal design and operation of such devices. One approach to combat this problem is to overdesign the exchanger. At the design stage a commonly used remedy is to increase the heat transfer surface area. Garret-Price et al. (1985) reported that in practice heat exchangers are designed with an average oversize of about 35%. While this strategy is widely accepted, it comes with enormous additional capital cost penalties. Heat exchangers which are designed with excess surface area are larger and heavier. This evidently results in extra costs to cover additional material, transportation and installation. During the operation of a heat exchanger, operators should commit periodic cleaning as a way of managing fouling. Periodic cleaning results in additional costs arising from loss of production and additional maintenance activities. Overdesign of the exchanger also applies to pumps which are again oversized to compensate the increased pressure drop.

It is estimated that fouling costs are about 0.25% of a country's Gross National Product (Müller-Steinhagen et al. 2005). Steinhagen et al. (1993) have also shown that fouling related costs constitute a significant portion of the industry's operating costs. Due to the increased energy prices over the last few years, as a solution, higher efficiency of heat exchangers is needed to minimize the use of energy and therefore the operating costs.

Fouling that is tenacious and difficult to remove is generally referred as "hard" or otherwise a softer deposit is sometimes called "sludge" (Bott, 1995). In both cases the result is a loss of efficiency. Unless suitable preventative measures are taken the problem can give rise to serious operating consequences. Over heating of scaled tubes or coils can also result in high metal temperature, which can decrease the allowable shear stress of metals dramatically. The reported allowable design temperature for pressurized parts of exchangers must not exceed 600°C (ASME, Sec. II). Thus fouling of the flow-side of furnaces and fire-tube boilers which are in direct contact to fire may result in metal failure due to a very high operating temperature between 900-1100°C of fire chambers. Consequently tube rupture may occur when the deposit causes a rapid rise in tube wall temperature (Betz, 1976). It is no surprise that the prices of materials that can withstand high temperatures are expensive. If fouling in such devices is under control, then considering a safe but lower "design temperature" reduces the construction cost.

Fouling occurs according to different mechanisms due to the type of working fluids, operating conditions and impurities. Common mechanisms include crystallization, bio-fouling, particulate, chemical reaction and corrosion. These mechanisms have been investigated to find approaches to mitigate deposit formation.

1.3 Challenges in Mitigating Deposit Formation in Tubular Heat Exchangers

The Global Strategic Business Report reports that the global heat exchanger market is estimated to top a total of $12.7 billion in 2012 with an increase of 3-5% per annum (Müller-Steinhagen et al. 2011). Despite this very positive market trend, manufacturers are

under increasing pressure to produce heat exchangers which are more efficient in terms of heat recovery and use of material, while at the same time being faced with fluids which are increasingly difficult to process. One major problem directly related to these requirements is the deposition of unwanted materials on the heat transfer surfaces, which occurs in the majority of heat exchangers.

Thermal performance of exchangers is profoundly affected by the fouling resistance, especially for water services. Figure 1-1 exemplifies how the fouling resistance may impact on the design of a typical shell and tube heat exchanger in water services as calculated by software Aspen B-JAC (see Appendix A). W_f/W_c denotes the weight ratio of the designed exchanger considering fouling and clean operation for the tube side. The figure indicates, for instance with a fouling resistance of 0.0007 m^2K/W, that the weight of the constructed heat exchanger would be increased by more than 100%. The weight of exchangers directly relates to the capital costs, as quite often the manufacturers sell tubular exchangers by weight. Fouling resistances for different fluids have been given in many heat exchanger handbooks. Values for water services based on the type of water whether from sea, river or demineralized range from 0.00009 to 0.0007 m^2K/W. These values for different types of water are listed in Table 1-1 (Thome, 2010). Figure 1-1 and Table 1-1 illustrate extra weight and costs by assuming different water for the construction of heat exchangers.

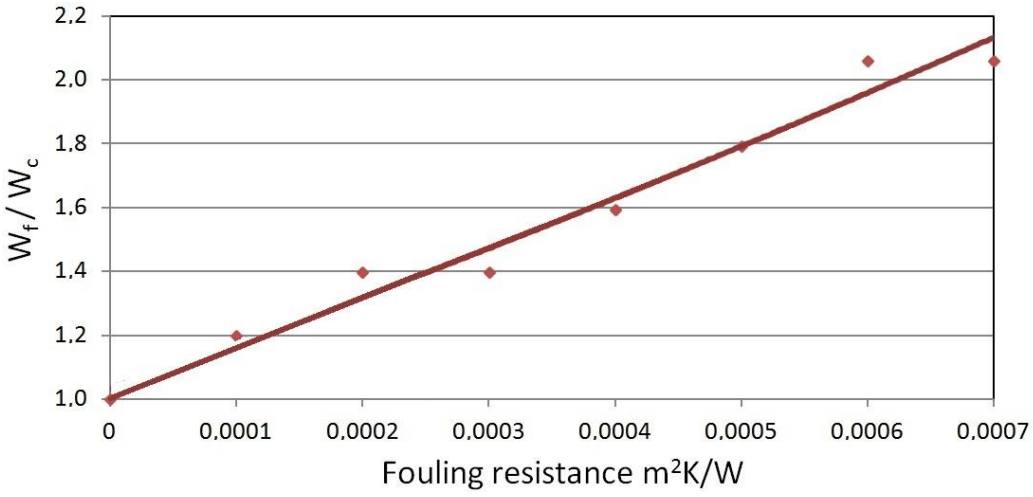

Figure 1-1 Extra weight from using different fouling resistances in the design of a typical heat exchanger (Calculated by Aspen B-JAC Software, see Appendix A)

Table 1-1 Fouling resistance for different water services in exchanger design standards (Thome, 2010)

Conditions	cooling water < 50 ˚C cooled fluid < 120 ˚C		cooling water > 50 ˚C cooled fluid > 120 ˚C	
Cooling Water Velocity	***v < 1 m/s***	***v > 1 m/s***	***v < 1 m/s***	***v > 1 m/s***
Type of Water	**m^2K/W**			
Sea	0.00009	0.00009	0.00018	0.00018
Brackish	0.00035	0.00018	0.00053	0.00035
Cooling tower with inhibitor	0.00018	0.00018	0.00035	0.00035
Cooling tower without inhibitor	0.00053	0.00053	0.00088	0.0007
City grid	0.00018	0.00018	0.00035	0.00035
River minimum	0.00018	0.00018	0.00035	0.00035
River average	0.00053	0.00035	0.0007	0.00035
Engine jacket	0.00018	0.00018	0.00018	0.00018
Demineralized or distilled	0.00009	0.00009	0.00009	0.00009
Treated boiler feedwater	0.00018	0.00009	0.00018	0.00018
Boiler blowdown	0.00035	0.00035	0.00035	0.00035

There are many different mitigation techniques available in the market to keep the surfaces of heat exchangers clean to some extent. Nevertheless, the successful application of any such technique requires in-depth understanding of the respective fouling mechanisms otherwise they may even lead to a counter-productive result of increased deposition. Apart from mechanisms, intensity of fouling, the type of heat exchanger, required cleanliness, cleaning costs and operating time intervals could be criteria for the selection of the mitigation techniques (Müller-Steinhagen et al. 2011).

Among different mechanical mitigation techniques, projectiles of different shapes e.g. sponge balls and wire brushes can be propelled through the heat exchanger tubes to mitigate deposition. Projectile cleaning is ideal as it can be applied at short intervals and can mitigate fouling on a continuous basis. Thus the degradation of heat exchanger efficiency can be controlled. The frequency and duration of the application depends on the severity of fouling and the strength of interaction between cleaning projectile and deposit. Nonetheless experimental data about the performance of various projectiles is scarce and non-conclusive (Al-Bakeri et al. 1993 and Hamed et al. 2007).

Projectiles have been used to mitigate deposit in tubular exchangers for decades. They circulate via a separate loop through the tubular heat exchanger. The advantages of this method are that it is very effective in fouling mitigation and provides stable operating conditions (Taprogge). It can also be used in food processes as it does not affect the consumables (Technos). The drawbacks of this method are that the projectiles can only clean the inner side and not the outer side of the tubes and that a special device for circulating the projectiles has to be installed. They must also be replaced regularly as they

wear out after a certain run time. As a result, the use of the projectile cleaning method is limited due to the following:

- structural integrity and chemical stability of projectiles at elevated temperatures
- insufficient force for propelling the projectiles in processes with low velocity
- random distribution of fouling pattern depending on the geometrical location of tubes

There are many unanswered questions such as optimum injection interval, size, stiffness, as well as minimum required shear force to remove fouling layers, applicability of projectiles at elevated temperatures and minimum required propulsion velocity of the projectiles that need addressing.

1.4 Research Objectives

The present study, as part of a European project entitled "Clean-Ex", aims at investigating the performance of various projectiles in harsh fouling environments. The main objectives of this work are:

- Design and construction of a test facility to investigate deposit formation with and without using projectiles.
- Online monitoring of the impact of injection on cleaning
- Investigation of optimum injection intervals for different projectiles
- Investigation of the influence of projectiles on the induction time during crystallization fouling
- Study of the influence of deposit hardening when projectiles are injected at different injection intervals
- Development of a criterion to select optimum projectiles for specified operating conditions
- Characterization of projectile performance in terms of operating conditions, projectile physical properties and structural specifications, i.e. shape, hardness and surface texture. This will include measurement of exerted shear forces by projectiles under propulsion of flow
- A theoretical study to predict asymptotic fouling resistances in case of projectile injection

1.5 Scope of Present Study

The present thesis comprises of six chapters. Chapter 2 provides a literature review on the present state-of-the-art of fouling mitigation techniques, specially cleaning projectiles and their technical limitations. Chapter 3 describes the experimental set-up and procedure for the attempted experiments. Experimental results and parameters that may influence fouling are presented and discussed in Chapter 4. Performance of various projectiles, compaction phenomenon, influence of sintering, shear stress analysis, injection effects on

induction time and the cleaning effect of metal projectiles are also discussed in this chapter. In addition, a criterion to compare the results and also one for the selection of efficient projectiles are introduced in this chapter. Chapter 5 presents a model for the prediction of asymptotic fouling resistances with and without projectiles. Conclusions and recommendations for future work are provided in Chapter 6. Figure 1-2 presents a flowchart highlighting various aspects of the experimental and theoretical studies carried out in this work.

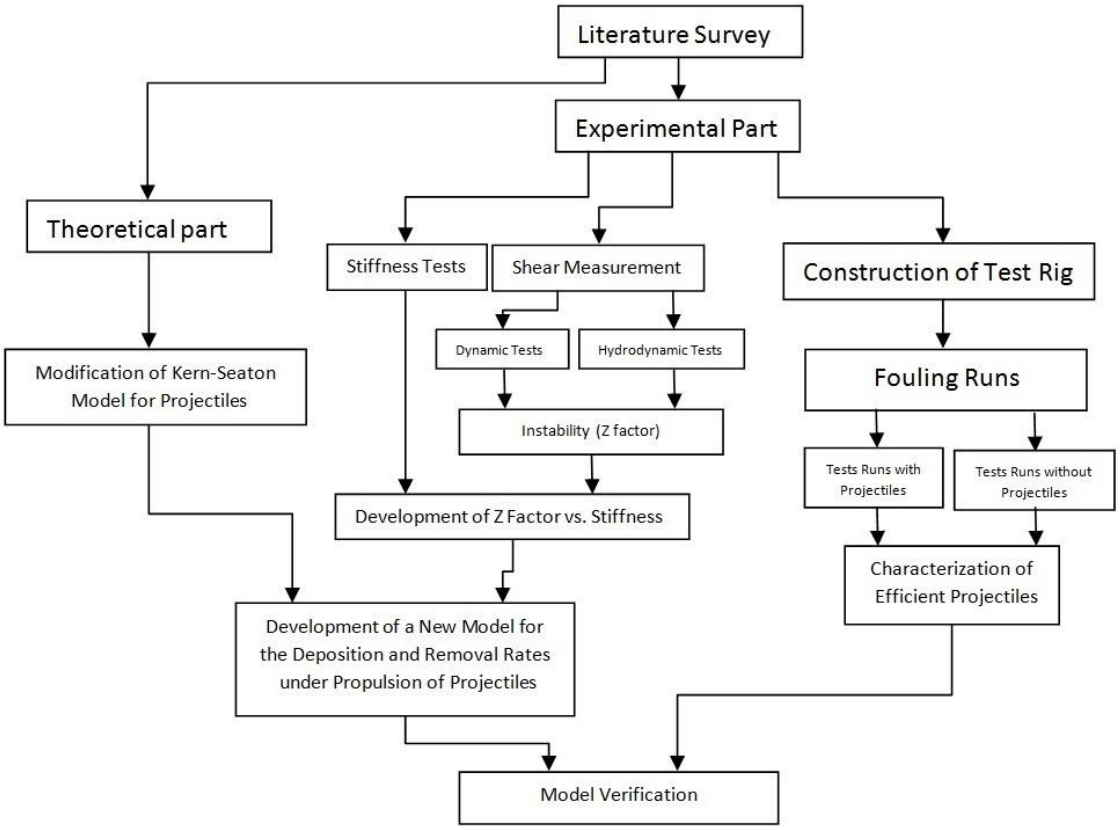

Figure 1-2 Flow chart of the scope of work in this study

2 LITERATURE REVIEW

2.1 Fouling Mitigation Techniques

If fouling cannot be prevented from forming, it is then necessary to remove it in periodic intervals or on a continuous basis. Figure 2-1 depicts the development of the heat transfer coefficient with and without cleaning. After the cleaning processes, the overall heat transfer coefficient *U* in an ideal case reaches again the clean state.

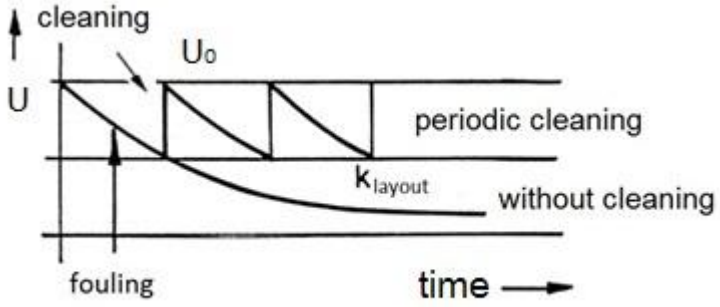

Figure 2-1 Change of heat transfer coefficient with and w/o cleaning (Bott, 1995)

There are several methods to mitigate or remove fouling in heat exchangers that can be divided into off-line and on-line methods. Each type, in turn, also divides into different sub-groups. They could be physical, mechanical, chemical or change of operating conditions. For off-line methods, the heat exchanger not only has to be stopped from operating, but may also need dismantling. There are also other methods that include design modification to reduce deposit formation. For instance, compact and fin-tube exchangers are prone to less fouling due to increased level of turbulence, lower surface temperature and homogeneous distribution of flow (Müller-Steinhagen et al. 2000).

2.2 Off-line Mititgation Techniques

Heat exchangers may be cleaned by different off-line methods as categorized in Figure 2-2.

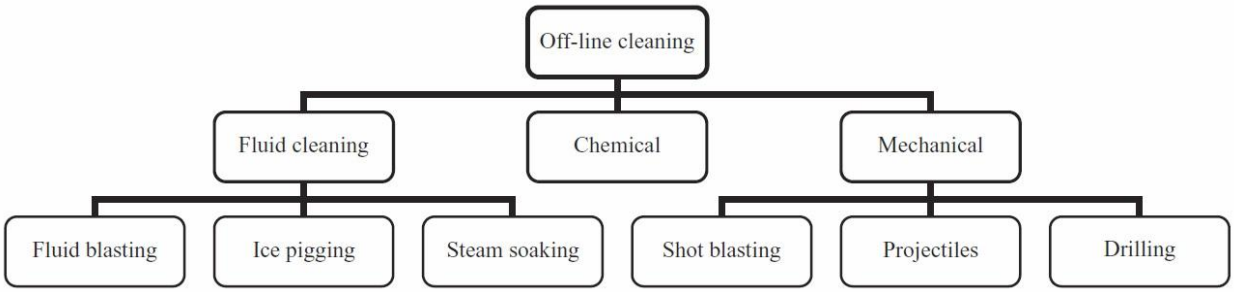

Figure 2-2 Various off-line cleaning methods (Müller-Steinhagen et al. 2011)

Disassembling and hand wash is the simplest method to clean a heat exchanger. This can involve wiping, brushing or scraping the deposits away. As it is labor intensive, the cost of manual cleaning may be high. Cleaning with high-pressure water is the most effective off-line cleaning method. It can operate with a pressure up to 3000 bar. Steam- and hydroblasting are probably the most common mechanical cleaning methods. They exist with a wide range of cleaning nozzles to suit many types of heat exchangers and deposits. If the deposits are very hard, sand can be added to the fluid to increase the efficiency.

Ice pigging is the pump-around of an ice-water slurry with different solid fractions, which is a combination of high velocity water jetting and pigging (forcing a solid through the pipe) to push the deposit away. It is reported as a successful technique to remove moderately adhering deposits, since the shear forces are increased by a factor of 4-5 due to the presence of the ice (Ainslie et al. 2009). Such a system can be applied for complex geometries and is reported to have a reduced cleaning downtime (Müller-Steinhagen et al. 2011).

Ultrasound is the only available alternative for the shell side of tube bundles but it is also used for the inner side of the tubes.

Techniques for the mechanical cleaning of tubes have a long history, the earliest mechanical cleaners being designed for cleaning boiler tubes (Müller-Steinhagen, 2000). Cecil M. Griffin and Vivian Griffin invented the first cleaner for condensers and shell and tube heat exchangers. The patent was granted in 1931 and then it was improved several times in 1939, 1947 and 1956. Brushes also are suitable to remove light organic deposits. They are suitable for spiral or finned tubes. The length and stiffness of brushes can be fitted for more effective removal and less damage to tubes.

The mechanical tube cleaners are made from metals, rubber or plastics. One of the concerns in the use of these mechanical cleaners is likely wear on the inside of heat exchanger tubes (Bott, 1995). Hovland et al. (1988) have demonstrated that the erosion effect of using these cleaner is negligible.

Due to aging phenomena deposits sometimes become harder. In such cases it is still sometimes necessary to apply acid cleaning, followed by cleaning with mechanical cleaners or high pressure water to remove any remaining debris (Müller-Steinhagen, 2000).

To remove hard deposits drills or scrapers may also be used. Drills and scrapers may be accomplished by water pressure which helps to lubricate and flush away the deposit as it is removed. Drilling and scraping is generally only applicable for the inner surface of the tubes (see Figure 2-3).

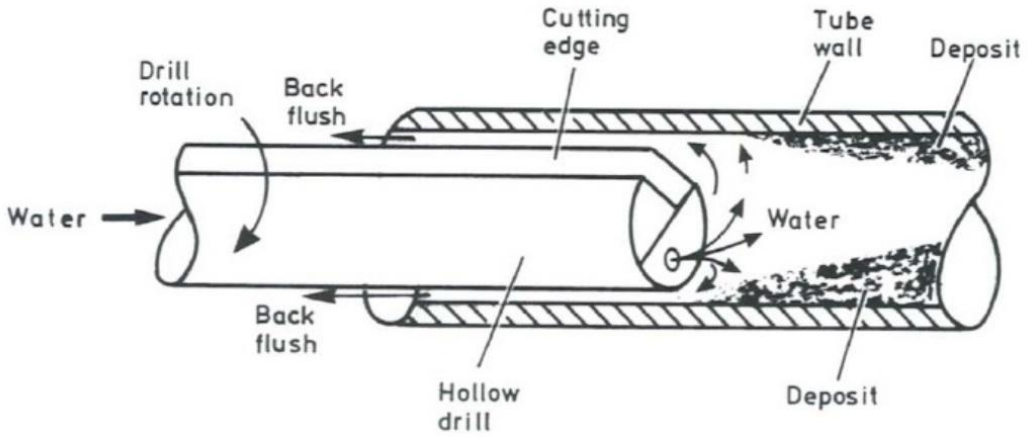

Figure 2-3 Drill and scraper cleaning system (Bott, 1995)

Chemical cleaning is another option. It is quick and does not cause mechanical damage to the surface, reaches inaccessible areas and does not need disassembling so it needs less labor, but problems may arise due to the danger of improper handling of the chemical agents (Müller-Steinhagen et al. 2011).

The biggest disadvantage of all off-line techniques is that the exchanger has to be stopped from operating and/or to be dismantled for cleaning. During this time the process is either stopped or a spare exchanger is used to enable a continuous process. Not only tend these methods to be time-consuming and expensive, the exchanger can possibly be damaged by untrained personnel.

2.3 On-line Mitigation Techniques

Periodical cleaning is necessary, even if the heat exchanger is properly designed. This gives impetus to develop on-line cleaning methods. Some of these are shown in Figure 2-4. Additives are effective if they do not lead to process contaminations or environmental hazards. They are usually anti-oxidants, metal de-activators, pH controller or scale inhibitors such as polyphosphate or aminophosphonic acid polyacrlyate. The advantages and disadvantages of using chemicals were already listed for off-line methods. They may apply to on-line methods as well. The most widespread mitigation strategy during on-line operation of heat exchangers is the use of chemical agents or inhibitors, which is particularly useful for heat exchangers with complex geometries where no other cleaning methods are possible (Müller-Steinhagen et al. 2011). Short time overheating (thermal shock) and flow pulsation deviates the process from steady-state operation, but they may have unfavorable impact on the exchanger and the quality of the products. Short time

overheating relies on the difference of thermal expansion between surface and deposit and whole deposit layers may spall off the surface instantaneously (Evangelidou, 2010).

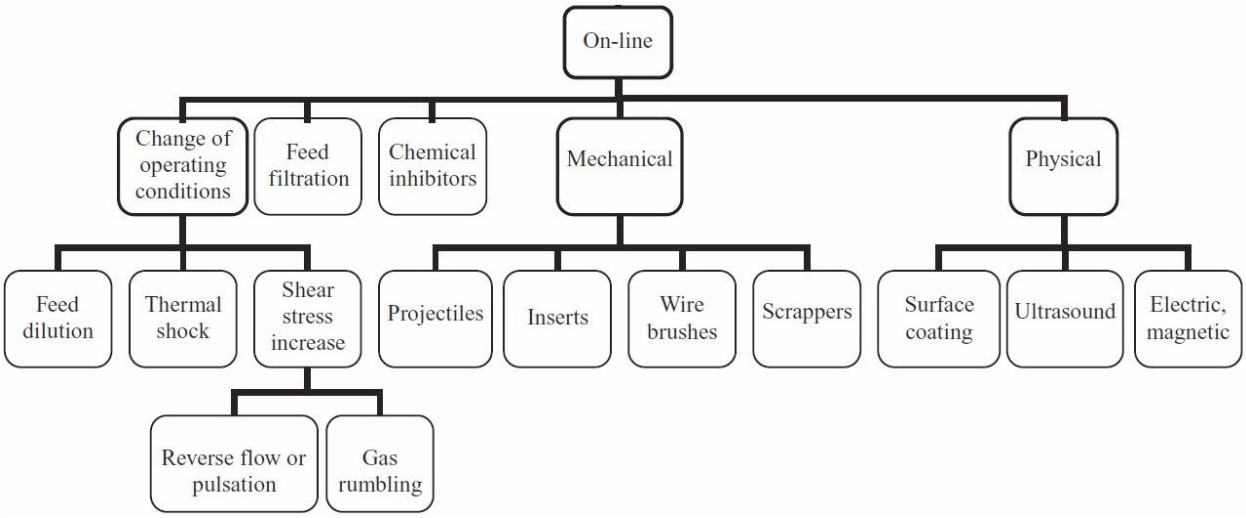

Figure 2-4 On-line cleaning methods (Müller-Steinhagen et al. 2011)

Surface coating can decrease the surface free energy and thus reduce the adhesion force between deposit and surface. A disadvantage is that the coating can be destroyed by particles in the fluid. Scraped surface heat exchangers have moving parts to remove continuously deposit from heat transfer surfaces (Solano et al. 2009).

Filters are recommended for particulate fouling (Bansal et al. 1997). It is a simple method to reduce deposits by installing a filter system before the fluid enters the heat exchanger. Sonic technology is another method. The principle of this method is to generate vibrations by sound. This disturbs and dislodges deposits from the surface. Cavitation produced by the propagation of sonic waves in a continuous manner near the deposit can also help the removal. This method, nevertheless, is not widespread and mainly limited to small exchangers. The drawbacks are structural damages to the heat exchanger by vibrations. There may also be some problems caused by the noise pollution.

2.3.1 Cleaning projectiles

The brush and cage system, as shown in Figure 2-5, is similar to the concept of sponge balls that will be addressed in this study. Brushes can dislodge the deposit from the surface. The brush system has capture cages at both ends of each tube and it needs a reversal flow to be returned. One advantage against rubber balls is that it requires less maintenance. The biggest drawback is when the process is stopped for flow reversal. This

interruption of steady conditions in the operation may be difficult to accommodate and may have implications on product quality.

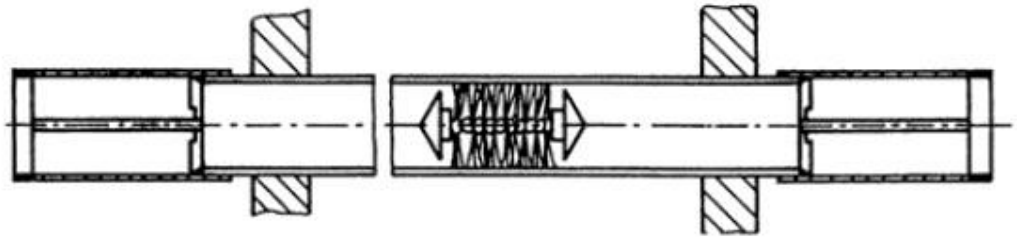

Figure 2-5 Brush and cage system (KALVO VOGLER GmbH)

Another option for projectile injection involves slightly oversized balls or other shaped objects made from sponge, rubber or metal which pass through the heat exchangers tubes. As the projectiles move, they remove the deposit depending on the exerted shear force. They circulate via a separate loop through the heat exchanger. Due to the fluid pressure, the projectiles are pushed through and will be re-injected after collection. During their contact with the tubes, they will actively rub the tubes inner surface, thus keeping it clean.

The technique was first introduced in 1957 (Aschoff et al. 1987). In the mid-1970s the Taprogge patent expired opening the way for other suppliers to enter the market. The dominant supplier however remains Taprogge, due to wide experience in the application of the technology (Bott, 1995). This innovative technique came into force from the need to clean heat exchangers without disrupting operation. The previous mechanical cleaning systems did not permit the cleaning of equipment without interrupting the process. The projectiles are used for processes with a high demand for maintaining a significant degree of cleanliness. The main characteristics of the projectiles are their size, texture and stiffness.

The advantages of this method are that the projectiles are very effective in mitigating fouling with reasonably stable operating conditions. This, in turn, reduces the primary energy cost and is also environmentally-friendly by saving energy which otherwise would have been needed to off-set the impact of fouling. Thus a longer lifetime of thermal equipment is expected. Other advantages include lower corrosion of heat transfer surfaces and avoidance of unscheduled shutdowns. This technique is extremely successful (Aschoff, 1987 and Bott, 1990) for cooling water applications.

On-line tube cleaning by circulating sponge balls along with the use of antiscalant is proved to be the most effective and economical means to avoid fouling of internal surfaces of tubes in Multi Stage Flash distillation and leads to reduced cost of additives as lower dose rates could be sufficient (Ghulam M. et al. 2001). Sludge can also be easily removed by employing on-line cleaning of the tubes. If not removed early after formation, these soft deposits could convert into solid scale (Ghulam M. et al. 2001). With optimum sponge ball

cleaning in additive dosed MSF plant, the tube fouling can be maintained as low as 0.04 m^2K/kW resulting in over 40% mean energy saving (Bohmer, 1993).

The drawbacks of this method are that the projectiles can only clean the inner side and not the outer side of the tubes and a special device for circulating projectiles has to be installed. Depending on material, e.g. rubber, the utilization of projectiles is limited to a maximum temperature of 120°C (Müller-Steinhagen et al. 2011). They also have to be replaced regularly since the projectiles have only a certain lifetime because of abrasion. Sponge balls are mainly used to remove soft deposits. For hard deposits, carborundum coated balls can be used (Bott, 1995). The selection of projectile material depends on whether or not it damages or wears the surface of the heat exchanger, which can result in even more fouling. Figure 2-6 presents a schematic diagram of the circulation of cleaning balls in industrial application.

A large amount of material may also stick to the sponge ball due to the removal of particles from the fouling layer. This, in turn, requires opening the systems and washing the balls to remove sediment from time to time. Moshe (1995) overcame the problem of cleaning the projectiles without opening the system by adding a collector, in which the balls are washed and the effluent water is released to the drain.

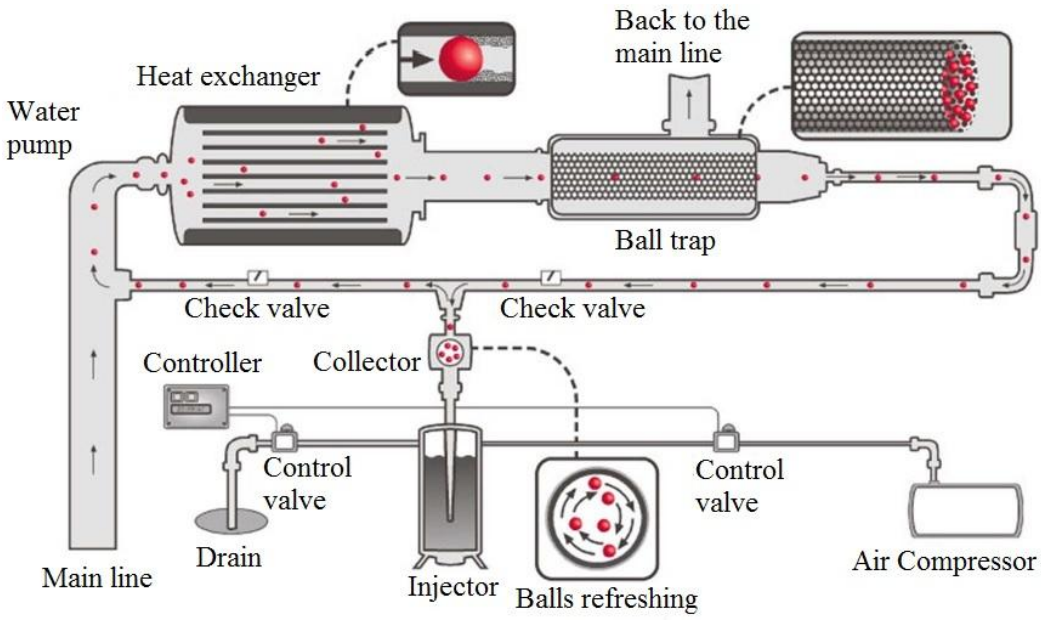

Figure 2-6 Cleaning ball system (CQM)

There are many types of projectiles available and any selection requires many considerations. The projectiles differ in size, density, hardness and texture. Here are some guidelines for the selection of suitable projectiles (Taprogge):

- Density of sponge balls can vary from 160 kg/m^3 (soft) to 300 kg/m^3 (hard). Any chosen density depends on tube material, tube contaminants, ball diameter and pressure drop across the exchanger and fluid properties.
- As for projectiles' hardness or coating, the type of deposit and the tube material need to be taken into consideration. Hard balls should be used only in stainless steel or titanium tubes, while soft balls are better used in brass tubes with delicate operating procedures. Abrasive balls are designed to be used only in extremely difficult cases of fouling and must not be used continuously. Abrasive sponge balls are coated fully or partially with carborundum for combating hard deposits.
- The long term use of projectiles may lead to an excessive tube wear.
- After some passages, sponge balls get smaller. Once they are smaller than the inner tube diameter, they should be replaced which is an additional cost factor. Tube conditions like roughness, corrosion and scaling will reduce the longevity of the balls. This fact determines the lifetime of sponge balls.

Eimer (1985) demonstrates how the ball frequency f_k (balls/h) may be determined. If n is the ratio of the number of balls to parallel tubes in the exchanger, then:

$$f_k = \frac{n \times 3600}{t_u} \tag{2.1}$$

where t_u is the average ball circulation time in seconds. For example if t_u=30s then f_k=12 balls/h. i.e each tube sees a ball 12 times per hour. According to Eimer (1985) this is a typical frequency (Bott, 1995).

This cleaning system must be operated continuously but based on intermittent application. The cleaning period, i.e. the time the balls are in circulation and the interval from the beginning of a cleaning cycle till the beginning of the next cycle must be taken into account (Bott, 1995). As an example by Eimer (1985) it can be used once per day during 1 hour with a ball injection interval of 12 balls/h (this could be considered as typical interval) or during 2 hours with an interval of 6 ball/h (Bott, 1995).

Sometimes to protect the inner side of heat exchanger tubes against corrosion, they are covered by a film or layer (Bott, 1995 and Eimer, 1985). It is imperative, therefore, that this coating is not destroyed by any on-line cleaning method i.e. sponge balls. This coating is also an extra thermal resistance. Therefore the thickness of this coating must be the optimum that guarantees a sufficient corrosion resistance with the minimum thermal resistance and is capable to resist the effects of sponge balls circulation. In this case the sponge rubber ball removes the bulk of the soft deposit, but leaves on the surface lacquer-like iron-rich coating. The result can be a protection against corrosion with minimal reduction in heat transfer efficiency, but the choice of operating conditions needs careful consideration (Bott, 1995).

Technos has developed a technique to blend the balls with the special materials that were previously used as coating on abrasive balls. The technique is claimed to provide a major advantage over ball coating technique since the desired abrasive effectiveness remains unchanged while the balls are being used (Al-Sofi,1989).

2.3.2 Technical limitations

Despite significant technological advancement, there are still several technical limitations that should be considered with respect to cleaning projectiles. Perhaps the first drawback is the behavior of cleaning projectiles at elevated temperatures. Due to the stability of the projectile material, they can presently not withstand temperatures above 120°C (Müller-Steinhagen et al. 2011). Thus the present projectiles are limited to low temperature systems.

The second limitation is the minimal flow velocity that is needed for the propulsion of projectiles through the heat exchanger tubes. Better mitigation is expected if the diameter of sponge balls is larger than the exchanger inner tube diameter but this in turn requires higher tube-side flow velocities for propulsion. These high flow velocities can become an operational barrier in some processes. Another limitation is the random distribution of the projectiles through the exchanger tube sheet. Due to this maldistribution, some tubes may be blocked due to excessive fouling if they are not cleaned as often as they should be, so a good pre-distribution is required. Problems may sometimes occur due to sticking of a ball in the tube.

3 EXPERIMENTAL SETUP AND PROCEDURE

A test facility was designed and constructed to investigate the online cleaning performance of projectiles in tubular conduits during crystallization fouling of calcium sulfate solution. Calcium sulfate dihydrate has an inverse solubility for temperatures above 40°C. Solution is heated up in a heated section so the deposit forms on the hot surface. More details will be explained in section 3.2.2. The test rig allowed the injection of projectiles at different intervals and velocities during fouling runs.

3.1 Description of Test Facility

3.1.1 Process Flow Diagram (PFD)

The test rig was designed to simulate conditions for fouling and mitigating in industrial scale with respect to tube and projectile sizes. The flow diagram of the test rig is presented in Figure 3-1. The projectile can be inserted from a position that is specified in this figure and would be directed into the heated test section by turning the flow from line 1 to line 2. This is done by a 3-Way-Valve (3WV). After passing through the heated zone, the projectile is returned to a transparent section to make sure that it does not get stuck somewhere in the rig.

A centrifugal pump was used to discharge the flow from the supply tank to the test rig. The flow rate was controlled by a flow meter and 3WV plus actuator. The flow meter sends signals to the actuator to allow that a certain flow passes through the valve. Excessive flow returns back to the tank through a bypass line. The tank was equipped with a cooling coil and 3 jacket heaters with a power of 3×500 W, a thermocouple and a temperature controller to adjust the bulk temperature to a certain value. The temperature controller receives the signals from a thermocouple located in the supply tank to adjust the required power for the jacket heaters or the flow in the cooling coil.

Some parts of the test rig were made from transparent material (normal glass) for tracing the projectile to make sure that the flow and projectiles were running smoothly. After passing the heated section the projectile could be returned to the transparent part. This part is a set of piping, including a glass valve and two T-junctions (see section 3.1.7 and Figure 3-17) to ensure that it was not stuck anywhere in the rig. Thereafter by opening a 2-Way-Valve, 2WV, a small flow would bring the projectile to its initial position for the next injection. Two check valves have been installed which avoid the reversal of the flow. The red crosses shown in Figure 3-1 are mechanical hindrances to prevent projectiles to enter the bypass lines.

The outer diameter of the heated tube where fouling occurs was 25.4 mm with a wall thickness of 2.5 mm, hence the inner diameter was 20 mm. The inner diameter of the tube had a minor variance of ±0.1 mm.

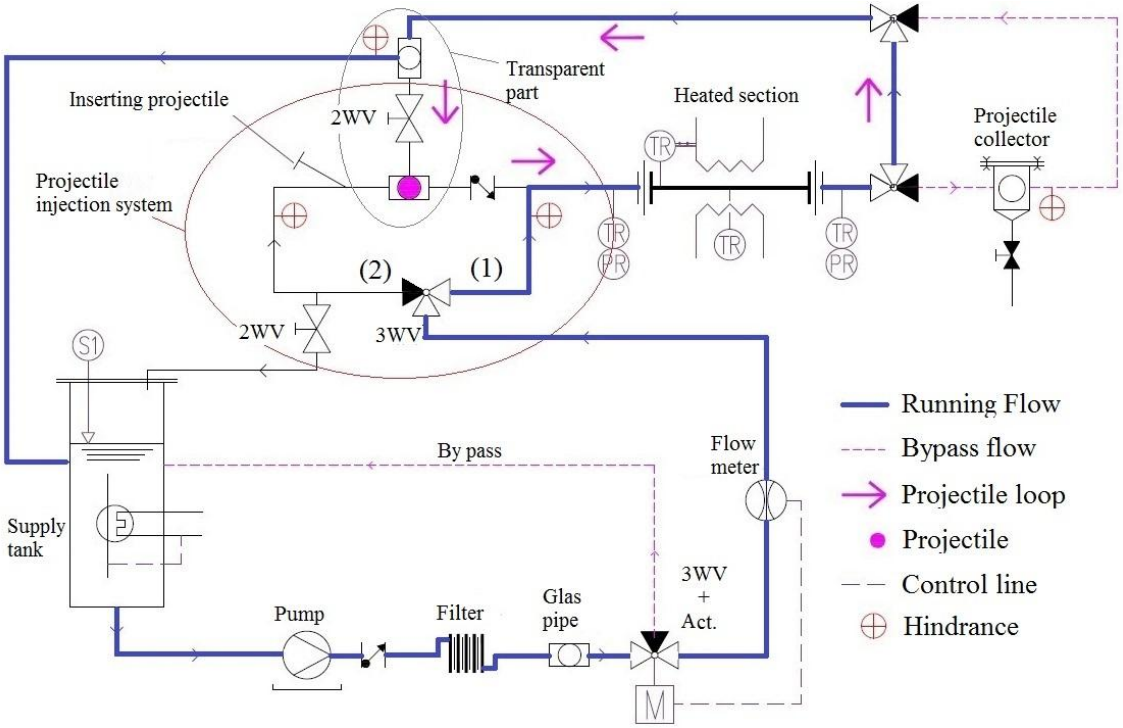

Figure 3-1 Flow diagram of the fouling test facility

The projectile injection system is highlighted in Figure 3-1 by an elliptic. The projectile was first inserted in the test rig via an inclined pipe shown in the upper left corner and identified as "inserting projectile". It was then shot into the heated tube by changing the flow through the 3WV such that the flow passes from outlet (2) of the 3WV to the heat exchanger tube. Figure 3-2 provides a picture of the experimental setup. The main components of the rig are; (1) 2200 W centrifugal pump, (2) transparent part, (3) a 3WV that is fully actuated by a motor and a flow controller, (4) a 10 kW electrical furnace, (5) projectile collector, (6) piping, (7) control panel for the furnace and (8) flow meter. The 60 L supply tank and filter are two other main parts that are not shown in the figure. A 70 µm in-line filter is used to remove suspended particles or broken deposits from the flow.

Figure 3-2 Photo of the experimental setup
(1) 3 hp centrifugal pump, (2) transparent part, (3) 3WV that is fully actuated by a motor and a flow controller, (4) 10 kW electric furnace, (5) projectile collector, (6) piping, (7) control panel of the furnace and (8) flow meter.

Figure 3-3 elaborates how the projectile could be injected into a closed loop in 5 steps. At first step the projectile is inserted from the inclined pipe shown in this figure. Then the 3 way valve was turned to L position (see Figure 3-3, step 2), so that the projectile is injected into the heated section by the flow before returning to the transparent part.

In step 3, the 3 way valve will be turned to R position (Figure 3-3, step 3). Both ball valves shown in step 4 should be opened and the projectile is returned back to its first position by a small flow. In step 5 both ball valves have to be closed again and the system is ready for the next injection.

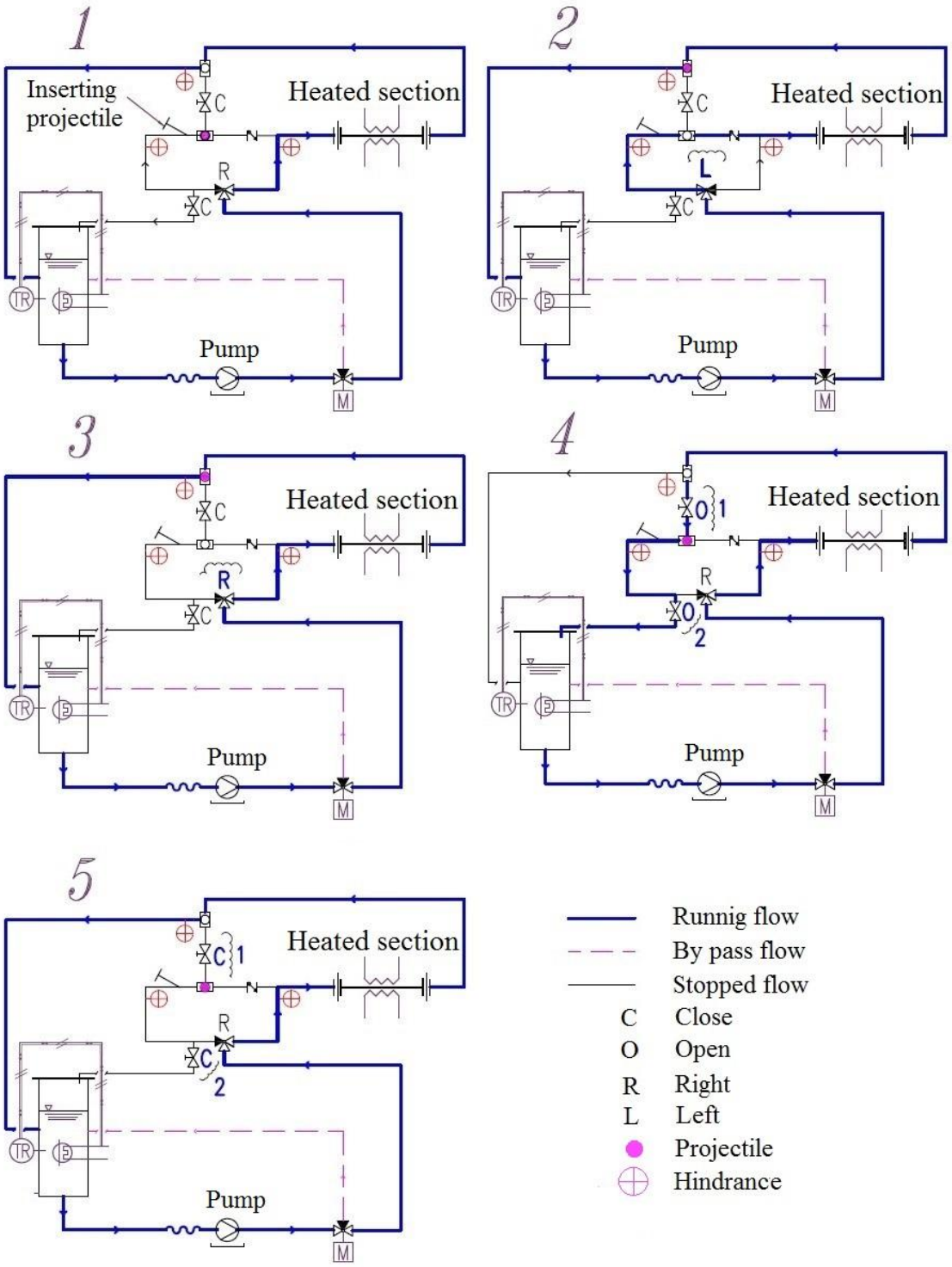

Figure 3-3-Procedure for the projectile injection and return in a closed loop

3.1.2 Furnace design and specifications

A 10.5 kW electrical heater was used as the heated section. The length of the heated test section was 280 mm (due to the length of the available electric elements). The heated section was positioned after 20 cm of straight line to achieve a fully developed turbulent flow. The heated section consisted of a circular tube heated from outside by the electric furnace. By considering the maximum surface temperature (60°C) at 3.5 m/s (the maximum velocity of the working fluid) plus 1 kW estimated heat loss, it was determined that an electric furnace with a power of around 10.5 kW was required. Heat was transferred from the electric furnace to the $CaSO_4$ solution passing through the heated tube which was made from stainless steel 316L. In Table 3-1 the desired parameters used for designing the furnace are listed.

Table 3-1- Desired parameters for designing the furnace

Parameter	Values
Max. surface temperature (at 3.5 m/s)	60 °C
Bulk temperature (Max. at 3.5 m/s)	40 °C
Maximum velocity	3.5 m/s
Inside diameter of heated tube	20 mm
Maximum heat flux (from the inner surface)	596 kW/m^2
Length of tube	28 cm
Power of furnace	10.5 kW

The dimensions of the furnace were 706 mm in length with 650 mm of width and 550 mm of height with a total weight of 80 kg. To avoid heat losses 125mm-thick insulation was used. The maximum temperature of the inner space of the furnace is 1600°C. The furnace has a control board which is equipped with temperature controllers, pointers and emergency instruments. A powerful transformator was used to provide the suitable power for the furnace. Figure 3-4 depicts the electric furnace where the locations of heating elements, insulation, and heated tube are identified.

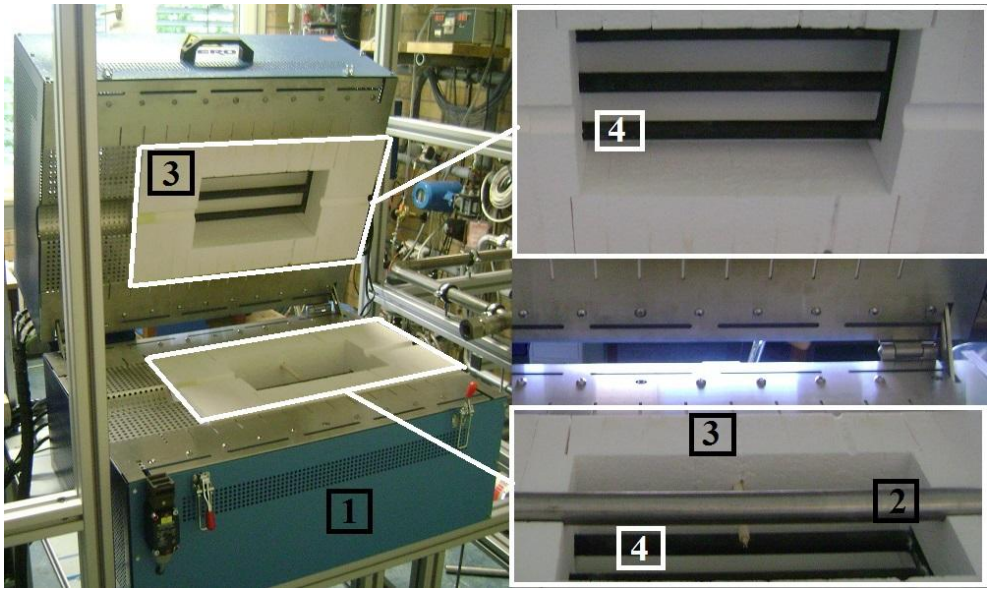

Figure 3-4- Photos of 1) furnace, 2) tube, 3) insulation and 4) heating elements

3.1.3 Wall temperature of heated tube in the furnace

A reliable means of determining the extent of fouling inside the tube is to measure the tube wall temperature. Because the fouling layer is a resistance against heat transfer, the tube wall temperature increases (see Figure 3-5). To measure the tube wall temperature it was firstly tried to pass two S-type thermocouples through the furnace chamber, but no thin thermocouples were available on the market that could withstand the high temperature of 1600°C. Therefore, it was decided to extend two holes into the tube wall, which was only 2.5 mm thick, from the insulation packing till the middle of the tube in the heated section as indicated in Figure 3-6. The 165 mm long holes (the longest possible) with a diameter of 0.8 mm were made to insert two K-type thermocouples with a diameter of 0.5 mm inside the tube wall. The gap was filled with high conductive paste (T12+Arctic Silver 5" with thermal conductivity of 9.8 W/m·K). The two thermocouples with 300 mm length and 0.5 mm diameter were positioned inside the two holes. Due to the high heat flux in a high temperature atmosphere, a finite element analysis was performed by ANSYS to be sure that the thermal stress in the tube will be less than the allowable stress for stainless steel 316L. Based on the calculation, a maximum wall temperature Max. T_w of 300°C was applied.

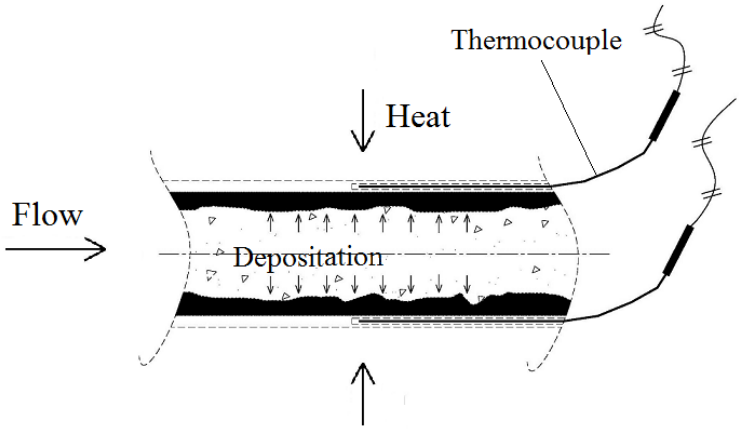

Figure 3-5 Tentative location of thermocouples

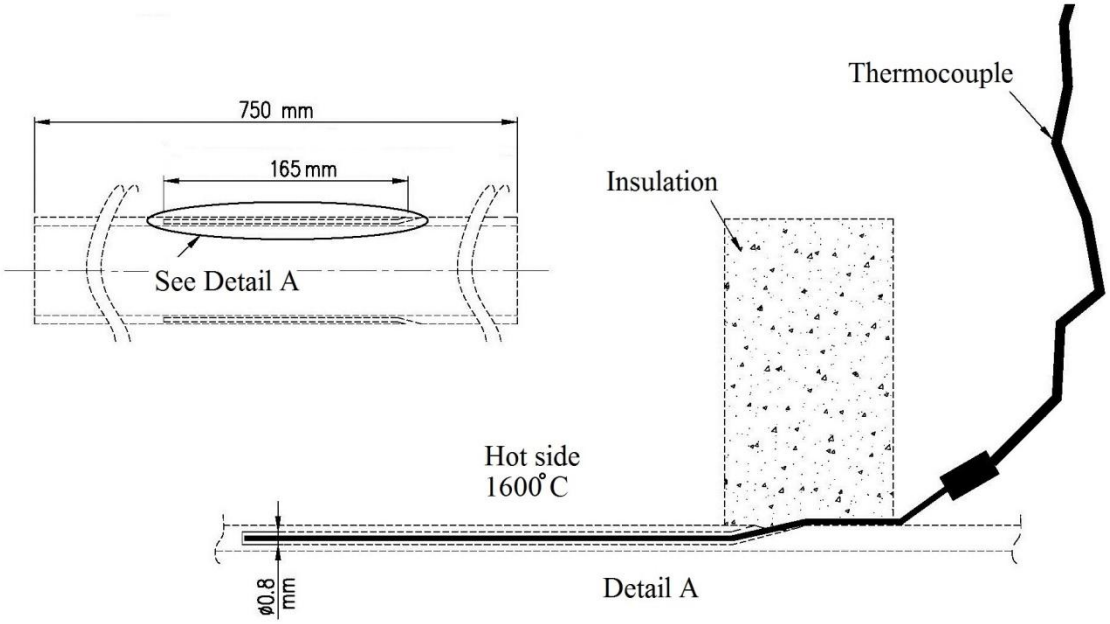

Figure 3-6 Method of inserting the thermocouples in the tube wall

In this study, the wall temperature (T_w) is measured by the two thermocouples on the left and right sides in the direction of flow (Figure 3-7). Ideally, because of the symmetric structure of the heating zone, the wall temperatures at the left and right sides should be identical. In reality though, during the experiments, sometimes there is a difference between the measured wall temperatures even at clean condition, thus the thermocouples are not located exactly at the same distance to the inner surface of the tube. This distance could be calculated by the Wilson plot method (see Appendix C). This method (Briggs, 1969) was used to find the exact positions of the thermocouples in radial direction and hence the distance between the thermocouples and the tube inner surface can be determined. Accordingly, several experiments were carried out at different surface temperatures.

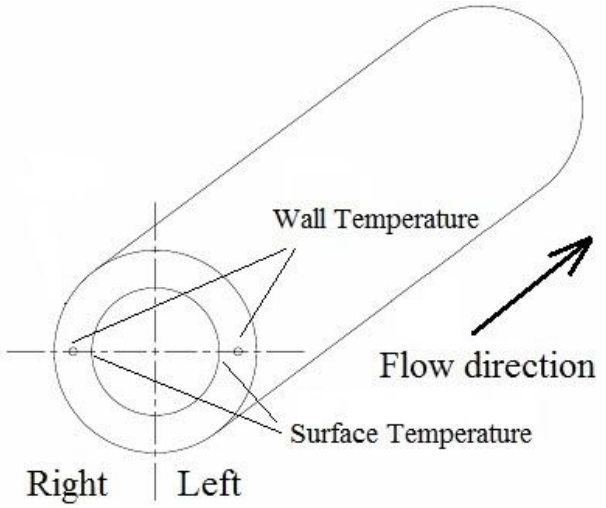

Figure 3-7 Position of the thermocouples inside the tube wall in flow direction

3.1.4 Projectile collector

The projectile collector was designed as a cyclone for collecting and removing the projectiles from the test rig whenever it was needed (Figure 3-8 and Figure 3-9). The cyclone was used in a bypass line and the projectile is directed by two 3WV into this cyclone. There is a hindrance (section A-A in Figure 3-8 and Figure 3-10) at the outlet that does not allow the projectiles to escape from the cyclone. When the projectile is located in the collector then both input and output lines will be closed (by the two 3WV) and the flow is passed through the main line again. By opening the 3" valve just beneath the collector, the projectiles were drained. The projectile collector was large enough to be used for many injections before it became full. Two glass windows were installed to track down the projectiles. The collector is positioned in a direct line toward the heated section to ensure the capture of spherical and non-spherical projectiles.

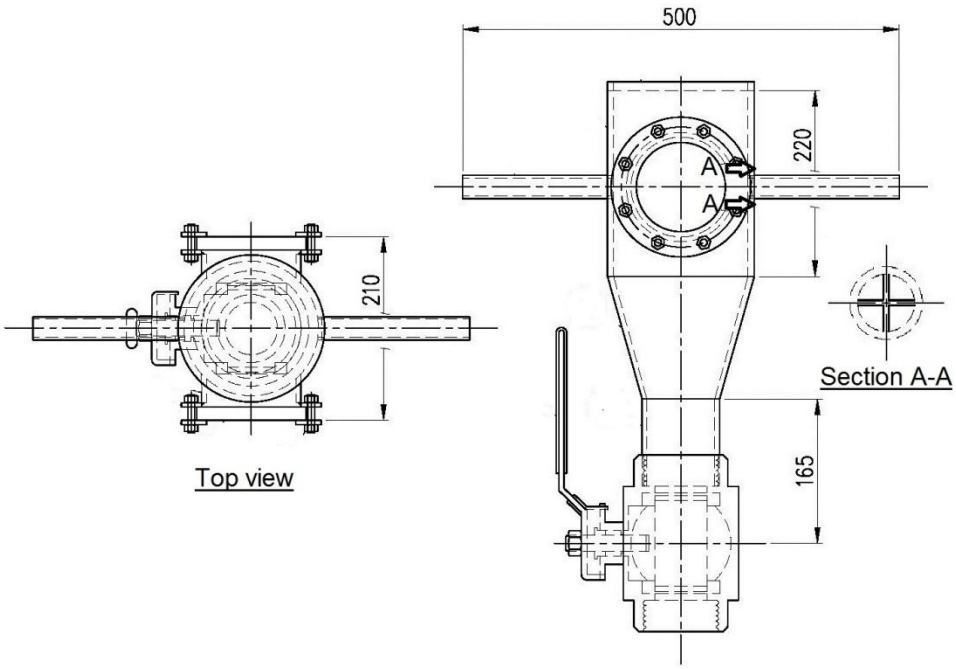

Figure 3-8 Drawings of the projectile collector

Figure 3-9 A picture of the projectile collector

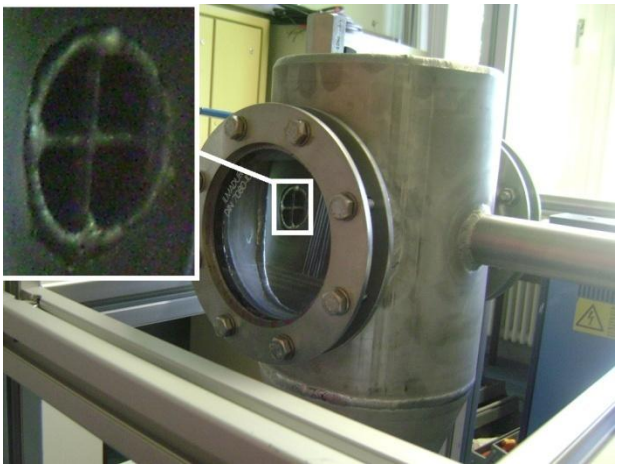

Figure 3-10 Mechanical hindrance at the outlet of projectile collector

3.1.5 Injection of projectiles

A simple devise was constructed for inserting the projectiles into the pipe. It is a plugged inclined pipe connected to the horizontal pipe through which the flow passes. The plug could be removed and the projectile could be inserted when the flow was passing through another line. By closing the plug, the projectile was ready for injection. Figure 3-11 and Figure 3-12 show the inclined connection which was equipped with a plug and a handle to be closed and opened easier if it was hot during operation. The connected rod with a spherical head was used to avoid that the projectile re-entered the inclined pipe (Figure 3-12). After inserting the projectile into the pipe, it was ready for injection. Then it was propelled by switching the flow from right to left by the 3 way valve as shown in Figure 3-13.

Figure 3-11 Projectile insertion assembly

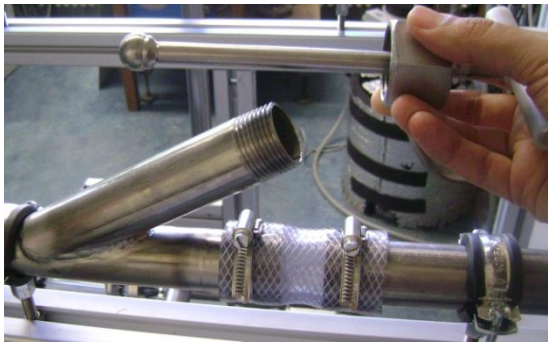

Figure 3-12 A rod with ball to push the projectile inside the pipe

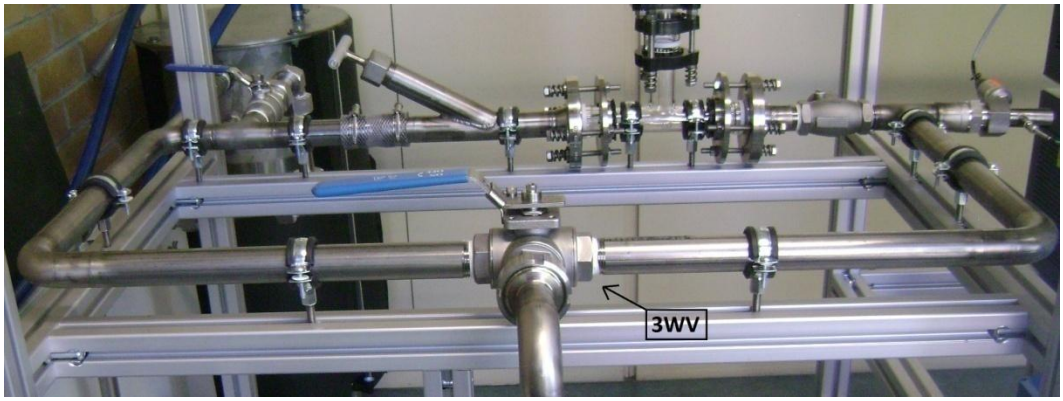

Figure 3-13 The 3 way valve used for switching flow direction for injection

3.1.6 Flow control system

To maintain the flow in the pipe at a desired value, several control instruments such as a flow meter, a 3 way valve plus actuator and a data acquisition system were used. Signals from the flow meter were sent to the data acquisition system. As shown in Figure 3-14, the signals were first analyzed by a program, which then again sent a signal to the actuator to set the flow to the required value by actuating the 3 way valve.

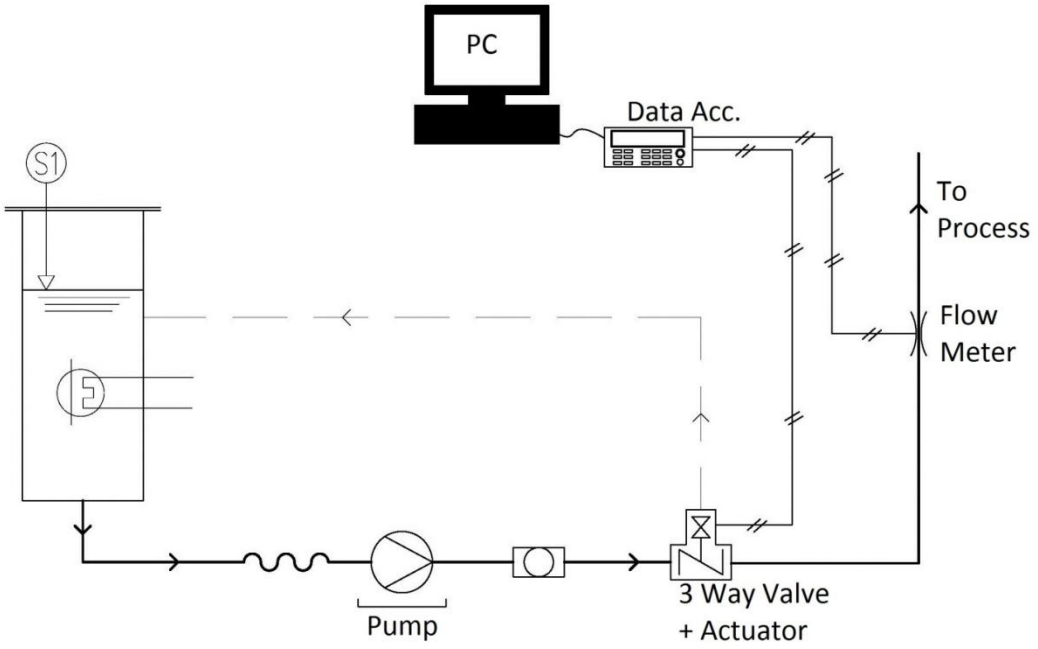

Figure 3-14-Flow control system

3.1.6.1 Flow meter

The magnetic flow meter (KFL-DC SERIALS a product of KAFLON M&C instruments Company) contained a display to show the flow directly and also a facility to send signals to the data acquisition system. It sends signals between 0-20 mA for a flow between 0-16 m^3/h, linearly (see Figure 3-15).

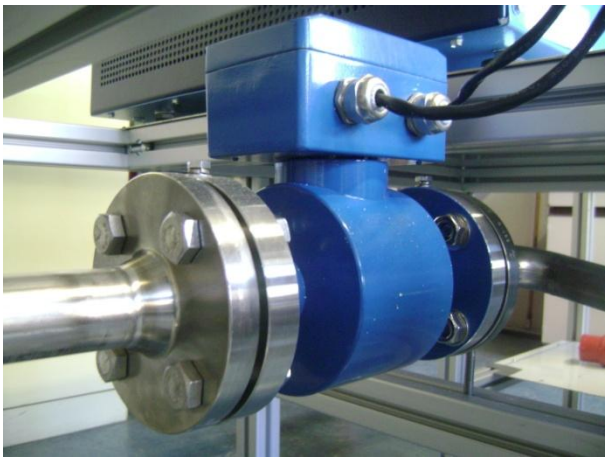

Figure 3-15 Flow meter

For actuating the desired flow rate, an electric actuator and a 3 way valve were used (see Figure 3-16). The actuator had a mechanical part with gears for connection to the 3 way valve.

Figure 3-16 The electric actuator and 3 way valve used for the flow control

3.1.7 Filter

An in-line 70 μm filter was also used to remove suspended particles or broken deposits in the flow. The filter was installed after the pump and before the heated section. It was made from polyethylene and polypropylene and it is 0.5 m long.

3.1.8 Visualization of projectile movement

Some parts of the test rig were completely constructed from glass, for observing the projectiles, as some may get stuck in the rig due to e.g. deposit formation. The main transparent parts are shown in Figure 3-17. The construction was not straightforward since the other parts were made from metal and metal-glass connections are prone to leakage. Another difficulty with these parts was the construction of a hindrance at the first T-junction. Figure 3-18 shows how a hindrance is connected to a glass T-junction.

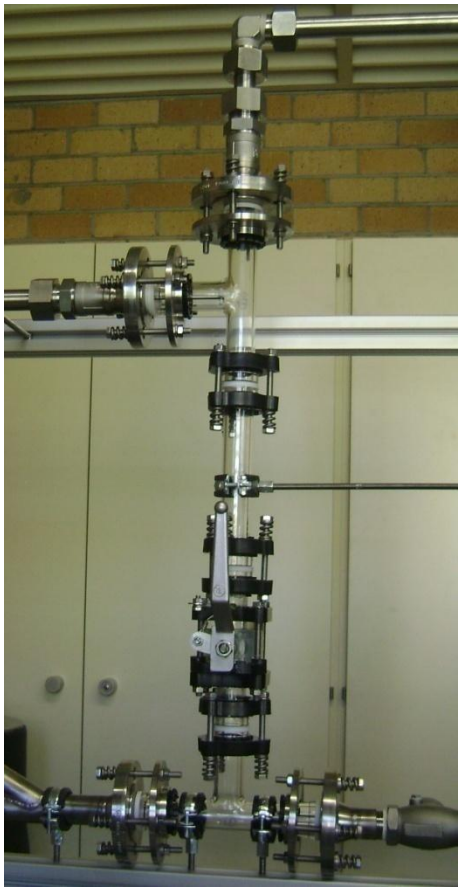

Figure 3-17 The construction of glass parts

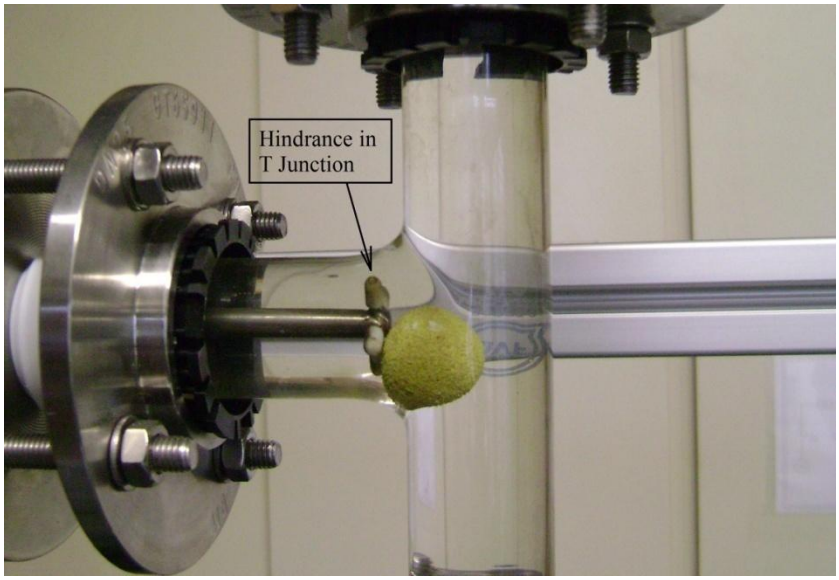

Figure 3-18 Hindrance at the glass T-junction

3.1.9 Measurement of pressure drop

Two tapings were installed before and after the heated section to measure inlet and outlet pressures. The employed pressure transducer was model DPX101 Series from Omega, with a sensitivity of reading the pressure every 1 μs which was then tuned to every 0.5 s because of limitations of the data acquisition program. The maximum error of the pressure transducer close to absolute vacuum was ±50 Pa. The normal fluctuations of pressure for flow were ±70 Pa. Thus the flow fluctuations did not allow obtaining a measurable value for the pressure drop since the difference between the input and output pressure was lower than the fluctuations themselves, but they were sensitive enough to recognize the produced shear when the projectile passed through the heated section.

A series of pressure measurements was conducted to discern the stability of projectile's contact with the tube. To eliminate the fluctuations, a long tube was used and the flow was discharged to the ambient. Then the pressure behind the projectile was recorded while it passed through the tube (see section 4.8.2 for more details).

3.1.10 Data acquisition system

A data logger is an electronic device that records data over time or in relation to location either via instruments or sensors. The devises used in this investigation were Data Acquisition Module 34970A (Main Device), a 34901A 20-Input Channel Multiplexer and two 34907A 2×2-Output Channel Multifunction, the products of Agilent Technologies. A 34830A BenchLink Data Logger Pro software was installed on a computer for configuring the input and output channels. The sensors used in the rig included thermocouples, pressure transducers and the flow meter. Data could be recorded at different intervals. In this work it is between 0.5 s – 1 min according to the nature of the attempted experiment. The data is recorded momentary based on the received analog electrical signal (of mA or mV) from different devices.

3.2 Experimental Procedure

3.2.1 Start-up at clean condition

At first, the furnace temperature for each specified surface temperature and fluid velocity was adjusted. For instance, for a surface temperature of 71°C and a velocity of 0.8 m/s, the required furnace temperature turned out to be 1200°C. Starting up the test rig took almost 2 hours to reach 1200°C because of the limited heating up ramp (maximum 10 K/min recommended by the furnace supplier). During heating up, firstly demineralized water was pumped through the rig. Figure 3-19 shows how all variables vary before reaching the set-points at steady-state conditions. When the bulk temperature reached the set-point (40°C) after 48 min, the control system for the cooling water started to adjust the

bulk temperature. Steady-state condition was maintained when the furnace reached its set-point after approximately two hours. In this study, the tube wall temperature (T_w) represented the temperature at the locations where the thermocouples were embedded, i.e. the two thermocouples on the left and right sides in the direction of flow. It was already mentioned that the constant difference between the two measured tube wall temperatures is related to the different positions of the thermocouples with respect to the interior surface, which was determined by the Wilson plot method.

The flow control system reacted to deviations from steady-state conditions fast. It adjusted the flow to set-point almost instantaneously. Figure 3-19 shows for demineralized water, that no changes in any parameter, temperatures and flow are expected in the absence of fouling. At fouling conditions, though, the tube wall temperature is expected to rise.

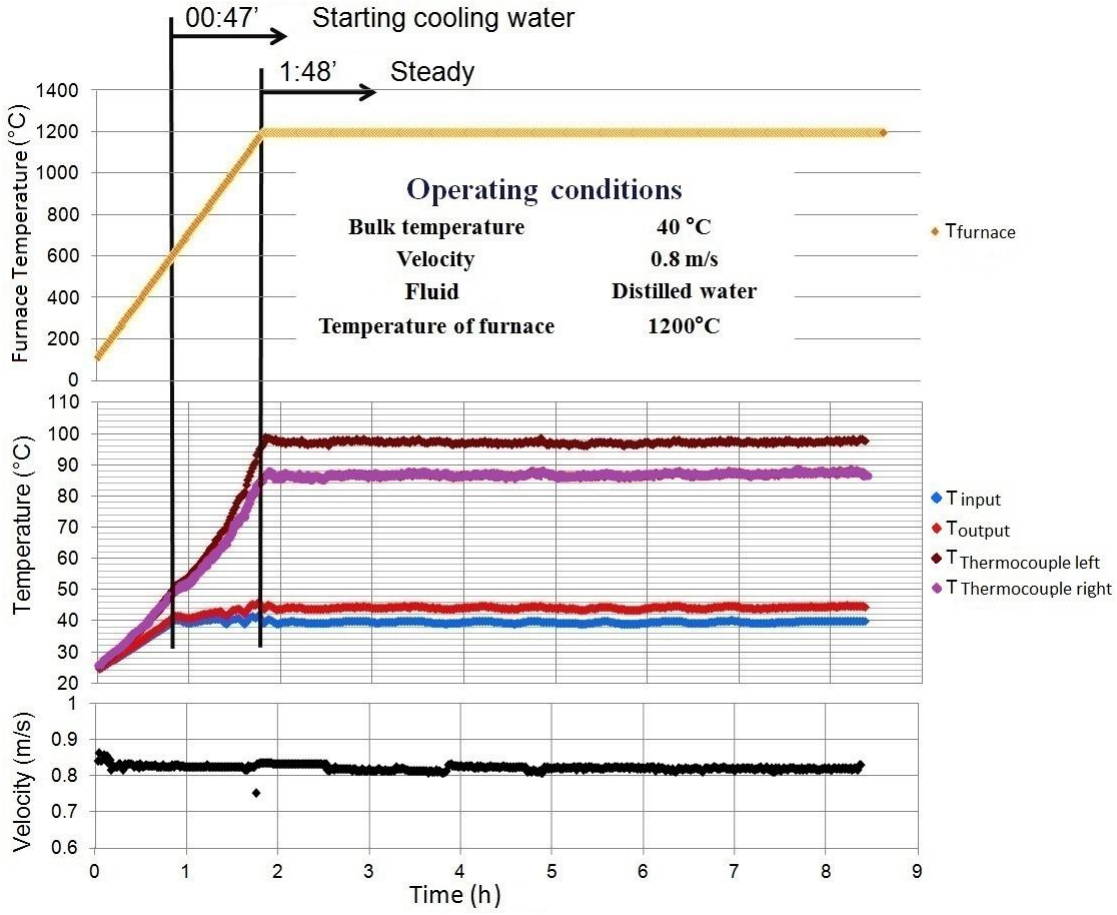

Figure 3-19 Variation of different parameters in the time span of 8.5 hrs

3.2.2 Preparation of chemical solution

Calcium sulfate dihydrate ($CaSO_4 \cdot 2H_2O$), which is used as foulant in this investigation, has an inverse solubility with temperature above 40°C (Jamialahmadi et al.

1993). The solubility is strongly influenced by of the presence of other ions (Marshall et al. 1964) in the solution, thus demineralised water with a conductivity of 50 µS/cm is used. Since calcium sulfate crystals do not dissolve easily in water, it was preferred to dissolve calcium nitrate tetrahydrate ($Ca(NO_3)_2 \cdot 4H_2O$) and sodium sulfate (Na_2SO_4) together in water to produce a calcium sulfate dihydrate solution. These two chemicals were chosen because their high solubility in water could provide a high enough concentration of foulant ions in the solution, as has been shown by Najibi (1997). The resulting sodium nitrate ($NaNO_3$) increases the solubility of calcium sulfate, as explained by Marshall et al. (1964) and Rizzo (2008). They attributed this to the electrostatic attraction between the sodium nitrate ions and the ions with opposite charge formed by the calcium sulfate.

Several experiments were performed to determine the suitable bulk concentration. It was observed that in order to produce fouling at measurable rates, the calcium sulfate solution had to be with a bulk concentration above 3.8 g/L. The prepared test solution has a bulk concentration of 4.6 g/L. In this concentration the pH is 8.2, though the calcium sulfate solubility is not significantly affected by pH (Jamialahmadi and Müller-Steinhagen, 2004).

Several tests have been performed to specifically investigate the possibility of bulk crystallization. In the experiments where the fouling layer had reached an asymptotic level, the experiments were kept running afterwards for several hours and the bulk concentration was continuously monitored. It was found that the bulk concentration did not change. Therefore, it can be concluded that bulk crystallization did not take place. Hence the possibility of crystallization in the bulk liquid was ruled out in all fouling experiments considering that heterogeneous nucleation on the heat transfer surface requires less activation energy than homogeneous nucleation in the liquid (Andritsos et al. 2003).

Half of the volume of the supply tank, i.e. 30 L, was filled with demineralised water at the beginning of each fouling experiment, and then the setup was switched on by turning on the pump and the electric furnace. Two 15 liter charges of calcium nitrate tetrahydrate and sodium sulfate solutions were heated to 40°C in separate thermostat tanks, then added to the supply tank once the temperature of the electric furnace as well as the bulk temperature of the circulating water had reached steady-state condition. The two solutions were then mixed immediately due to the high turbulence in the supply tank forming $CaSO_4$ based on the following chemical reaction (Bansal et al. 2008 and Al-Janabi et al. 2009).

$$Ca(NO_3)_2.4H_2O + Na_2SO_4 \text{ -----> } CaSO_4 \cdot 2H_2O + 2NaNO_3 + 2H_2O$$

The concentration of $CaSO_4$ during the fouling experiments was determined by a complexometric Ethylene-Diamine-Tetra-Acetic Acid (EDTA) acid titration (Fritz et al. 1987) and then controlled by the addition of the respective solutions. The titration was carried out every half hour; details about the titration method can be found in Appendix B.

To maintain the concentration of $CaSO_4$ at the desired value a highly concentrated solution of calcium nitrate and sodium sulfate was added to the supply tank.

3.2.3 Preparation for fouling experiment

At the beginning of each fouling experiment, various components of the test rig i.e. supply tank, filter and heated section had to be checked to see if there was any deposit left from the previous experiment. A fouling experiment was then started by turning on the pump and the electric furnace. The furnace temperature was set to increase at a rate of 10 K per minute. This was in order to maximize the lifetime of the furnace (recommended by the supplier). When the supply tank reached a bulk temperature of 40°C, the temperature was controlled by a water cooling system. The flow velocity was also adjusted by the flow-meter and the 3WV plus actuator. The data acquisition system was then switched on to assess the stability of the operating conditions. As mentioned before the electric furnace reaches steady-state condition after approximately 2 hours of heating. Once steady-state conditions were confirmed, then the fouling process was started by adding the calcium nitrate tetrahydrate and sodium sulfate solutions to the supply tank. The data acquisition system was then set to record all input signals every 1 minute and store it as a Microsoft Excel spreadsheet.

3.3 Cleaning the Fouled Tube

When the fouling experiment was finished, it was necessary to clean the tube before using it for the next experiment. To clean the surface from the deposit, a chemical agent, anti-gypsum, was used. This chemical was added inside the tube at 60°C for 3 to 6 hours, depending on the hardness of the deposit, in a bath with an ultra-sonic stirrer.

3.4 Specification of Projectiles

Two main types of projectiles were used in this study. The first group included cleaning balls while the second group consisted of metal projectiles. Cleaning balls were also divided into hard and soft balls. Measurements on how to determine the stiffness of a projectile will be explained later. Two shapes of metal projectiles, which were designed and supplied by CQM Company, were also investigated. More specifications of the investigated projectiles are listed in Table 3-2, Table 3-3 and Table 3-4. The reported dynamic shear force (τ_{dyn}) in the tables will be introduced in section 4.7.1.

Table 3-2 Specification of suggested soft projectiles

Projectile				
Code	P01	P02	P05	P06
Diameter (mm)	21	22	24	21x22
Type	Sponge-ball	Sponge-ball	Silicon-Hollow-ball	Silicon-Solid-ball notch on surface
Stiffness (N/ % def.)	0.178	0.558		
τ_{dyn}(kPa)	14.2	75.0	80.1	95.6
Projectile				
Code	P09	P10		
Diameter (mm)	22	23		
Type	Sponge-ball	Sponge-ball		
Stiffness (N/ % def.)		0.178		
τ_{dyn}(kPa)	51.0	36.2		

Table 3-3 Specification of suggested hard projectiles

Projectile				
Code	P04	EX06	P11	P12
Diameter (mm)	19.8	19.8	20.0	20.2
Type	Rubber-ball Smooth surface	Rubber-ball Structured surface	Rubber-ball Structured surface	Rubber-ball Smooth surface
Stiffness (N/ % def.)	1.040	1.040	1.040	1.040
τ_{dyn}(kPa)	loose	loose	negligible	932

Table 3-4 Specification of suggested metal projectiles

Projectile				
Code	EX04	EX05		
Diameter (mm)	19.5	20		
Type	Metal bullet	Metal spring		
Stiffness (N/ % def.)				
τ_{dyn}(kPa)				

3.5 Matrix of Operating Conditions

The range of operating conditions in this work is listed in Table 3-5. The important point to note here is that the velocity of 3 m/s corresponds to a Reynolds number of around 10^5. Thus to perform fouling runs and to have measurable deposits a very high furnace temperature is required.

Table 3-5-Range of operating conditions

Parameters	Range
Bulk temperature	40 °C
Velocity	0.5 - 3.0 m/s
Chemical concentration	3.0 – 5.0 g/L
Surface temperature of heated tube	71-80°C
Inside diameter of heated tube	20.0 mm
Length of heated section	28 cm
Min. projectile interval	20 s
Max. Power of furnace	10.5 kW
Maximum heat flux (from the inner surface)	596 kW/m^2
Maximum temperature of furnace	1600°C

Table 3-6 lists the operating conditions of the performed fouling experiments with or without projectiles. These experiments were carefully planned to discern the performance of various projectiles at different operating conditions.

Table 3-6 Matrix of operating conditions for the experiments (fouling runs), T_b=40°C

Exp. No.	Surface Temp. of Tube (°C)	Concentration (g/L)	Type of Projectile	Projectile Inj. Interval (per min.)	Velocity (m/s)	Descriptions
001	80	5.0	P01	Not Regular	0.8	
002	80	4.0	P01	Not Regular	0.8	
003	80	4.0	P01	Not Regular	0.8	
004	80	4.0	P01	30	0.8	
005	80	4.0	P01	5	0.8	
006	80	4.0	P01	5	0.8	
007	80	4.0	P01	2	0.8	
008	80	3.0	N/A	W/O	0.8	
009	80	3.5	N/A	W/O	0.8	
010	80	3.5	N/A	W/O	0.8	
011	80	3.7	N/A	W/O	0.8	
012	80	4.0	N/A	W/O	0.8	
013	80	3.8	P02	30	0.8	
014	80	3.8	P02	2	0.8	

Table 3-6 (continue)

Exp. No.	Surface Temp. of Tube (°C)	Concentration (g/L)	Type of Projectile	Projectile Inj. Interval (per min.)	Velocity (m/s)	Descriptions
015	80	3.8	P02	5	0.8	
016	80	3.8	P02	10	0.8	
017	80	3.8	P02	15	0.8	
018	80	3.8	N/A	W/O	2.2	
019	80	3.8	N/A	W/O	2.2	
020	80	3.8	EX06	5	0.8	
021	80	3.8	P04	5	0.8	
022	80	3.8	N/A	W/O	0.8	
023	80	3.8	N/A	W/O	2.2	
024	80	3.8	P10	60	2.2	
025	80	3.8	P10	10	0.8	
026	80	3.8	P02	10	0.8	
027	80	3.8	P02	5	0.8	
028	80	3.8	P10	5	0.8	
029	80	3.8	P10	5	0.8	
030	80	3.8	N/A	W/O	0.8	
031	80	3.8	N/A	W/O	0.8	
032	80	3.8	N/A	W/O	0.8	
033	80	3.8	N/A	W/O	0.8	
034	80	3.8	N/A	W/O	0.8	
035	80	4.3	N/A	W/O	0.8	
036	80	3.8	N/A	W/O	0.8	
037	80	4.8	N/A	W/O	0.8	
038	80	4.6	N/A	W/O	0.8	
039	80	4.6	P05	5	0.8	
040	80	4.6	P06	5	0.8	
041	71	4.6	N/A	W/O	1.3	
042	71	4.6	P06	5	1.3	
043	71	4.6	P06	10	1.3	
044	71	4.6	P06	15	1.3	
045	71	4.6	P11	5	1.3	
046	71	4.6	P12	5	1.3	
047	71	4.6	P12	10	1.3	
048	71	4.6	P12	10	1.3	
049	71	4.6	P12	15	1.3	
050	71	4.6	P02	5	1.3	
051	71	4.6	P04	5	1.3	
052	71	4.6	P04	5	1.3	
053	71	4.6	P04	10	1.3	
054						Failed
055	71	4.6	P12	10	1.3	
056						Failed
057	71	4.6	P12	2x10	1.3	
058	71	4.6	N/A	W/O	2.2	

Table 3-6 (continue)

Exp. No.	Surface Temp. of Tube (°C)	Concentration (g/L)	Type of Projectile	Projectile Inj. Interval (per min.)	Velocity (m/s)	Descriptions
059	71	4.6	N/A	W/O	0.8	
060	71	4.6	N/A	W/O	3.0	
061	71	4.6	N/A	W/O	1.3	
062	71	4.6	P12	10	2.2	
063	71	4.6	P12	10	3.0	Injecting air each 10 minutes
064	71	4.6	N/A	10	2.2	Taking sample
065	71	4.6	P12	10	1.3	Injecting air each 5 minutes
066	71	4.6	N/A	5	2.2	Injecting air each 10 minutes
067						Failed
068						Failed
069	71	4.6	N/A	W/O	2.2	
070	71	4.6	P12	3x10	1.3	
071	71	4.6	P12	3x10	1.3	
072	71	4.6	P12	2x15	1.3	
073	71	4.6	P12	3x15	1.3	
074	71	4.6	P12	3x15	1.3	
075	71	4.6	P12	2x20	1.3	
076	71	4.6	P12	3x20	1.3	
077	71	4.6	P12	20	1.3	
078	71	4.6	P09	10	1.3	
079	71	4.6	P09	2x10	1.3	
080	71	4.6	P09	3x10	1.3	
081	71	4.6	EX04	10	2.2	
082	71	4.6	EX04	10	3.0	
083	71	4.6	P07	5	1.3	
084	71	4.6	P09	2	1.3	
085	71	4.6	P12	2	1.3	
086	71	4.6	P02	2	1.3	
087	71	4.6	N/A	W/O	1.3	At the end of experiment C* and C** were measured
088	63	4.6	N/A	W/O	1.3	At the end of experiment C* and C** were measured
089	76	4.6	N/A	W/O	1.3	At the end of experiment C* and C** were measured
090	71	4.6	P12	5	1.3	
091	71	4.6	P12	10	2.2	
092	71	4.6	P12	5	2.2	
093	71	4.6	EX05	5	3.0	

3.6 Data Reduction

Consistency of the experimental procedure was of prime importance due to the dominant influence of initial conditions on the subsequent deposition of $CaSO_4$. The fouling process is characterized by the thermal resistance R_f of the fouling layer, which is calculated from the overall heat transfer coefficients at clean and fouling conditions as follows,

$$R_f = \frac{1}{U_f} - \frac{1}{U_c} \tag{3.1}$$

where U_f and U_c are the overall heat transfer coefficients at fouling and clean conditions, respectively. The overall heat transfer coefficient U was calculated from the following equation,

$$U = \frac{\dot{Q}}{A_i(T_s - T_{bb})} \tag{3.2}$$

where T_s is the temperature at the inner surface of the heated tube. T_{bb} is the bulk temperature in the heated section, A_i the inner surface area of the heated tube, and $\dot{Q}$ is the rate of heat transfer via the heated test tube which can be calculated from Eq. 3.3. T_s was calculated from the measured tube wall temperature by the thermocouples and the distance between their positions to the inner surface of the tube, S, by using Eq. 3.4. S is determined by the Wilson plot method (Appendix C). Here only the left side thermocouple was considered for the determination of heat transfer coefficient. The thermocouple on the right hand side (see Figure 3-7) was installed only to make sure that the fouling layer in the tube is sufficiently uniform. The relevant temperatures with respect to the fouling layer and the heated tube are shown in Figure 3-20.

$$\dot{Q} = \dot{m} c_p (T_o - T_i) \tag{3.3}$$

$$T_s = T_w - \frac{\dot{Q} ln(\frac{r+S}{r})}{2\pi L \lambda} \tag{3.4}$$

In Eq. 3.3 $\dot{m}$ is the mass flow rate, c_P is the specific heat capacity of the fluid and T_o and T_i are the outlet and inlet temperatures of the flow from and to the heated section, respectively. T_{bb} was obtained by averaging the two bulk thermocouple readings, T_o and T_i. In Eq. 3.4, r is the inner diameter of the tube, L the overall length of the heated section and λ is the thermal conductivity of the tube. T_w was measured by the thermocouples. The

temperature at the inner surface of the fouling layer $T_{FL,i}$, i.e. near the fluid, is determined from,

$$T_{FL,i} = T_{FL,o} - \dot{q}R_f \tag{3.5}$$

where $T_{FL,o}$ is the temperatures of the outer surface of the fouling layer, i.e. at the heated tube, which is equal to T_s. $\dot{q}$ is the heat flux calculated from,

$$\dot{q} = \frac{\dot{Q}}{A_i} \tag{3.6}$$

After each experiment where deposition has taken place, the heated tube was disassembled from the test rig and analyzed. Photographs of the inner surface were taken in order to see the fouling layer in the heated section. The photographs would help to discern the texture and coverage of the deposit layer. Thereafter, the tube was chemically cleaned before using it for the next experiment. The washing chemicals were inert such that they did not react with the surface of the tube. The repeatability of the performed experiments has been checked by repeating several experiments. It has been found from the performed tests that the repeatability of the performed experiments varies between 75 – 95% (definition the percentage of the repeatability is discussed in section 4.3.1.1).

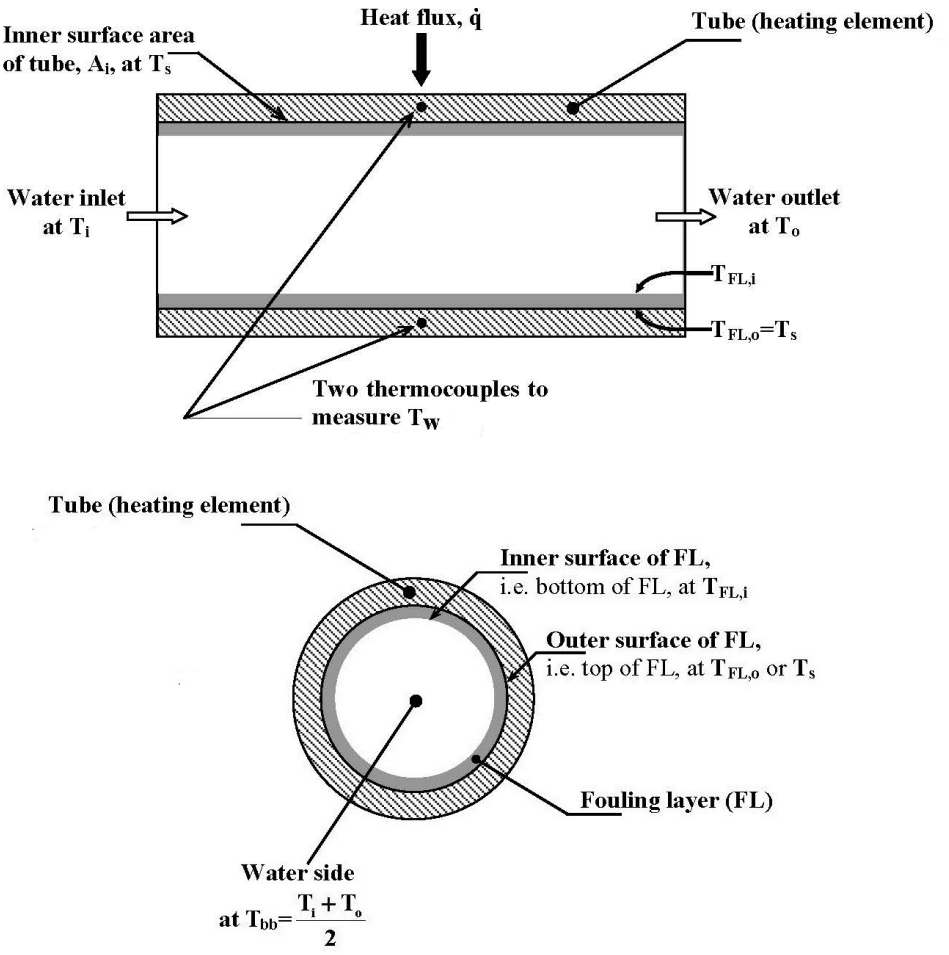

Figure 3-20 Fouling layer position with respect to the heating element and the solution side

3.7 Probing of the Heterogeneous Deposit Layer

Not only the measurement of fouling resistance would determine how effective the projectiles were at any specified injection interval but the fouled surface was also examined after each run to see how the deposit was developed. After each experiment, the inside of the tube was fully scanned by an endoscope camera and a sketch of the area covered by deposit was prepared. Furthermore the circumferential orientation of deposit was detected. Such information was useful, as will be exemplified later, to explain discrepancies and contradictions in the reported results.

3.8 Experimental Uncertainty and Error Analysis

Experimental errors consist of bias and precision errors, which determine the uncertainty in the measured quantity. The knowledge of the uncertainty in a single experiment is important as it helps in evaluating the results. The uncertainty C is related to the bias error B and the precision error P for a 95% confidence by (Al-Janabi et al. 2009 and Figliola et al. 1991),

$$C = \sqrt{\left[B^2 + P^2\right]} \tag{3.7}$$

The thermal resistance R and the resulting bias error B_R are calculated from,

$$R = \frac{T_s - T_b}{q_b} = \frac{\Delta T}{q} \tag{3.8}$$

$$\left(\frac{B_R}{R}\right)^2 = \left(\frac{B_q}{q}\right)^2 + \left(\frac{B_{T_s}}{\Delta T}\right)^2 + \left(\frac{B_{Tb}}{\Delta T}\right)^2 \tag{3.9}$$

respectively. B_q, B_{Ts} and B_{Tb} are the bias error of the heat flux q, surface temperature T_s and the bulk temperature T_b, respectively. The precision error P_R of the measured thermal resistance R is calculated from the standard deviation of a set of n observations as follows,

$$P_R = \sqrt{\left(\frac{\sum_{i=1}^{n}\left(R - \overline{R}\right)^2}{n(n-1)}\right)} \tag{3.10}$$

where $\overline{R}$ is the average thermal resistance of the n observations. For example, based on experiment #022, the uncertainty at the beginning and at the end of the experiment is determined. This experiment was chosen because it did not have projectile injection and it demonstrates a typical fouling process. The precision error is calculated based on 20 readings, i.e. n=20.

Given Eq. 3.8 - Eq. 3.11, it is obvious that the highest uncertainty occurs at the beginning of the experiment because the temperature differences are smaller. In Table 3-7 the calculated values are presented. Uncertainty for the heat transfer coefficient changes from 2.73% at the beginning to 2.49% at the end of the experiment while for fouling resistance the uncertainty is 2.08% at the end of the experiment. Uncertainty of R_f is given

only at the end, because R_f is defined as zero at the beginning, hence its uncertainty would be zero.

Table 3-7 Calculated uncertainties for various variables

	Bias error B		Precision error P		Uncertainty C	
	Start	End	Start	End	Start	End
Heat flux $\dot{q}$ [W/m²]	± 2%	± 2%				
Surface temp. T_S [K]	± 0.4	± 0.4				
Bulk temp. T_b [K]	± 0.4	± 0.4				
Heat trans. Coeff. α [W/m²·K]	101.3	22.5	72.15	17.37	2.73	2.49
Fouling resistance R_f [m²K/W]		4.573E-06		1.324E-05		2.071

4 EXPERIMENTAL RESULTS AND DISCUSSION

A total of 6 clean and 93 fouling runs were performed for forced convective heat transfer to investigate the performance of various projectiles during the precipitation of $CaSO_4$ deposits. The accumulation of deposits on the surface has continuously been monitored by measuring the variation of surface temperature with time. Both fouling rate and induction time were used to evaluate the effect of various projectiles on fouling mitigation. For doing so the variation of fouling resistance, R_f, as a function of time with and without injection of projectiles was investigated.

4.1 Heat Transfer at Non-Fouling Condition

4.1.1 Effect of velocity on surface temperature

A series of experiments was performed to determine the surface temperature of the tube as a function of fluid velocity and furnace temperature. Such experiments with demineralized water were imperative in order to obtain the surface temperature from which the fouling resistance could subsequently be determined. Figure 4-1 shows that the surface temperature is profoundly influenced by the fluid velocity. Because the heat transfer coefficient is a function of the Reynolds number, it increases when the velocity is increased. Hence the surface temperature decreases with increasing flow velocity for constant furnace temperature. For constant flow velocity, the surface temperature increases with increasing furnace temperature.

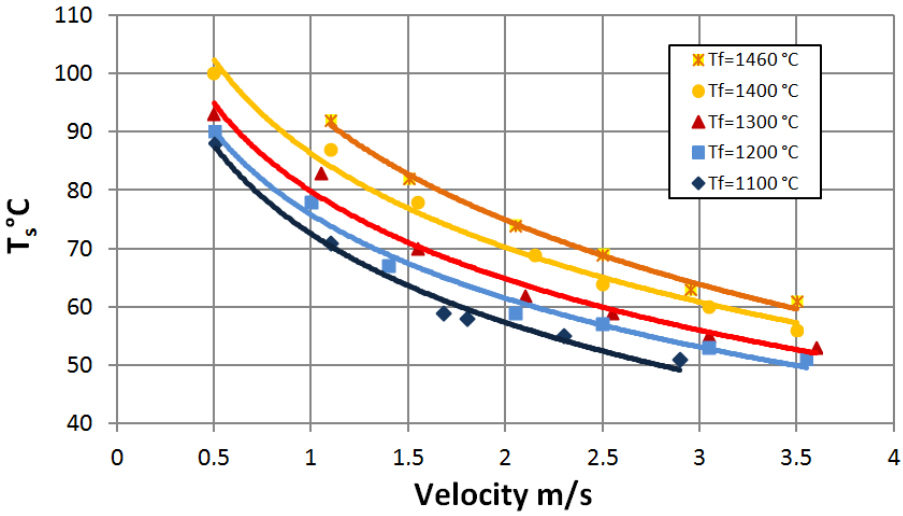

Figure 4-1 Surface temperature vs. velocity for different furnace temperatures and the bulk temperature of 40°C

4.1.2 Effect of projectile movement on surface temperature and heat transfer rate

The hydrodynamic boundary layer is momentarily agitated when the projectile passes through the tube. It is, therefore, always likely that the surface temperature and the heat flux will change even at clean conditions. Furthermore, the furnace temperature was usually higher than 1000°C, so if projectile injection produces high fluctuations it may be possible that an elevated thermal stress may deform the tube. Apart from that, it may cause a non-uniform surface temperature which is very important in this investigation. Figure 4-2 shows the effect of projectile injection on the surface temperature for projectile P01 which was quite soft and spongy. The projectile has a nominal diameter of 21 mm which is 5% larger than the tube inner diameter. The data were recorded every 0.5 s. It was first examined for clean conditions to discern if there is any improvement in heat transfer when the projectile agitates the boundary layer. The heat flux at different injections intervals i.e. 1 inj./min and 2 inj./min was investigated. The furnace and bulk temperatures were 1240°C and 40°C respectively. It turned out that fluctuations of the surface temperature did not exceed ±2 K for a fluid velocity of 0.8 m/s which was the minimum velocity required for the propulsion of projectiles in this investigation. Heat transfer coefficient and heat flow rate were calculated and the results are shown in Table 4-1. To define U_c and $\dot{Q}$, Eq. 3.2 and Eq. 3.3 were used. U_c and $\dot{Q}$ were calculated from recorded data ($\dot{m}$, T_i and T_o) every 0.5 s during a 20 minute period, then their average was reported. Table 4-1 confirms that the clean heat transfer coefficient does not change significantly when P01 is injected. In Table 4-1, the measured U_c without projectile has been compared with the predictions of some correlations i.e. Dittus-Boelter, Sieder-Tate and Gnielinski correlation (Incropera, 2006). However as shown in Figure 4-2, injections impact the surface temperature by ±2 K but their effect on the heat flux is less than what could be measured. An underestimation error of 27% with the Sieder-Tate correlation and 38% with the Dittus-Boelter equation was observed. This error for Gnielinski correlation was 24% overestimation. To calculate the friction factor in the Gnielinski correlation the equation of Colebrook was used.

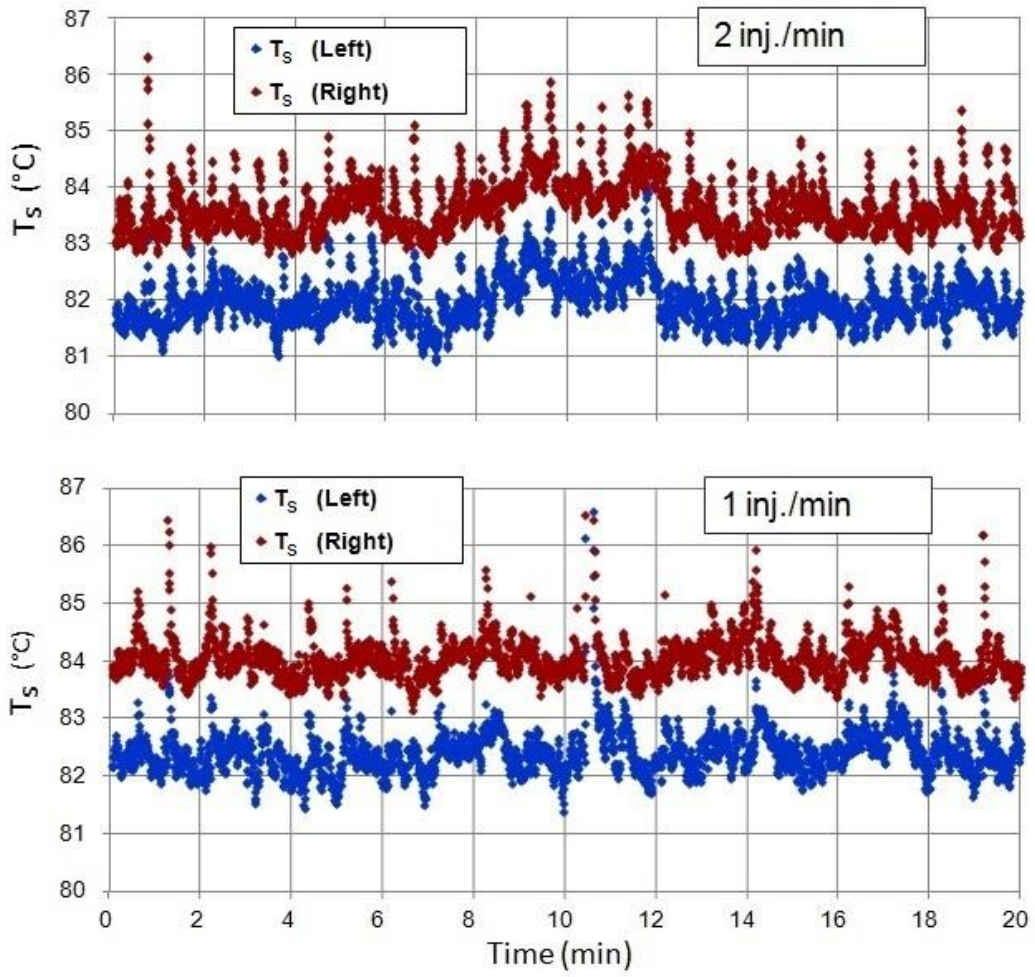

Figure 4-2 Effect of projectile P01 on surface temperature of the tube in the two positions where thermocouples are located Bulk temperature 40°C, flow velocity 0.8 m/s, furnace temperature 1240°C

Table 4-1 Variation of clean heat transfer coefficient and heat flow rate for different injection intervals of P01 Bulk temperature 40°C, furnace temperature 1240°C

	v (av.) (m/s)	U_c Sieder-Tate correlation (W/m²·K)	U_c Dittus-Boelter correlation (W/m²·K)	U_c Gnielinski correlation (W/m²·K)	Uc (av.) Measured (W/m²·K)	$\dot{Q}$ (av.) (W)
W/O projectile	0.815	5707	4870	9803	7873	3621.8
1 inj./min	0.814	-	-		7969	3642.5
2 inj./min	0.826	-	-		8051	3624.7

Figure 4-3 shows the impact of injection on the inlet and outlet temperatures. The inlet bulk temperature was set to 40°C and injection intervals were every 1 and 2 minutes at

clean conditions. Two types of fluctuations could be observed. The long term variations are due to the cooling control system which tries to maintain the bulk temperature at a set point. They were also observed without injections. The sharp fluctuations are due to the injections. These sharp fluctuations owing to the inlet and outlet temperature are clean-cut and could be discerned easier than fluctuations in the surface temperature. The reason for these sharp fluctuations is that the projectile before injection is located in a pipe outside of the normal circulation path. The stationary liquid inside this pipe is not circulated to the supply tank and hence is not cooled to the set point bulk temperature by the cooling coil. This volume of the flow in the pipe was hotter than that in the circulating flow. Injecting a projectile causes the hotter flow to enter into the cycle and causes a peak of about +1 K in the measured inlet and outlet temperature as well as in the surface temperature (see Figure 4-2). For an insulated system the maximum temperature of the stationary liquid would be equal to the outlet temperature due to the last injection and depend on the velocity, e.g. 43.5°C for low velocity v=0.8 m/s. But the pipe was not insulated on purpose to cool down to ambient temperature until the next injection takes place. It was tried in the design of the test rig to reduce the length of this part to a minimum of 400 mm, and a volume of 246 cm^3 (diameter of tube was 28 mm). The recorded peak due to this stationary liquid was maximum +1°C for low velocities around 0.8 m/s.

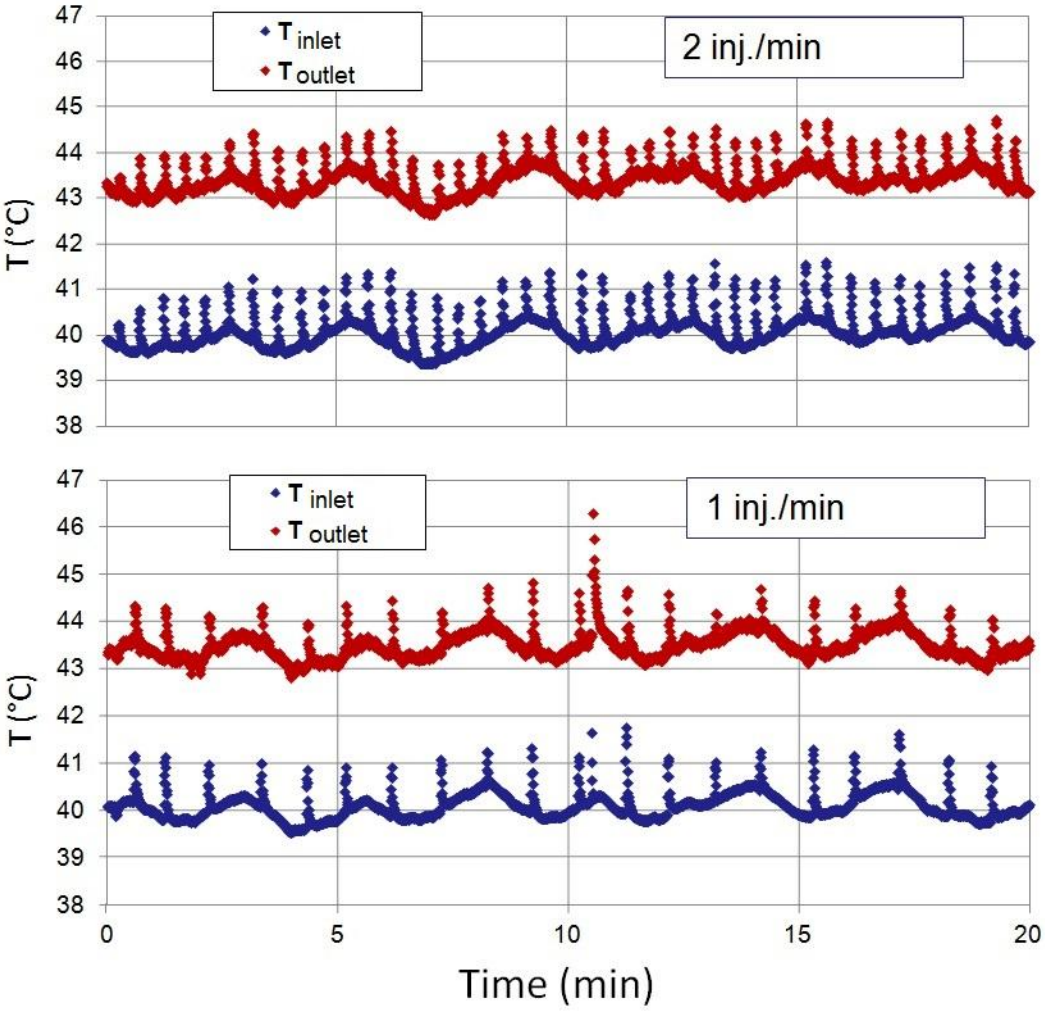

Figure 4-3 Effect of projectile P01 on the inlet and outlet temperatures
The bulk temperature 40°C, flow velocity 0.8 m/s, furnace temperature 1240°C

4.2 Fouling Runs without Projectiles

4.2.1 Fouling curves for different velocities

Fouling experiments were initially performed without injecting projectiles under different operating conditions to discern if the resulting findings were consistent with previous investigations. The results can also be used to assess the performance of projectiles under similar operating conditions. Figure 4-4 shows the variation of the fouling resistance for two velocities of 0.8 and 2.2 m/s. The bulk temperature is 40°C, surface temperature and concentration are 80°C and 3.8 g/L. As stated before, in this investigation the tube diameter and the flow velocities are comparable with of those in industry. As it can be seen for a higher velocity of 2.2 m/s, the rate of fouling is slower. Sudden and sharp drops of fouling resistance can be explained by the flow shear that can remove parts of the fouling layer. Contrariwise, increase in fouling resistance is more difficult to explain, but

may be due to incidental deposition of crystals on spots where the wall thermocouples were embedded. Both occurrences can evidently be seen in this figure. However filter was used in the system, but this means detached particles can settle on the surface before they exit from the heated section and could be caught by the filter.

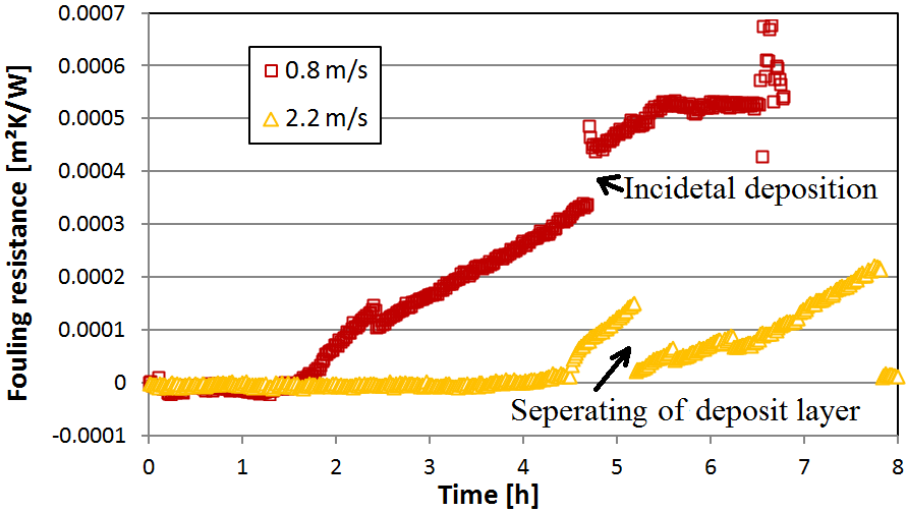

Figure 4-4 Fouling resistance vs. time for different velocities without injecting projectiles Bulk temperature 40°C, surface temperature 80°C and concentration 3.8 g/L

4.2.2 Fouling curve for different concentrations

Figure 4-5 shows the variation of fouling resistance vs. time for different concentrations of $CaSO_4$. The bulk temperature is 40°C the flow velocity and surface temperature are 0.8 m/s and 80°C. At a concentration of 5.0 g/L, fouling was so severe that the test had to be terminated after only approximately 0.5 hr to avoid tube burn-out. With this concentration, no induction time was observed and the fouling rate was high. The runs with concentrations of 3.5 g/L show no fouling during the time exposure of 7 hrs. At a concentration of 4.0 g/L, the fouling resistance starts to rise after one hour of induction time.

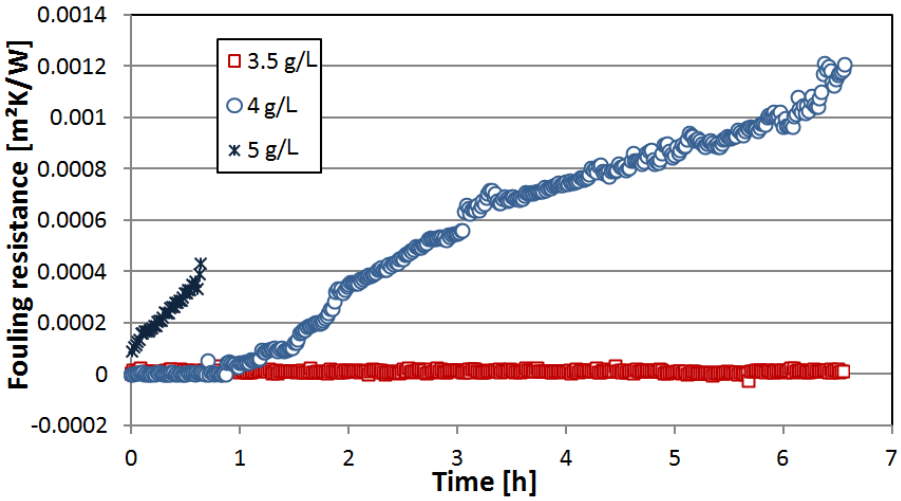

Figure 4-5 Fouling resistance for different concentrations without injecting projectiles Bulk temperature 40°C, flow velocity 0.8 m/s, surface temperature 80°C

4.3 Fouling Runs with Projectile Injection

4.3.1 Impact of projectile injection on cleaning

4.3.1.1 Effect of injection intervals

The first investigated projectile for fouling mitigation was P01. It consisted of spongy material and was quite soft. Each projectile had a nominal diameter of 21 mm. The injection intervals were every 2, 5 and 30 minutes. Figure 4-6 presents the fouling resistance without and with injection as a function of time. The bulk temperature is 40°C. Even though smaller injection intervals provided better efficiency, the tube cannot be kept entirely free from deposit even with an interval of only two minutes. In this case, the fouling resistance is reduced to about one third of the value without injection. The curves are close together and injection intervals do not have a significant effect. Since the projectile is very soft, for all cases only little removal of the deposit layer has occurred.

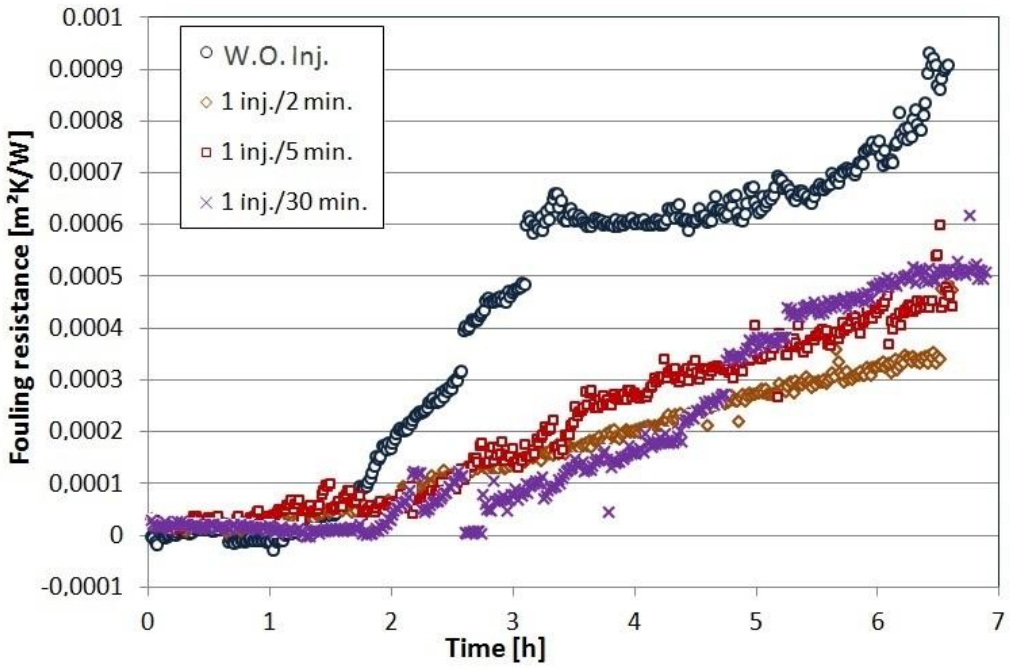

Figure 4-6 Fouling curves for projectile P01 with different injection intervals
Bulk temperature 40°C, flow velocity 0.8 m/s, surface temperature 80°C, concentration 3.8 g/L

For projectile P02, the injection intervals are one injection every 2, 5, 10, 15 and 30 minutes. The fouling resistances are shown in Figure 4-7. Up to an interval of 1 inj./10 min the fouling resistance remains below 0.0002 m²K/W during the run. For less frequent injections, fouling can only be mitigated a few times, but after that, the fouling layer starts to grow. Surprisingly, the efficiency of fouling mitigation is better with one injection every 30 min when compared to one every 15 min. Experiments with longer injection intervals e.g. every 15 and 30 min had poor repeatability. Hence for long intervals the effect of cleaning by projectiles diminishes and other mechanisms take over to make the results more unpredictable. Figure 4-7 indicates that 1 inj./10 min would be an optimum interval to keep the tube at an acceptable level of cleanliness, about one fifth of that without injection. Considering that injection decreases the fouling resistance substantially, the size of the heat exchanger would also be smaller for the construction, because the heat exchanger is designed based on a higher overall heat transfer coefficient (See also Appendix A). This series of experiment proved that induction time (the time before the fouling resistance starts to rise substantially) is shorter with injection. This will be explained in section 4.4 in detail.

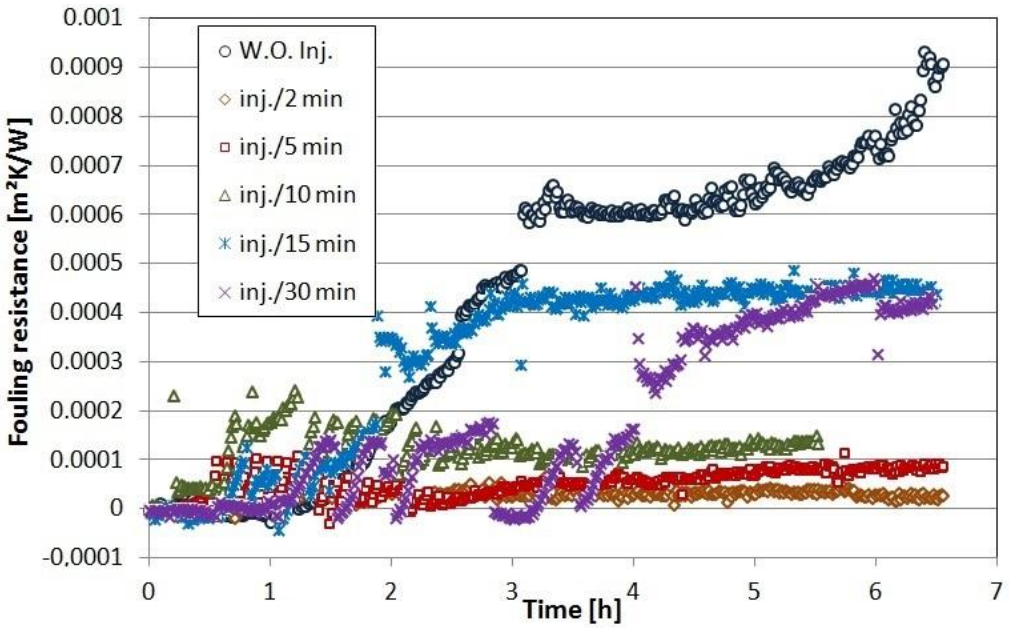

Figure 4-7 Effect of P02 on cleaning with different injection intervals
Bulk temperature 40°C, flow velocity 0.8 m/s, surface temperature 80°C, concentration 3.8 g/L

The repeatability of the performed experiments has been checked by repeating them in random manner especially for dubious results. Repeatability above 75% is quite acceptable for experiments of such nature. Figure 4-8 is an example for the repeatability of P02 with injection in 2 minute intervals. As indicated in this figure, the data are more reproducible at the early stage of the experiment while at the end large variation becomes obvious. The biggest difference was observed for the asymptotic period (0.00005 m^2K/W for the first experiment and 0.00009 m^2K/W for the second experiment). Compared to the maximum reported fouling resistance in this series of experiments (0.0009 m^2K/W), a repeatability of 95% for P02 is considered.

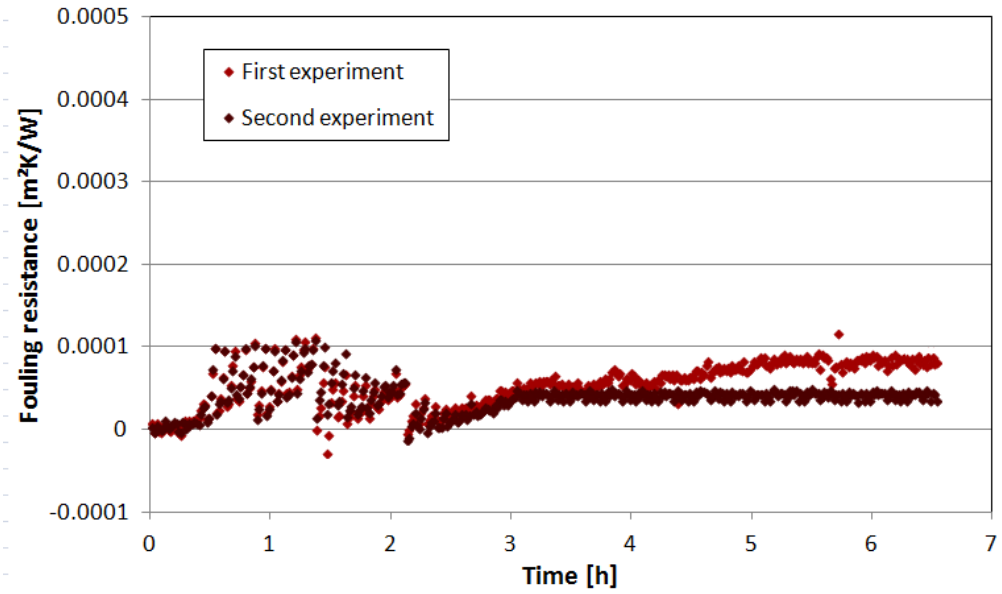

Figure 4-8 Repeatability test for P02 with injection interval of 5 min
Bulk temperature 40°C, flow velocity 0.8 m/s, surface temperature 80°C, concentration 3.8 g/L

4.3.1.2 Effect of projectile type

In addition to the comparison of projectile performance at different injection intervals, the effectiveness of various projectiles has also been investigated. Figure 4-9 presents similar results for the same operating conditions but for four different projectiles. The bulk temperature was 40°C, velocity, surface temperature and concentration were 0.8 m/s, 80°C and 3.8 g/L respectively. The injection interval was each 5 minutes. P01 and P02 were spherical sponge-type projectiles with a diameter bigger than that of the tube; hence they could be deformed and then pass easily. P02 was harder and bigger than P01 (see Table 3-2). The results show that P02 plays a better role in keeping the surface clean than P01. EX06 and P04 were rubber type projectiles and stiffer than P01 and P02. Their sizes fit loosely into the tube; with a clearance of just 0.1 mm. A loose projectile means that it does not have any firm contact with the tube. The surface of EX06 was ribbed and that of P04 was smooth. As it can be seen, both did not have any impact on cleaning the surface. Instead, they even worsened fouling for the last 3.5 hrs when compared with the curve for no-injection. It seems that crystal nucleation is accelerated when P04 and Ex04 were used. This excitement could be due to either scratch on the surface by the projectile or air bubbles that could not be fully avoided to enter into the system when the projectile is injected. In sections 4.4.4 and 5.31 this point will be discussed in detail. Overall, the soft sponge balls perform much better than the hard rubber projectiles.

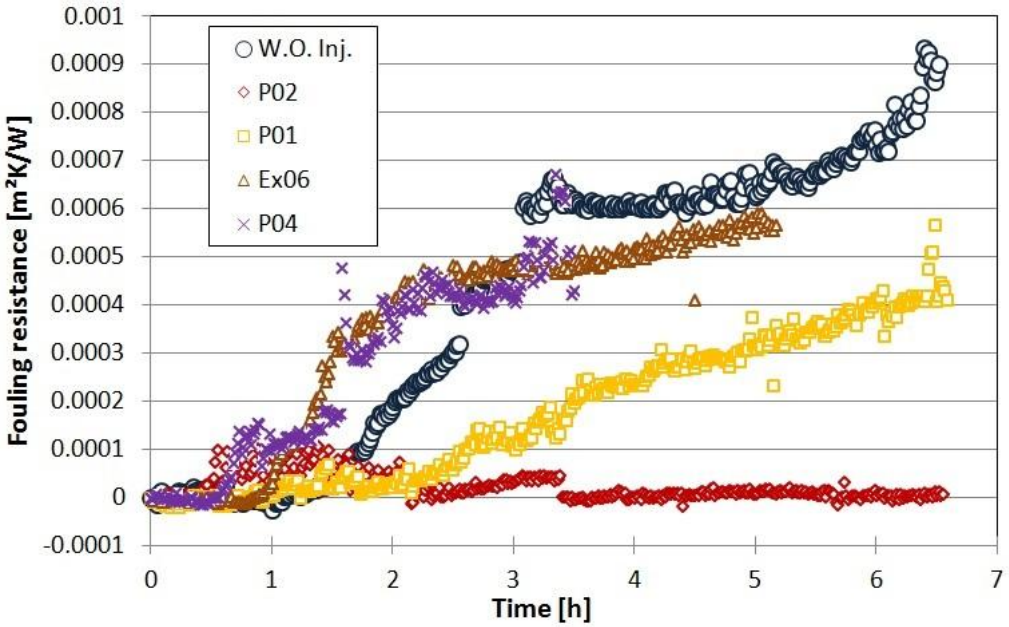

Figure 4-9 Comparison of various projectiles on cleaning for the same injection interval of 5 min Bulk temperature 40°C, flow velocity 0.8 m/s, surface temperature 80°C, concentration 3.8 g/L

Figure 4-10 compares the performance of several other projectiles, again for an injection interval of 5 min. The bulk temperature is 40°C and the velocity, surface temperature and concentration were 1.3 m/s, 71°C and 4.6 g/L respectively. For the investigated projectiles, the cleaning performance of P06 is the best, followed by P12. P12 is a hard projectile but P06 is soft. P12 exerts much more shear on the tube than P06 but the cleaning results for P06 are better than for P12. This means that other parameters, like contact area of projectile, may have an impact on the cleaning efficiency as well. This will be explained in more details in the following sections. The diameter of P11 matches exactly the tube inner diameter. Thus a poor performance is expected as can be seen in this figure, because of poor contact between the surface and the projectile. The results show that P11 even facilitates fouling such that for the first 4 hrs the fouling resistance is even higher than that of no injection. It seems that despite the poor contact, nucleation excitement is unavoidable. P04 fits loosely into the tube with a clearance of 0.1 mm and performs worse than P11. One important conclusion from this figure is that the magnitude of exerted shear force is decisive for an efficient cleaning. Nevertheless, if the projectile produces significant shear but the contact area is not enough, then it may compact the deposit further and instead enhance fouling. There is a sudden drop in fouling resistance for P12 after about 2.75 hrs. Such drops would be common for hard projectiles because they have the potency of sticking which may produce a thermal shock. A short time sticking produces a short time overheating, so the different thermal expansion between the tube and the deposit layers may cause the deposit layers to crack and be separated from the surface. After every short time sticking, many deposit particles were observed in transparent section.

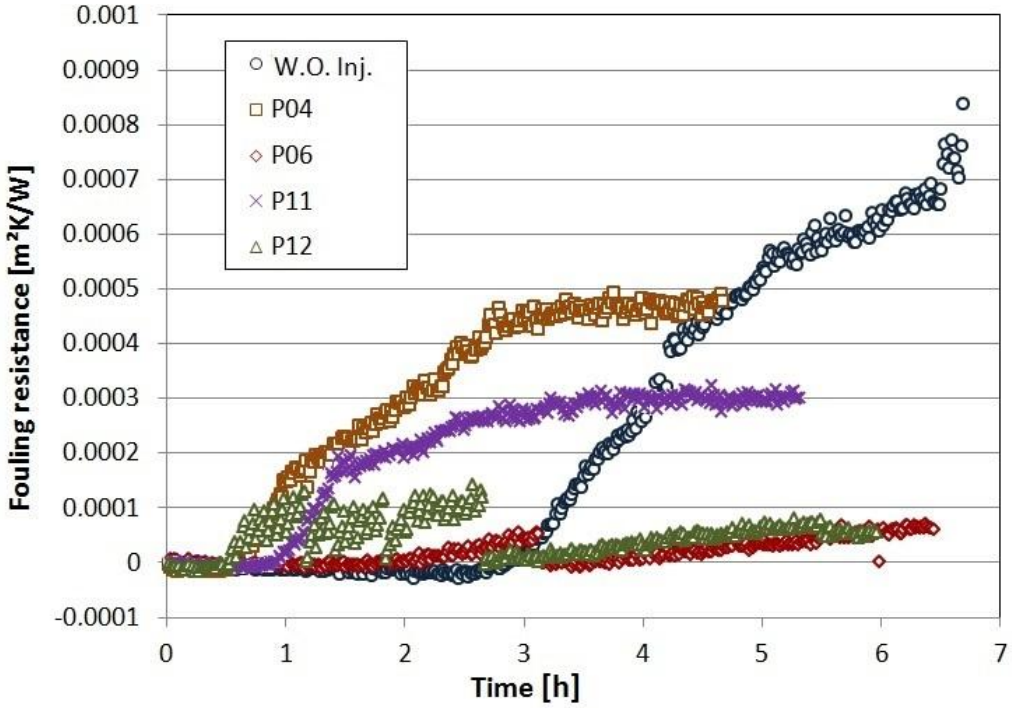

Figure 4-10 Comparison of various projectiles on cleaning for the same injection interval Bulk temperature 40°C, flow velocity 1.3 m/s, surface temperature 71°C, concentration 4.6 g/L, injection interval of 5 minutes)

Figure 4-11 and Figure 4-12 show the performance of loose projectiles, P04 and P11 individually, with different injection intervals. The diameters of P04 and P11 are 19.8 mm and 20.0 mm. Like the previous runs, the bulk temperature was 40°C and velocity, surface temperature and concentration were 1.3 m/s, 71°C and 4.6 g/L. Injection intervals were 5 and 10 minutes. Not only the projectiles did not clean the tube, but also they accelerated the deposit formation in the first hours. It seems that nucleation accelerates the crystallization for P04 and P11. This could be due to either scratch on the surface or air bubbles that will be investigated in sections 4.4.4 and 5.31. It was also observed for an injection interval of 10 min, that projectiles got stuck when they encountered the deposit in the tube. Sticking is obviously an important problem in projectile system processes.

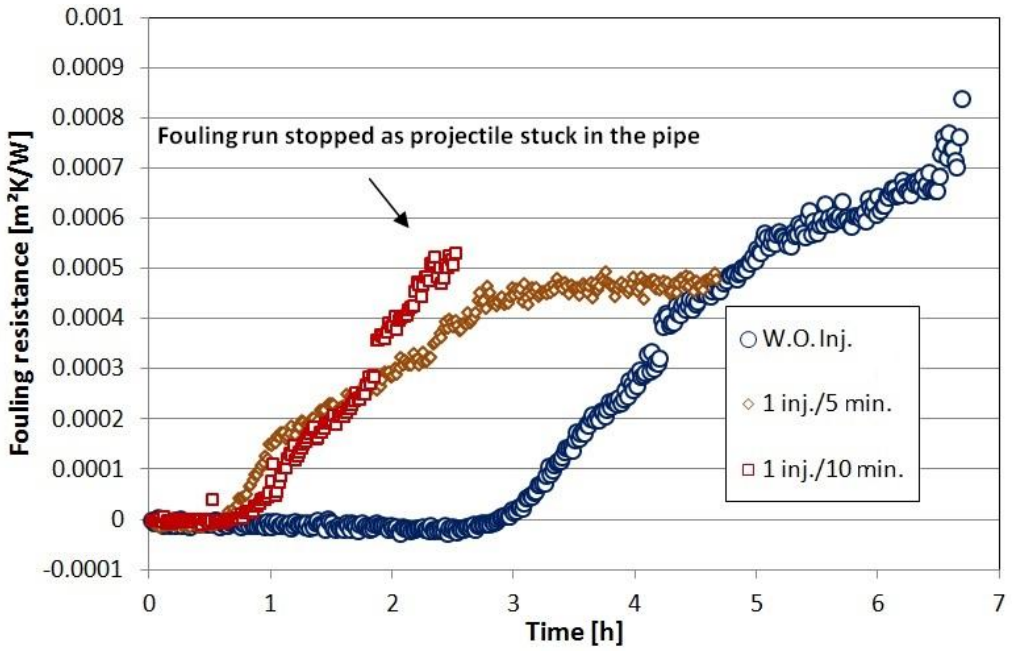

Figure 4-11 Impact of P04 on fouling resistance for different injection intervals
Bulk temperature 40°C, flow velocity 1.3 m/s, surface temperature 71°C, concentration 4.6 g/L

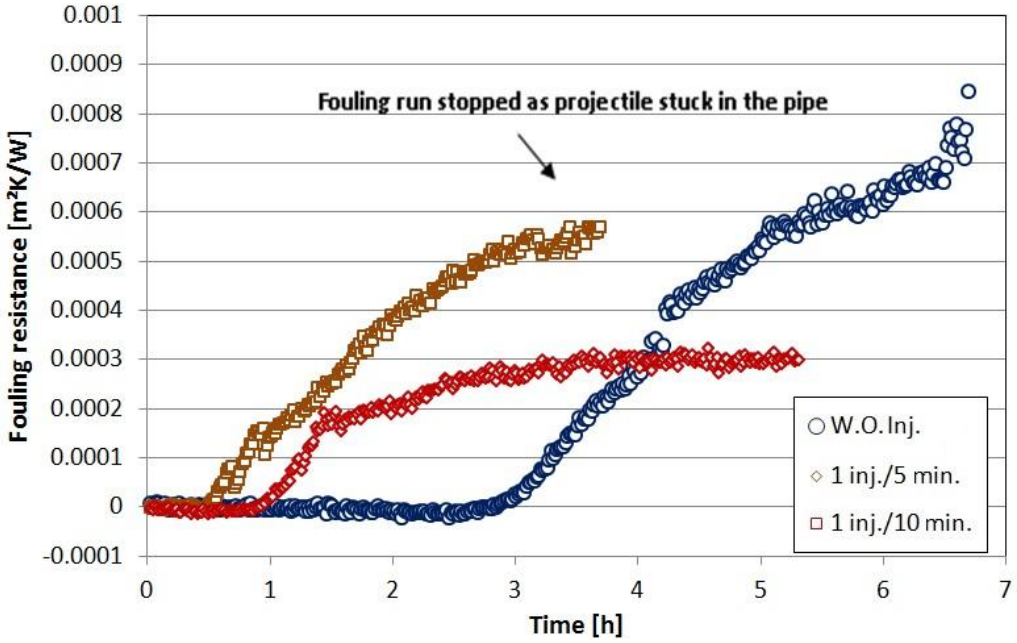

Figure 4-12 Impact of P11 on fouling resistance for different injection intervals
Bulk temperature 40°C, flow velocity 1.3 m/s, surface temperature 71°C, concentration 4.6 g/L

4.3.1.3 Performance of hard projectiles

Figure 4-13 indicates that for the hard projectiles, sometimes long injection intervals have negative consequences on cleaning. For these experiments, the bulk temperature was 40°C and velocity, surface temperature and concentration were 1.3 m/s, 71°C, 4.6 g/L. Injections were every 5, 10 and 15 min and there was a run without injection. For example, an injection interval of 5 minutes provides a relatively good cleaning performance, while for 10 and 15 minutes the results are totally different and indicate even worse deposit formation. It means that long intervals such as 10 or 15 minutes are insufficient for cleaning because the presence of air bubbles from the injections and maybe the deposit residues left on the surface after the previous injection intensify nucleation and hence deposit growth. These phenomena will be explained in the next sections in detail.

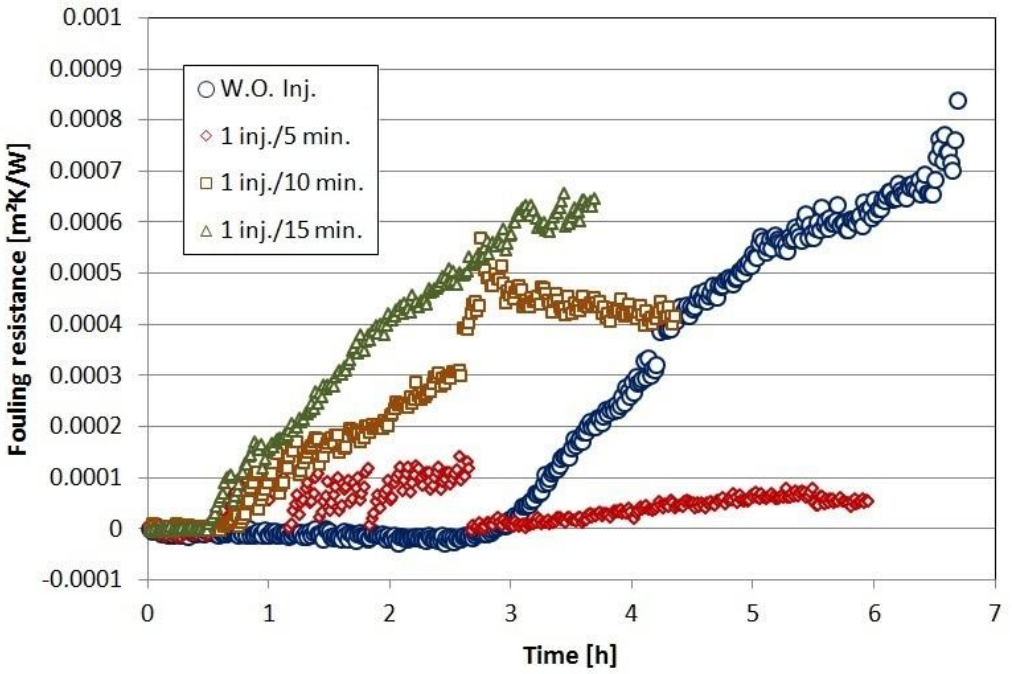

Figure 4-13 Effect of P12 on cleaning for different injection intervals
The bulk temperature 40°C, flow velocity 1.3 m/s, surface temperature 71°C, concentration 4.6 g/L

4.3.1.4 Effect of extra-large and soft projectiles

An experiment was performed with projectile P05, which is hollow with a diameter of 24.0 mm (20% bigger than the inner diameter of the tube). The operating conditions for this experiment are listed in Table 4-2:

Table 4-2 Operating conditions for experiment No. 039

Parameters	Range
Bulk temperature	40 °C
Velocity	0.8 m/s
Surface temperature	80°C
Concentration of $CaSo_4$	4.6 g/L
Inside diameter of tube	20.0 mm
Length of heated section	28 cm
Projectile interval	1 inj./5 min
Diameter of projectile	24 mm
Temperature of furnace	1200°C
Type of Projectile	P05

This projectile had the biggest diameter which has been investigated in this study. Insertion of the projectile in the tube was difficult, but it passed very well even with a small flow rate of 0.8 m/s. Without heating the tube, this was checked several times to make sure that the projectile would not get stuck anywhere in the rig. For the fouling run, the concentration of $CaSO_4$ was 4.6 g/L. Figure 4-14 presents the resulting fouling resistances as a function of time for an injection interval of 5 min. The deposit formation started just after 20 minutes into the induction time. The deposit process was fast enough to reach a fouling resistance of 0.0001 m^2K/W just in 5 minutes. Nonetheless each injection was successful to clean the tube to near zero fouling resistance again. It seemed that injections were very effective to produce a high shear force for removing a large amount of deposit from the tube.

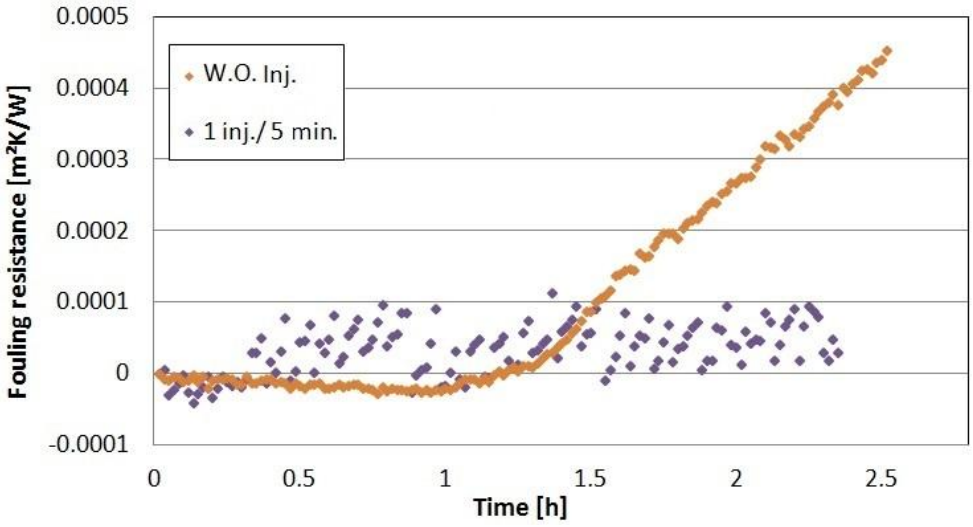

Figure 4-14 Effect of mitigation in each 5 minutes interval
Bulk temperature 40°C, flow velocity 0.8 m/s, surface temperature 80°C, concentration 4.6 g/L, Projectile P05

The experiment did not last for a long time, since after 2 hours and 15 minutes the velocity started to fluctuate during the injection, as shown in Figure 4-15. Possibly, the inner surface of the tube was not smooth any more due to some deposit. This secondary

roughness produced a strong friction between the tube and the projectile, to the extent that the projectile got stuck inside the tube. The temporary sticking, in turn, disturbed the flow control system and caused fluctuation. The projectile stuck in the tube twice. The first sticking lasted about 30 seconds before the projectile released itself. The second sticking lasted for more than 2 minutes; then again the projectile was released when the flow rate was momentarily increased. Thereafter, the experiment was terminated. During these two minutes blockage the temperature of tube reached 850°C (see Figure 4-15) and thus the tube was deformed. When the door of the furnace was opened, it was found that the outer surface of the tube had turned black where the projectile got stuck. Figure 4-16 shows the place where the projectile had been stuck. Figure 4-17 shows the location of deformation.

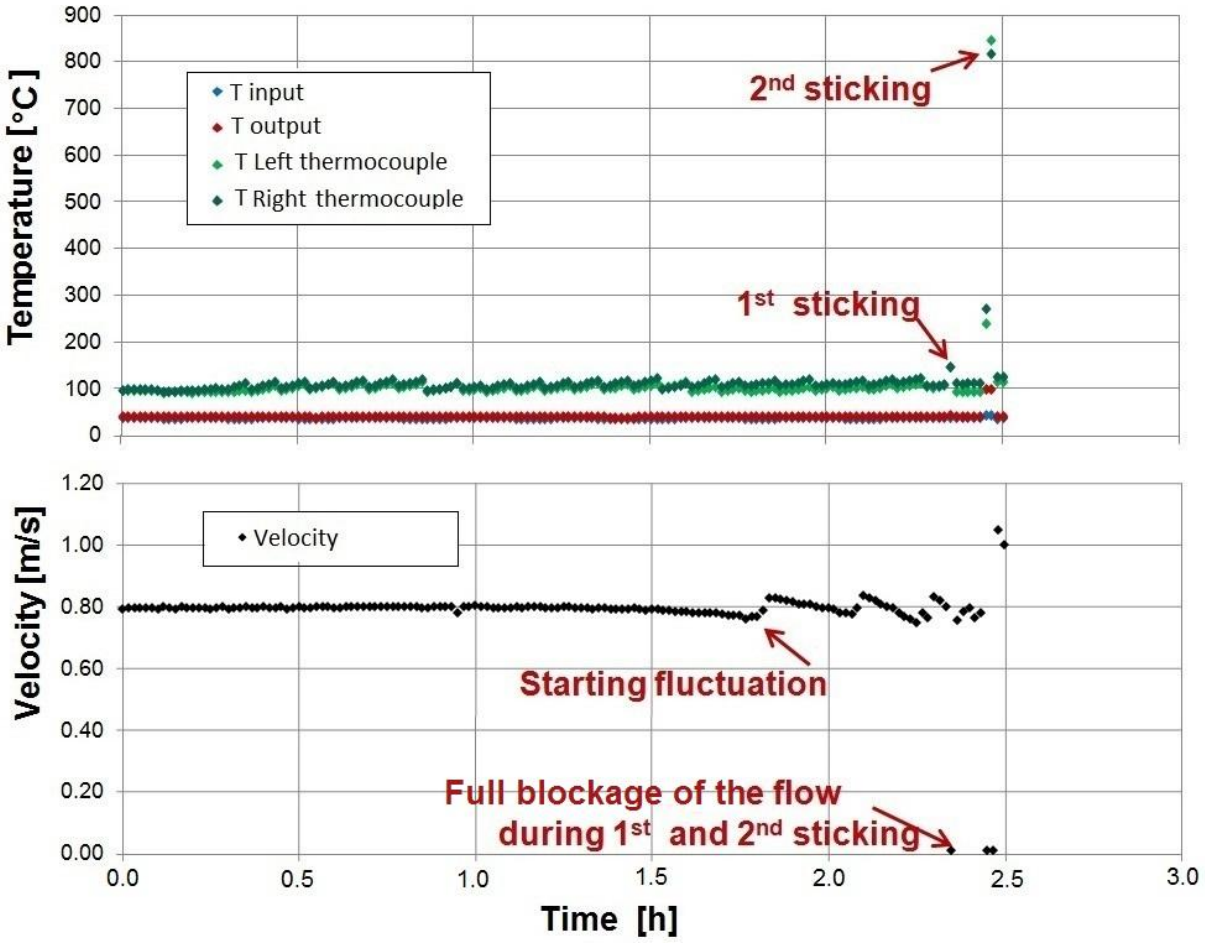

Figure 4-15 Variation of operating conditions that led to the shutdown of the rig when P05 got stuck in the tube

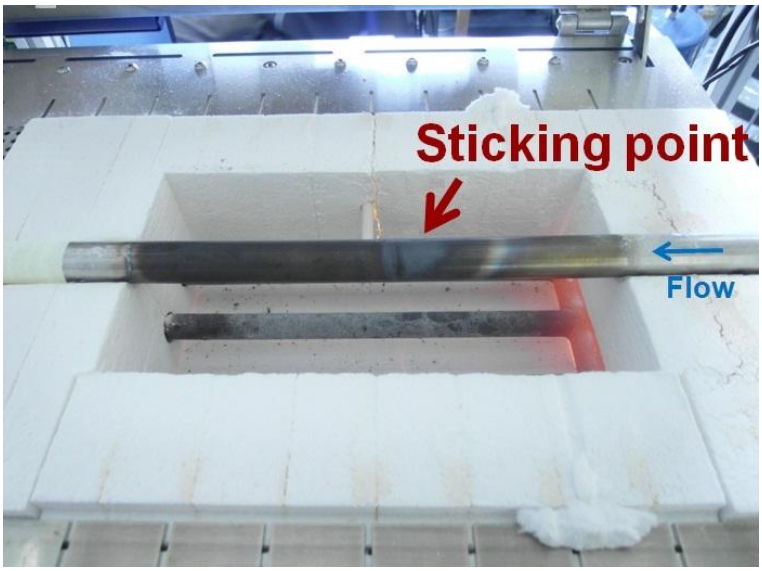

Figure 4-16 The location where the projectile got stuck and the tube turned black

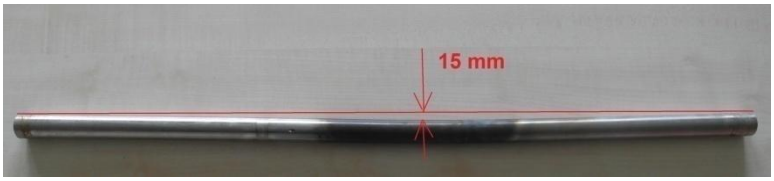

Figure 4-17 The 15mm tube deformation in middle of the heated section

This experiment shows that a large but soft projectile may also have a short lifetime. To avoid that the projectile gets stuck requires a balance between size and softness. A large projectile should be soft enough to pass through the tube, although it cannot last for more than an expected time due to the large deformation. In other words it would be extremely under stress and would be damaged. Thus projectiles are divided into two groups, i.e. those which get stuck in the tube and those with short lifetime. It seems very large projectiles that can pass through the tube are defined as very soft with a short lifetime, even though they can clean acceptably. As it can be seen in Figure 4-18, it seems that projectile was strongly under stress during the just 28 injections.

Figure 4-18 Torn P05 projectile after being stuck and released

4.3.2 Compaction phenomenon

During the experiments with EX06 and P04 some rises were noted in tube wall temperature, immediately after each injection. Figure 4-19 shows these sudden rises of temperature on the left and right sides. Black arrows indicate when the projectile injection takes place and the red arrows show the rising of temperature. These results indicate that these projectiles did not improve cleaning but instead the fouling resistance increased after several injections. When the tube was opened and scanned, the texture of the deposit was very hard and glassy. This implied that the compacted deposit was sintered at high temperature of more than 85°C (for more information about sintering see section 4.3.4). As the projectile was hard, it pressed the deposit onto the surface. Thus, if the deposit was porous before injection it then gets compact and sintered after injection. The compacted layer would have a higher thermal resistance against heat transfer, because the molecular density of the deposit is higher and while the layer gets thinner the flow cannot pass through the porous layer anymore and eventually loses contact with the surface of tube. Figure 4-20(a) shows projectile EX06 which has a 0.1 mm clearance to the tube. The experiment shows that this clearance of hard projectiles intensifies compaction. This phenomenon was confirmed again for a hard projectile with a diameter exactly the inner diameter of the tube (P11). Figure 4-20(b) shows schematically how the injection may turn a porous deposit in to a highly compacted one.

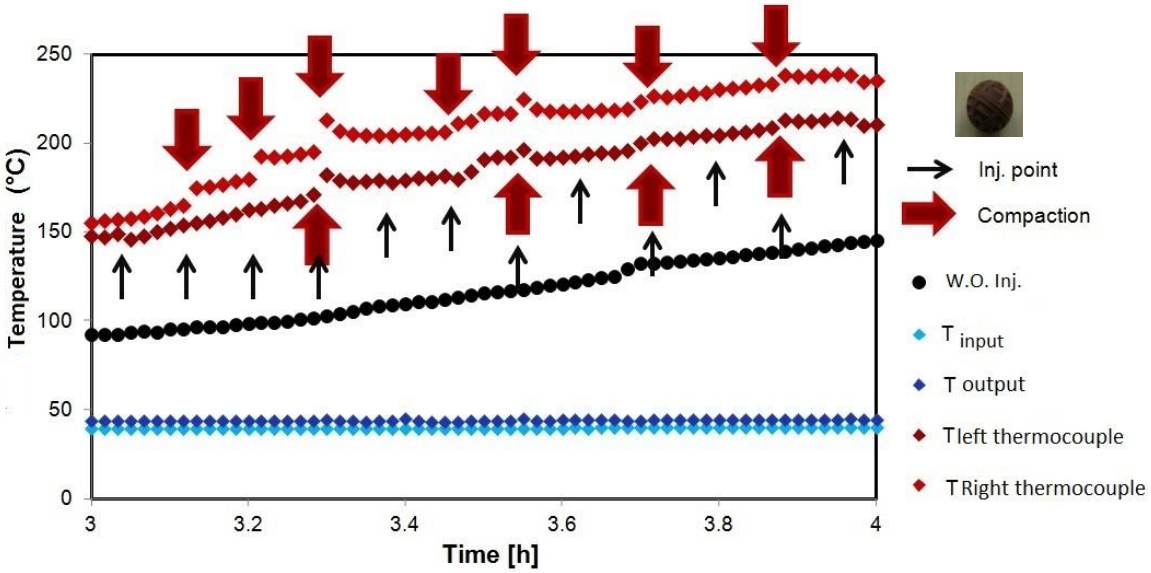

Figure 4-19 Increases in the tube wall temperature for the left and right thermocouples after each injection of P04 Bulk temperature 40°C, flow velocity 0.8 m/s, surface temperature 80°C, concentration 3.8 g/L

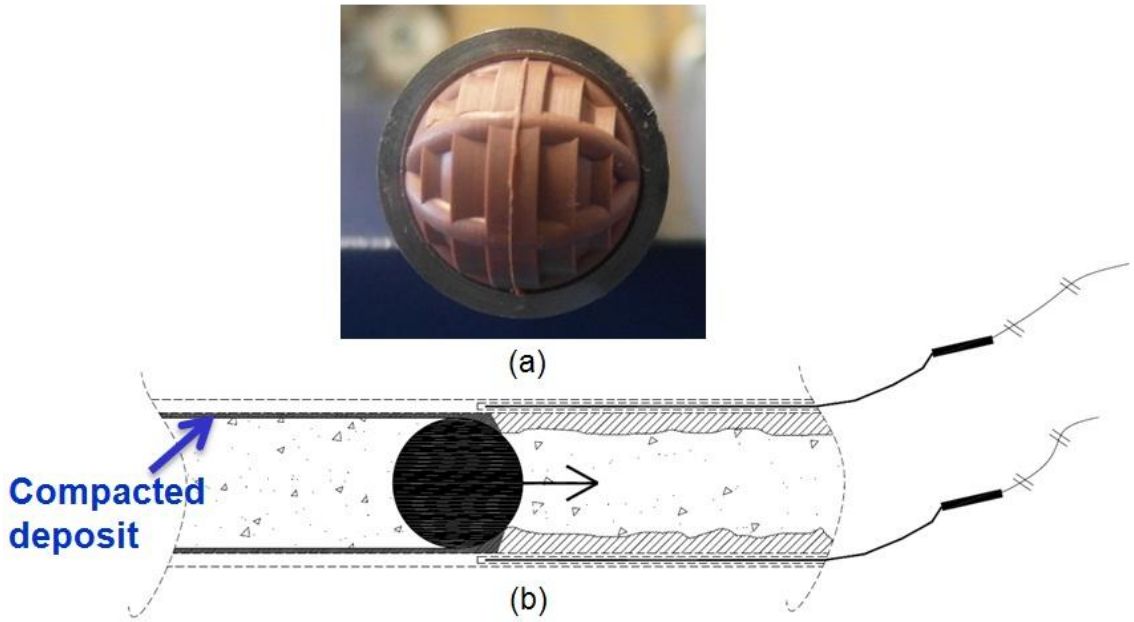

Figure 4-20 (a) 0.1 mm clearance between EX06 and the tube. (b) schematic illustration of compacted deposit by hard projectiles

4.3.3 Cleaning action of projectiles in initiation, transition and asymptotic phases

Based on many investigations and observations, the deposit formation and mitigation by projectile injection included three steps. The criterion for recognizing these steps is the behavior of the fouling resistance. These steps are:

- Initiation stage or induction time, no observation of deposit and zero fouling resistance.
- Transient stage, with the maximum deposition rate and maybe simultaneously maximum cleaning of projectiles. The deposit is primarily soft and the mitigation by the projectiles is more effective.
- Asymptotic stage, deposit formation and mitigation of projectile are in the same rate hence the fouling resistance remains constant till the end of the experiment.

These stages are shown in Figure 4-21 and were commonly observed in the majority of the attempted experiments. In the initial stage or induction time, no fouling was observed.

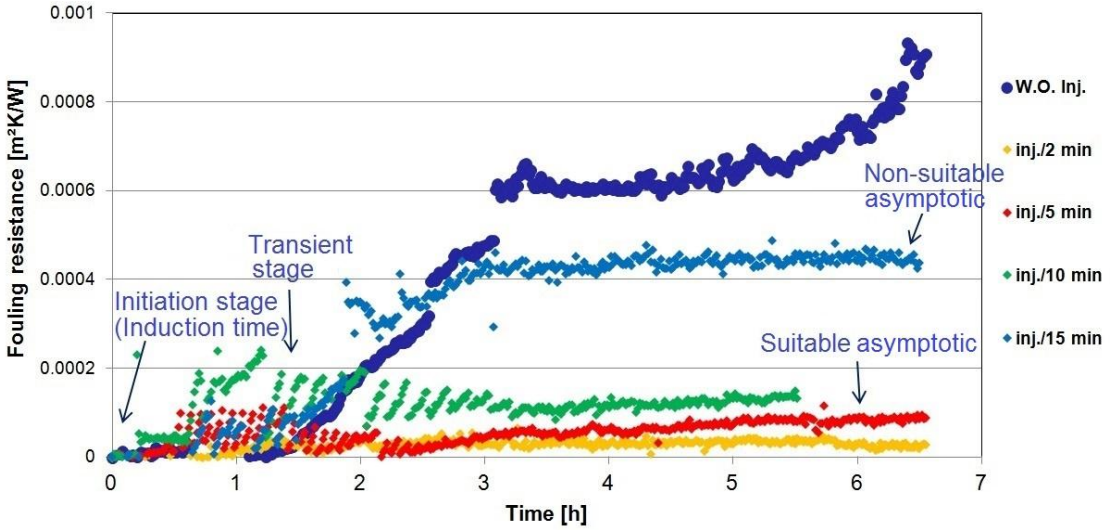

Figure 4-21 Three stage of cleaning actions; induction, transition and asymptotic
Bulk temperature 40°C, flow velocity 0.8 m/s, surface temperature 80°C, concentration 3.8 g/L, Projectile P02

During the transient stage, the maximum deposition rate occurs as the data show the maximum increase in fouling resistance vs. time. Though the rate of fouling is high, the deposit is nevertheless crystalline (see Figure 4-22(a)) and hence the maximum cleaning by projectiles takes place. Figure 4-22 shows the cross-section of the deposit layer in the transient stage. The difference in deposit structure between flow and wall sides indicates that the structure of deposit on the flow side is crystalline and soft, and thus may be removed easier by the projectiles. Thus the effects of cleaning are expected to be stronger and because of crystalline texture of the surface, the formation rate of deposit is also high. Sometimes, at the transient stage (for example transient stage in Figure 4-21), an increase of 1.8 K/min was recorded by the left and right thermocouples. It could be determined from Figure 4-22 that the thickness of deposit is about 800 µm. The transient stage is very critical, since there are two possibilities with respect to the cleaning action of the projectiles. If the shear exerted by the projectiles is large enough to dislodge a big part of the deposit then it keeps the fouling resistance very low (like P02 in Figure 4-9 and P06 and P12 in Figure 4-10). Contrariwise if the shear force is not large enough, then the majority of the deposit stays on the tube after each injection. After a while when it is compressed and sintered, further injection has no big effect on removing any deposit from the surface. It may also happen that the investigated projectile produces the right amount of shear but the injection interval is too long (see Figure 4-21, injection in 10 and 15 min intervals) thus an appreciable cleaning would not take place, in comparison to injection in 2 and 5 min intervals in Figure 4-21.

At the last stage, the fouling rate and cleaning rate become equal and the fouling curve reaches an asymptote. Hence no further mitigation takes place if additional injections are performed. The reason for the asymptotic behavior may be explained by sintering as will be elucidated in section 4.4. Based on the magnitude of fouling resistance, the asymptotic

stage can either be suitable or non-suitable. For a well-selected projectile with proper injection intervals, the fouling resistance in this period is low and could provide a suitable asymptotic. Contrariwise, for a projectile with poor cleaning action, even if the injection interval is short, the fouling resistance is still high which is termed here as non-suitable asymptote. In Figure 4-21 two data sets of suitable and non-suitable asymptotic are presented. For these experiments some parts of the deposit layer were extracted and analyzed. The thickness of the deposit layer was much lower for the data specified as suitable asymptotic. Figure 4-22(b) shows the cross section of deposit in a typical asymptotic period. It could be observed that it is sintered and hard. This could be the reason why injection is not effective anymore in this period. As the fouling resistance has a direct relation to the thickness of deposit, a thin deposit results in a suitable asymptotic value. Thicker layers correspond to larger fouling resistances and are considered as non-suitable asymptotes. In this series of experiments a thickness of 500 µm is recognized as a "non-suitable asymptote" and of 200 µm as the "suitable asymptote". 200 µm is thin enough to keep the fouling resistance below 0.0001 m^2K/W. This value is 90% less than the fouling resistance without the use of projectiles. For the non-suitable asymptotic behavior injection reduced the fouling resistance to only 50% compared to the operation without injection. Figure 4-23 shows schematically the difference of suitable asymptotic and non-suitable asymptotic fouling.

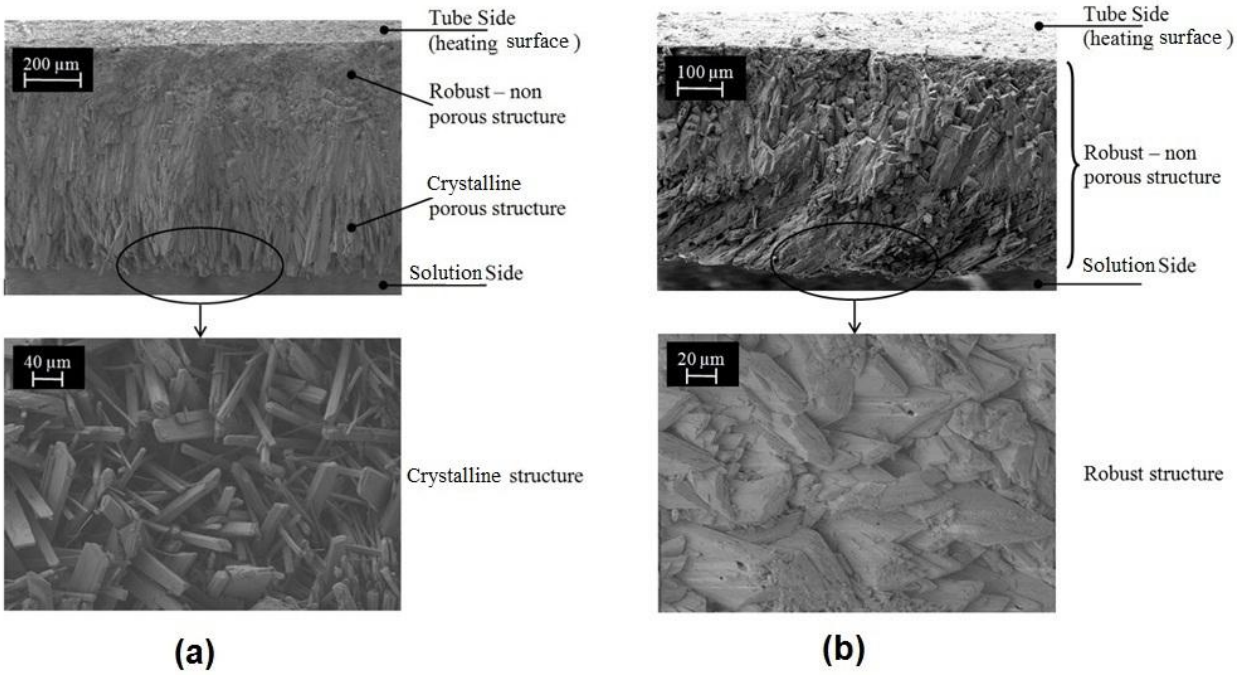

Figure 4-22 (a) Crystalline layer in the transition period, (b) Sintered layer in the asymptotic period

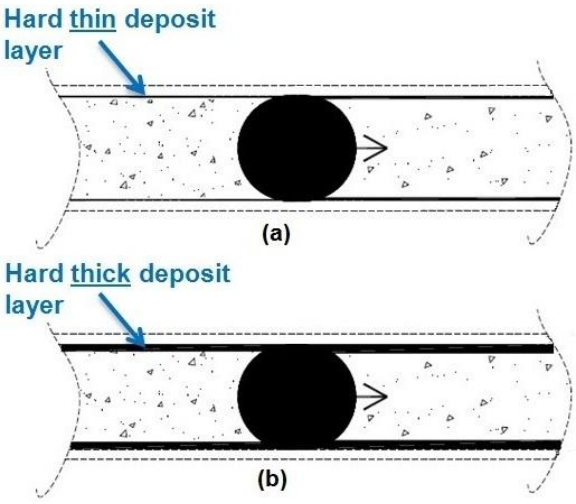

Figure 4-23 Schematics of (a) suitable asymptotic (b) non-suitable asymptotic fouling layer

4.3.4 Influence of sintering on the cleaning action of projectiles

The variation of fouling resistance, R_f, as a function of time with and without injection of the projectiles is shown in Figure 4-24(a). The projectile P12 has been injected every 15 minutes, the $CaSO_4$ concentration has been adjusted to 4.6 g/L and the flow velocity was 1.3 m/s. The fouling experiment lasted approximately 6.5 hr. The fouling resistance increased continuously in case without projectile injection, but many investigations have established that it should reach an asymptote (Peyghambarzadeh et al. 2012). Nevertheless, here the experiment had to be terminated as the surface temperature exceeded a set temperature above which the run could not be continued for safety reasons. With injecting a projectile, an asymptotic level has been approached after approximately 5 hr of operation, as can be seen in Figure 4-24(a). The final asymptotic resistance with injecting a projectile is 0.00045 m^2K/W. However, the fouling resistance without injection reached 0.0008 m^2K/W after 6.5 hr of operation and was still increasing, i.e. the asymptotic behavior is not approached yet and the final asymptotic resistance without injection would be much higher than when projectiles were injected. The results indicate that using projectiles accelerates the fouling process such that the asymptotic behavior is approached quickly but the final asymptotic resistance is much lower than in case without injection. In case of injection, the induction time is decreased from 2 hr and 50 min to just 50 min when injecting the projectile every 15 min.

The fouling resistance without injection increases continuously in the investigated time. In case of projectile injection, it is intermittent and fluctuating due to the removal of same parts of the fouling layer by the injected projectiles. The fouling resistance decreases as soon as a projectile is injected and then increases again with time, i.e. the fouling layer builds up. The discontinuity and the size of fluctuation in the fouling resistance are quite noticeable at the early stage of fouling and decrease with time until they are diminished when an asymptote is reached. Furthermore, the intermittence of the fouling resistance

coincides with the time of injection, and there are four intermittences per hour which is in agreement with the injection rate, i.e. 1 injection every 15 minutes. It can be concluded that the projectile is capable of removing parts of the fouling layer at the early stage of the fouling process, and this capability decreases as the fouling layer builds up such that the projectile is not effective anymore when the asymptotic region is approached. Furthermore, the removal efficiency of the injected projectile is a function of the fouling layer structure.

The fouling resistance at point (A), as indicated in Figure 4-24(a), is 2×10^{-4} m^2K/W, then decreased to approximately 1×10^{-4} m^2K/W, i.e. point (B) after injecting the projectile. The decrease in the fouling resistance from (A) to (B) is about 50%. The fouling resistance is also equal to δ/λ_d, where δ and λ_d are the thickness and thermal conductivity of the fouling layer, respectively. The change in the thermal conductivity λ_d of the fouling layer from (A) to (B) may be assumed negligible, i.e. $\lambda_d \sim$ constant, due to the negligible changes in the fouling layer structure in that short period of time. Therefore, it can be concluded that the decrease in the fouling layer thermal resistance from (A) to (B) by 50% is mainly due to the decrease in fouling layer thickness, which implies how powerful the cleaning effect of the injected projectile is at the early stage of the fouling process. A large amount of $CaSO_4$ material may also stick to the sponge ball due to the removal of particles from the fouling layer. This, in turn, requires opening the systems and washing of the balls to remove sediment from time to time so they can be used further.

The temperatures at the outer surface of the fouling layer, $T_{FL,o}$, i.e. near the heated tube, and at the inner surface, T_{FLi}, i.e. near the solution side, are shown in Figure 4-24(b). If the outer surface temperature of the fouling layer becomes higher than the minimum sintering temperature (MST) (Al-Otoom et al. 2000), then sintering takes place. Sintering changes the fouling layer structure from a porous-crystalline structure to a robust and non-porous structure. The minimum sintering temperature is usually far below the melting point of the fouling layer material (Skrifvars et al. 1992 and Kuczynski et al. 1949), and it ranges from 2/3 to 4/5 of the melting point of the concerned material (Production sintering practices, ASM Handbook). The developing fouling layer inside the heating tube is calcium sulphate dihydrate (Bansal et al. 2008) which has a melting point of about 128°C (Alfa Aesar, 2012). Therefore, it can be concluded that the MST for $CaSO_4.2H_2O$ ranges from 85 to 102°C depending on the purity of the material. The range for the minimum sintering temperature is indicated in Figure 4-24(b). It can be concluded from Figure 4-24(b), that the inner surface of the fouling layer should be in a crystalline form during the whole experiment, since $T_{FL,i}$ < MST. However, the outer surface should change from a crystalline structure at the beginning of the experiment, since $T_{FL,o}$ < MST, to a robust and a hard structure at the end of the experiment, because $T_{FL,o}$ becomes greater than the MST. Samples of the fouling layer are taken for analysis using scanning electron microscopy (SEM). The first sample is taken after 3 hr of operation and the second sample at the end of the fouling experiment, as indicated in Figure 4-24(a). While the first sample is taken from a fouling experiment that has lasted for 3 hr, the second sample is taken

when the same experiment was repeated till the asymptotic behavior is approached. SEM Images of the samples are shown in Figure 4-25 and Figure 4-26.

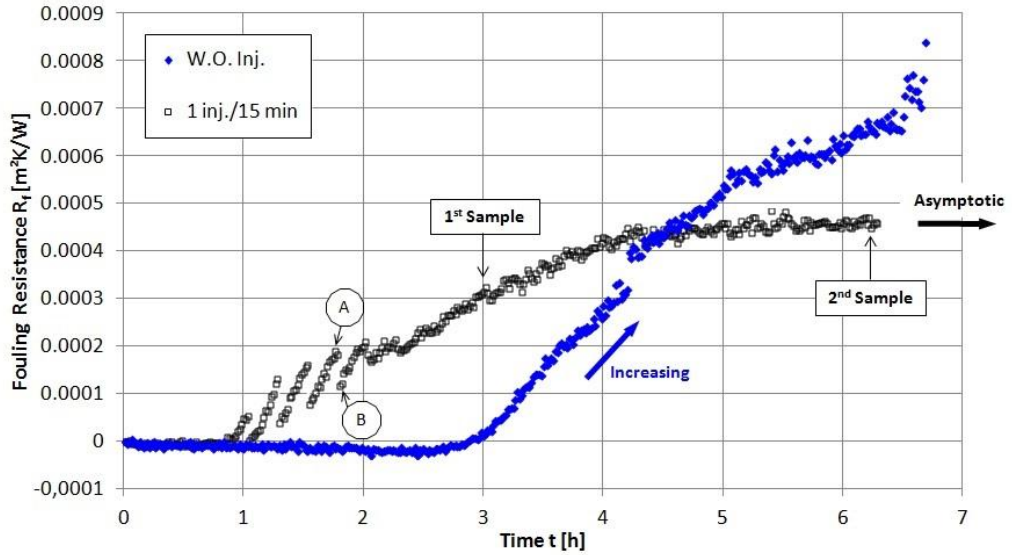

(a)

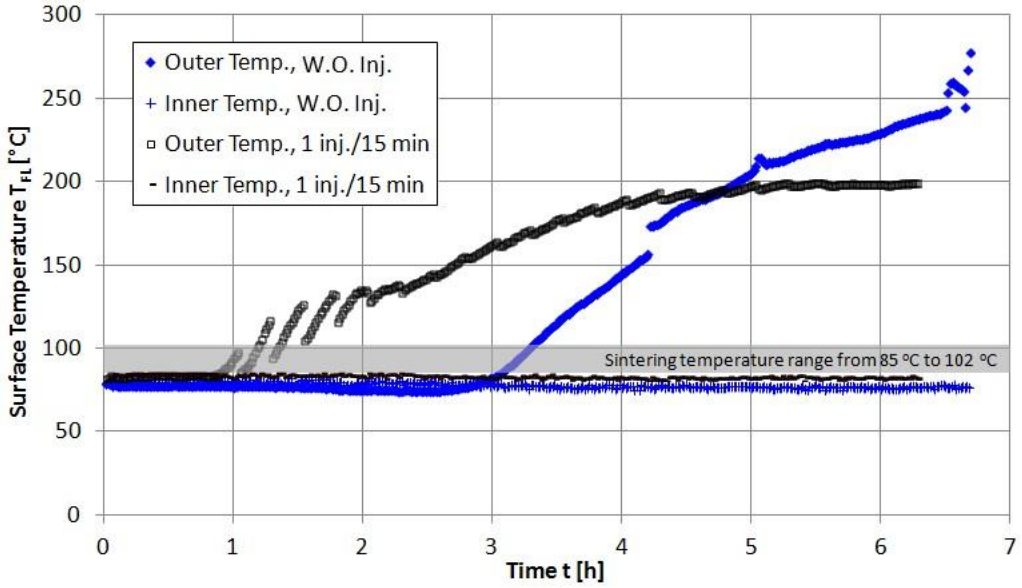

(b)

Figure 4-24 Fouling resistance (a) and surface temperature (b) vs. time with injection (P12) and no injection Bulk temperature 40°C, flow velocity 1.3 m/s, surface temperature 71°C, concentration 4.6 g/L, Projectile P12

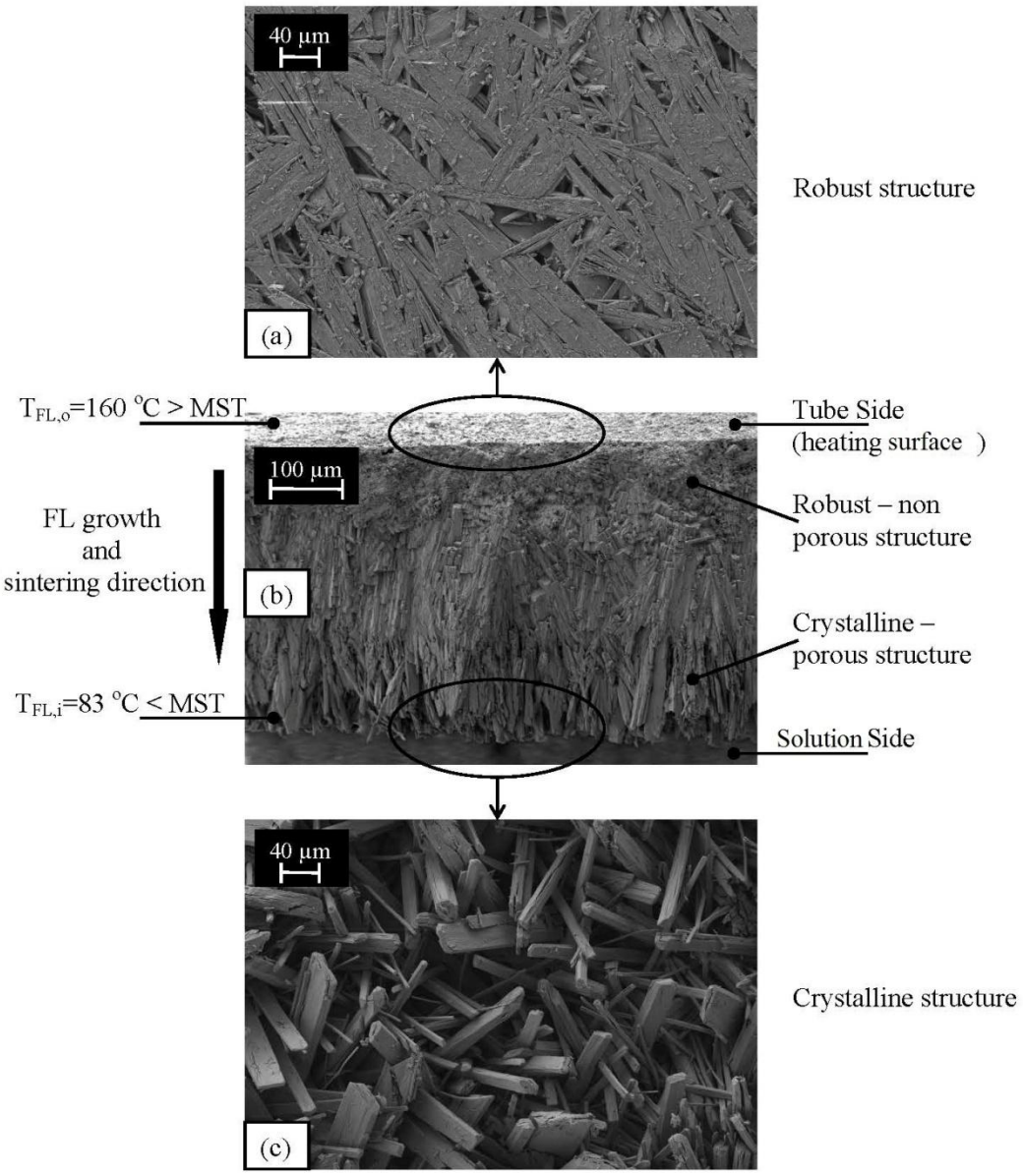

Figure 4-25 SEM images of 1st sample taken after 3 hours of operation; (a) top view (b) cross section (c) bottom view

It can be concluded from the 1st sample taken that the fouling layer near the heating surface has a robust and non-porous structure while the fouling layer near the solution side is crystalline and porous, as can be seen in Figure 4-25. The surface temperature of the fouling layer near the heated surface is 160°C that is well above the MST, therefore sintering of the layer has taken place. Nevertheless, the surface temperature of the fouling layer near the solution side is 83°C, which is below the MST and thus not prone to sintering. The degree of sintering across the fouling layer is decreasing from top to bottom, i.e. from the tube side to the solution side, due to the temperature gradient across the layer. Sintering has started at the top of the fouling layer, near the heating element where the

temperature of the layer is higher than the MST, and it has spread across the layer. The porous structure of the fouling layer near the solution side assists the removal of crystals by the injected projectiles. It can be seen from Figure 4-26 (b) that the structure of the fouling layer of the 2nd sample has a non-porous structure, with a highly sintered structure near the tube side and less sintered at the solution side. The change in the fouling layer structure from porous to a non-porous hard structure stops the projectile from eroding the layer.

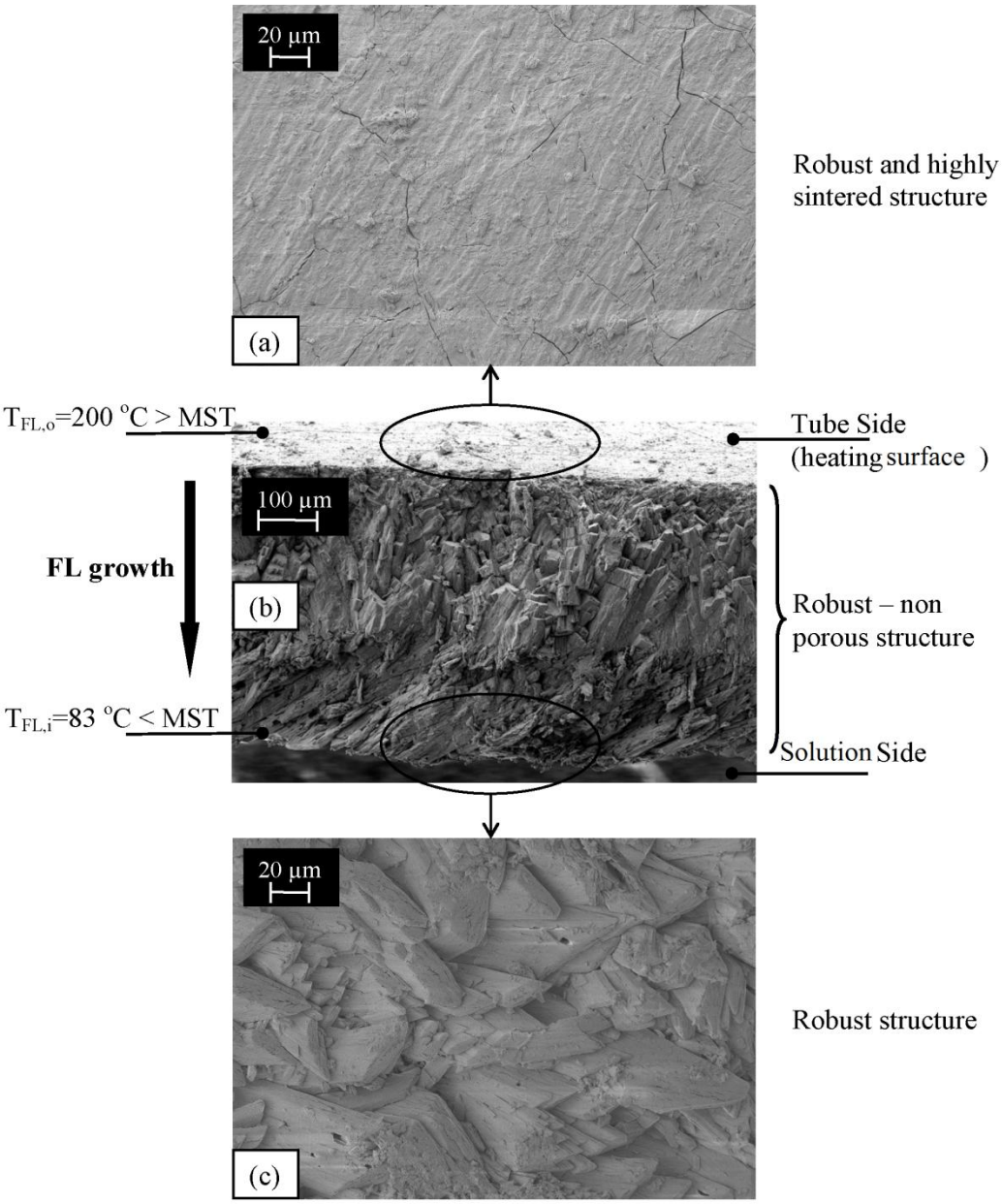

Figure 4-26 SEM image of 2nd sample taken at the experiment, (a) top view, (b) cross section (c) bottom view

The behavior of the fouling resistance and the temperature of the outer surface of the fouling layer as a function of the injection intervals are shown in Figure 4-27. The injection intervals have been varied between 1 injection every 10 and 15 minutes. It can be seen that the fouling process consists of three consecutive stages; induction time, fouling, and finally the asymptotic behavior. In the second stage, the fouling layer is developing but at the same time there is a cleaning process taking place due to the injected projectiles, which are the reason behind the discontinuity in the curves. The discontinuity in fouling resistance with 1 injection every 10 minutes is much higher than in case of 1 inj./15 min, and that is due to the increased removal of deposits with the increased injection interval. However, the discontinuity decreases as the fouling layer develops, which indicates less removal of crystals until it ceases when the asymptotic level is approached. The range of the minimum sintering temperature is also shown in Figure 4-27(b). It can be concluded from the minimum sintering temperature that sintering has occurred across the FL. In the third stage, i.e. the asymptotic behavior, the fouling layer becomes hard such that projectile is not capable of removing any particles out of the fouling layer. The asymptotic resistance with 1 injection every 10 minutes is 1.5×10^{-4} m^2K/W, while in case of 1 inj./15 min is 4.5×10^{-4} m^2K/W.

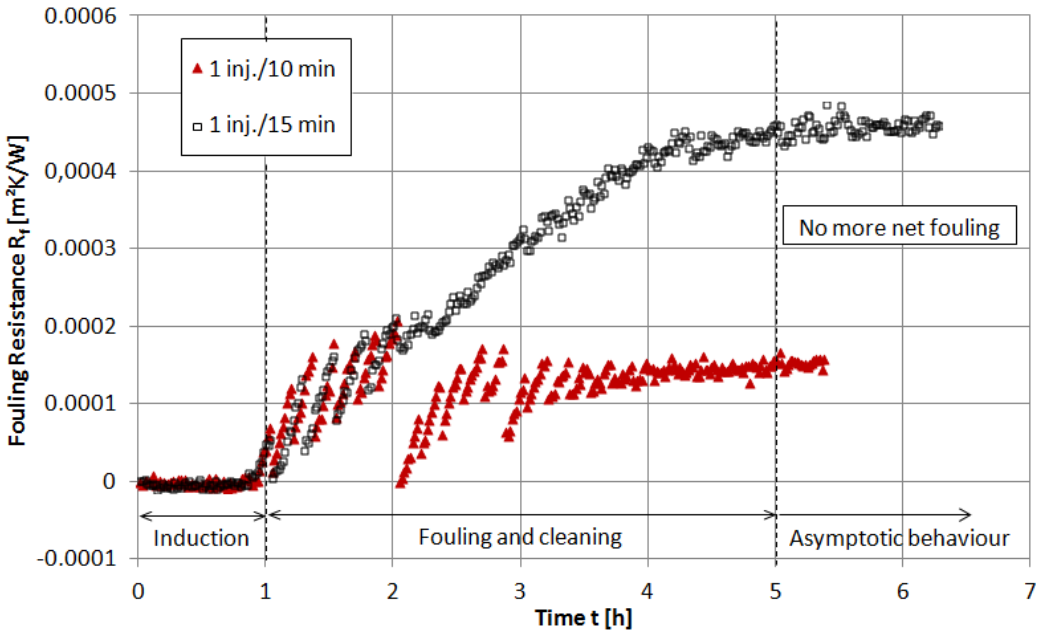

(a)

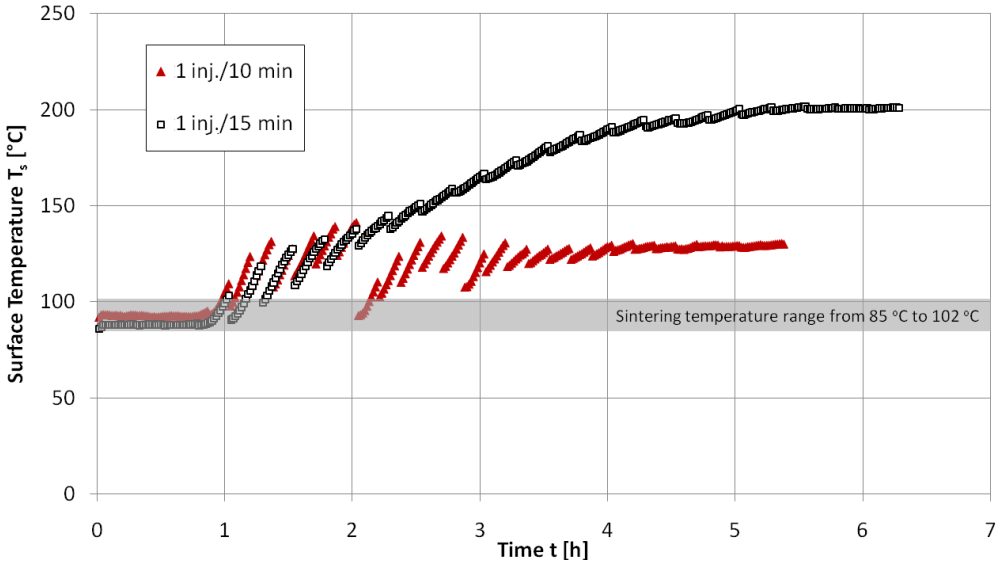

(b)

Figure 4-27 Fouling resistance (a) and outer surface temperature (b) as function of the projectile injection interval

A schematic diagram of the fouling process during online cleaning, i.e. by injecting projectiles in regular intervals, is depicted in Figure 4-28. During the fouling process two mechanisms are simultaneously occurring but opposing each other. The first mechanism is the development of a crystalline fouling layer near the tube surface, and the second mechanism is the removal of material from the porous crystalline layer near the solution due to projectiles, as shown in Figure 4-28(a) and (b). If the removal rate is slow enough to allow building up of the fouling layer, as in the case of one injection every 15 minutes or no injection at all, see Figure 4-24, then a thick fouling layer with a very high surface temperature T_s will result. The outer surface temperature of the fouling layer, i.e. T_s, increases as the fouling layer develops due to the increased R_f. The temperature of the outer surface T_s of the fouling layer, i.e. near the heated surface is the highest temperature across the fouling layer, while the temperature of the inner surface $T_{FL,i}$ of the fouling layer, i.e. near the solution side, is the minimum temperature. If the fouling layer temperature becomes higher than the MST sintering takes place, which changes the layer from a fragile, crystalline and porous structure to a hard and non porous structure. Sintering prevents the projectiles to remove deposits from the fouling layer. Sintering starts near the heating element side and spreads across the layer, as shown in Figure 4-28(c). The rate of sintering is a function of the heating temperature and time (Ristic, 1979). If the sintering rate is faster than the removal rate then hardening of the layer will be faster than the cleaning action of the projectile, leading to a thicker fouling layer. If the removal rate is faster than the sintering rate then a very thin fouling layer is expected, as in the case of one injection every 10 min. The change in the fouling layer structure from a porous crystalline structure to a non-porous and robust structure due to sintering is the main cause for impeding the cleaning action of projectiles. Developing of new crystals over the fouling

layer is greatly reduced once the whole layer has sintered completely as has been explained recently by Esawy et al. (2010), which also leads to an the asymptotic behavior as depicted in Figure 4-28(d). Injecting a projectile removes the porous crystalline structure at the top of the fouling layer, until the sintered layer at the bottom of the fouling layer is approached. Therefore, it can be concluded that the speed to reach a totally sintered layer is dependent on the injection interval. Injecting a projectile accelerates the process to reach a totally sintered fouling layer, and hence to reach asymptotic behavior. Furthermore, the success of injecting projectiles on mitigating fouling is highly dependent on the early stage of scale formation, especially the induction time. The influence of injected projectiles on the induction time will be the next stage of this investigation.

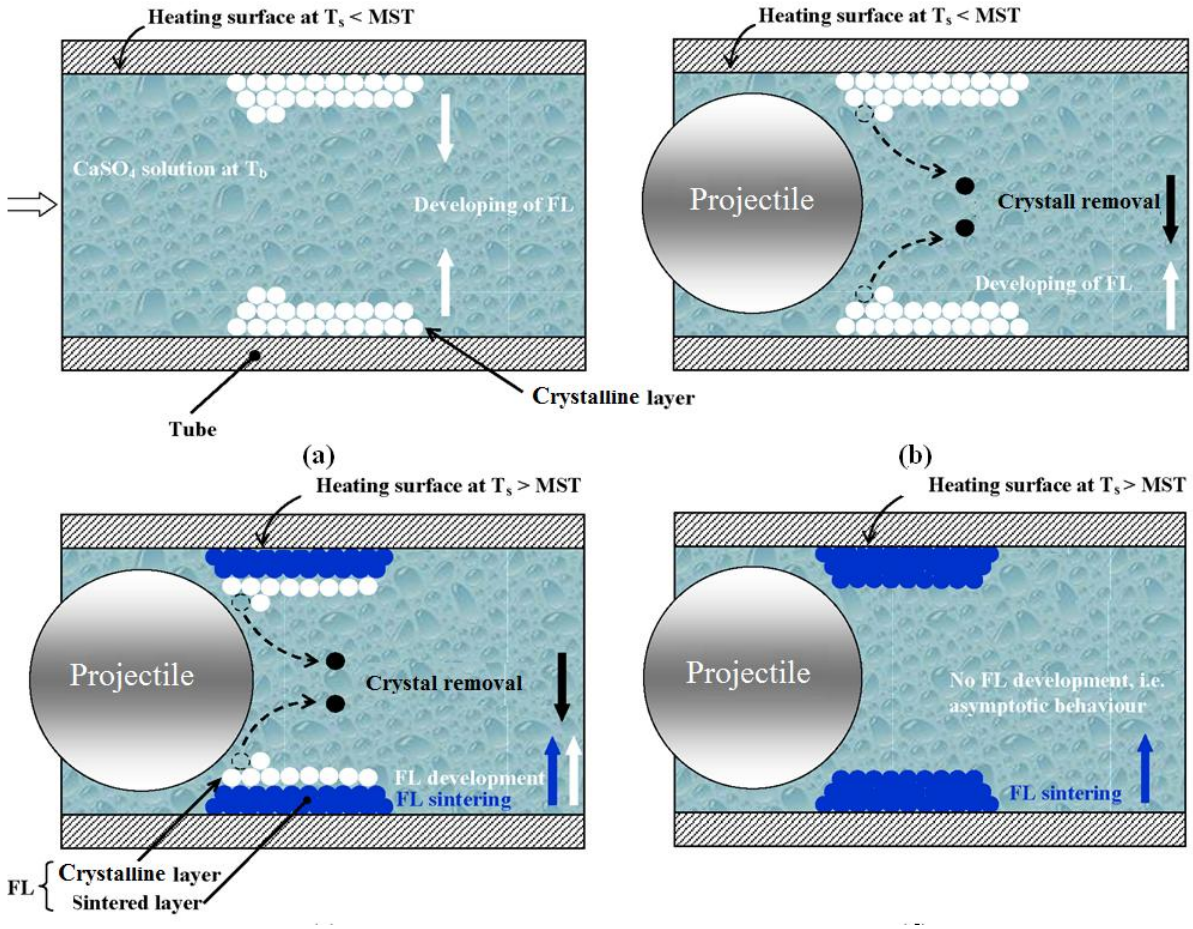

Figure 4-28 Development of the fouling layer during online cleaning using projectiles

4.4 Impact of Projectile Injection on the Induction Time

Several experiments have been performed to investigate the impact of projectile injection on the induction time (IT) at different flow velocities. The development of fouling resistance R_f with and without projectiles is shown in Figure 4-29. The flow velocity was 2.2 m/s and the injection interval is one projectile every 10 min. The induction time without injection of projectiles is 2.05 h, but with projectiles it is 0.65 h

which is a reduction by approximately a factor of three. The discontinuity in the fouling resistance with injection is due to the cleaning action of the projectiles, i.e. partial removal of deposits from the fouling layer. The discontinuity and the size of the fluctuations in fouling resistance are quite noticeable at the early stage of fouling and decrease with time until they diminish to zero when asymptotic fouling is approached. The final asymptotic fouling resistance is reached after 3.5 h with projectiles, but without injection, the asymptotic fouling resistance was not approached even after 5 h of operation.

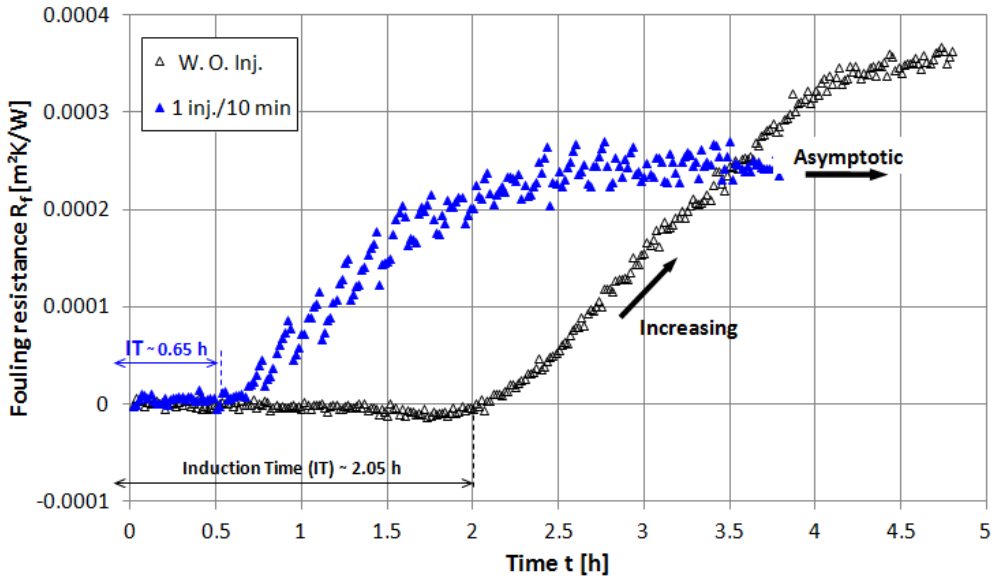

Figure 4-29 Comparison of fouling resistance with and w/o projectiles (P12) versus time
Bulk temperature 40°C , injection interval every 10 min, flow velocity 2.2 m/s, surface temperature 71°C, concentration 4.6 g/L

Figure 4-29 also confirms that injecting a projectile expedites the initial fouling process, i.e. the fouling process starts early and the asymptotic behaviour is reached quickly though it is much lower compared to that without injection. This figure also shows that the fouling resistance R_f becomes slightly negative during the induction time. This behavior has been observed and reported by many researchers, e.g. Bansal et al. (2008), Fahminia et al. (2005) and Albert et al. (2009). Only few crystals of $CaSO_4$ are formed on the surface during the induction time of crystallization fouling, as has been visualized and shown by Kim et al. (2002). These crystals cause turbulence in the fluid boundary layer near the heat transfer surface which would in turn improve the local heat transfer, as has been explained by Crittenden and Aldermann (1988). The enhancement in the local heat transfer by the primary deposited crystals, over-rides the heat transfer resistance of the scale only during the induction time, which results in a negative fouling resistance.

Due to the sensitivity of the performed experiments, the repeatability of these experiments has been checked by repeating the experiments. The repetition of the first

experiment performed, which has been shown in Figure 4-29 without injection of projectiles, is presented in Figure 4-30. The induction time in the first experiment is approximately 2.0 h and in the repeated experiment is approximately 1.8 h, which is about 0.2 h (12 min), i.e. 10 % difference. It has been found from the performed tests that the repeatability of the performed experiments varies between 85–90% which is quite acceptable for experiments of such nature.

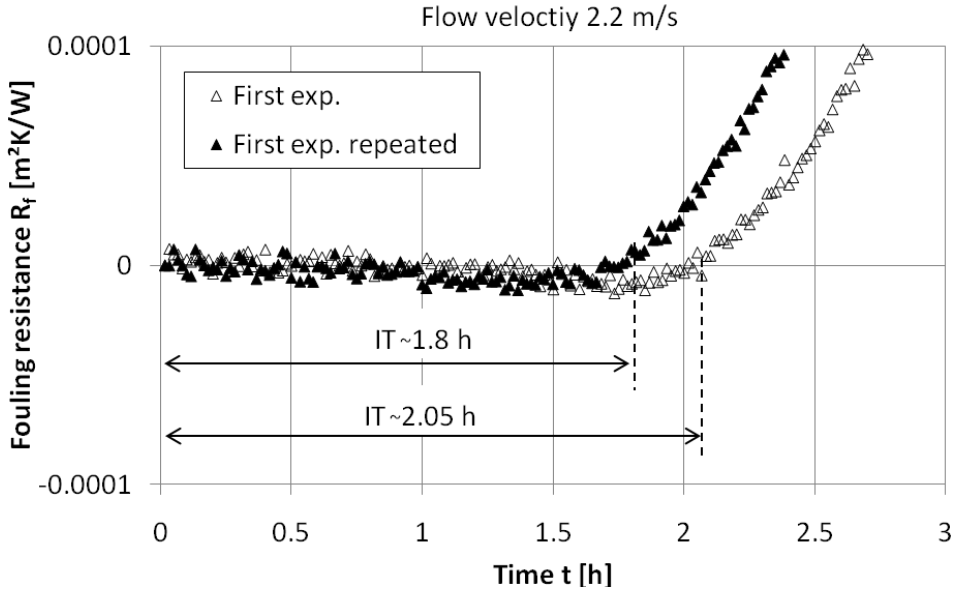

Figure 4-30 Repetition of the experiment presented in Figure 4-29
Bulk temperature 40°C , flow velocity 2.2 m/s, surface temperature 71°C, concentration 4.6 g/L, no projectiles

The above experiment has been repeated but for other flow velocities, i.e. 0.8 m/s, 2.2 m/s and 3 m/s. The development of fouling resistance as a function of the flow velocity with and without projectiles is demonstrated in Figure 4-31. The induction time without projectile injection, increases with the flow velocity, which is in agreement with the work of Kim et al. (2003) and Yang et al. (2002). The fouling rate dR_f/dt, which is defined as the slope of the fouling resistance curve in the progressive region of fouling, is depicted on the upper right corner of Figure 4-31(a) as a function of the flow velocity. It confirms that the fouling rate decreases with the flow velocity highlighting that the fouling process is a reaction-controlled process otherwise the higher flow velocity would have resulted in a higher fouling rate for a mass transfer-controlled fouling process. This is in agreement with the findings of Konak (1974).

The net rate of fouling is the difference between the deposition and removal rates. Deposited crystals can be removed from the fouling layer by the fluid shear stress. Increasing the flow velocity, increases the shear forces on the deposited crystals, and consequently increases the removal rate. Increasing the removal rate of crystals delays the fouling process and increases the time needed for the fouling process to start up in a substantial way. However, the induction time with injection of projectiles is almost

constant, i.e. independent of the flow velocity, as can be seen in Figure 4-31(b). This implies that the influence of the flow velocity is dominated by the injected projectile as long as the injection rate is constant. The induction time is extracted from the previous set of experiments, and plotted as a function of the flow velocity in Figure 4-32. The induction time is linearly proportional to the flow velocity without injection, and it is almost independent of the flow velocity if projectiles are passed through the tube.

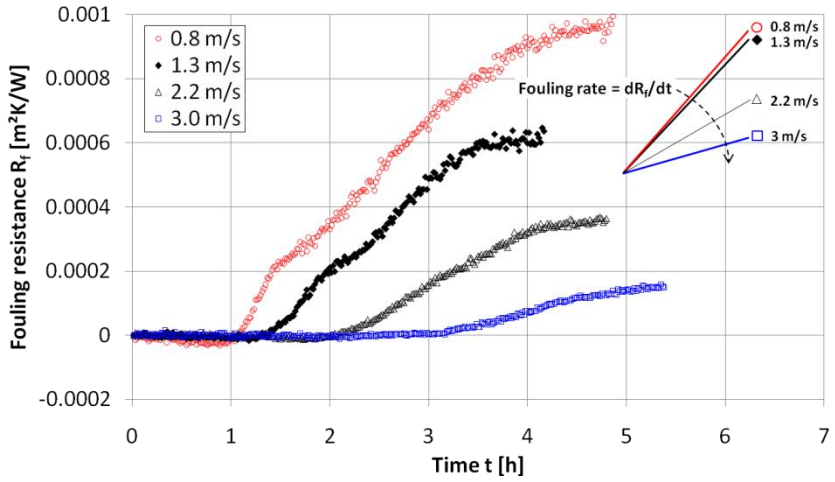

(a)

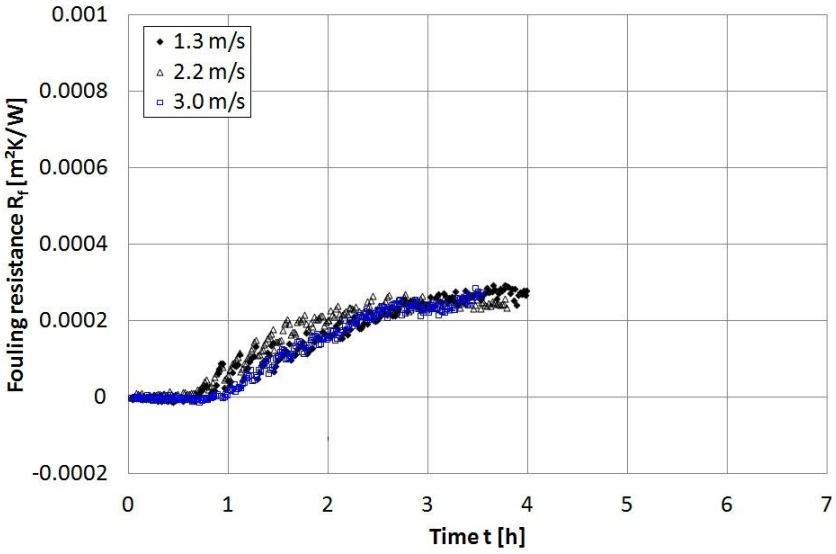

(b)

Figure 4-31 Fouling resistance versus time as a function of the flow velocity (a) without and (b) with projectile (P12) injection every 10 min

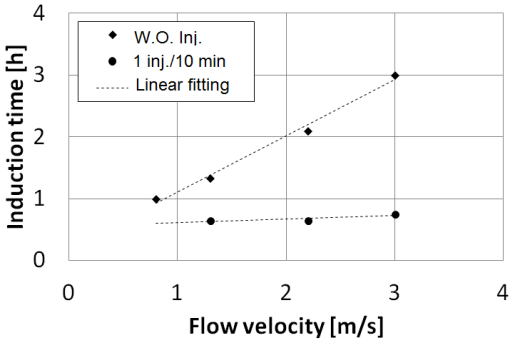

Figure 4-32 Induction time versus flow velocity with and w/o projectiles (P12)

4.4.1 Injection after induction time

It can be concluded from the experiments in section 4.4 that it is highly recommended to inject projectiles only after the induction time. This makes use of the longer induction time without injection. This strategy of operation, i.e. injecting projectiles at the end of the induction time, could be taken as a new operational criterion for mitigating fouling using projectiles. A new experiment has been performed to examine this strategy of operation, such that the projectiles were injected at the end of the induction time. The development of the fouling resistance in case of i) without injection, ii) injecting projectiles from the beginning of the operation and iii) injecting projectiles at the end of the induction time which is recorded in case i. The results are shown in Figure 4-33. The flow velocity is 2.2 m/s and the injection interval was one projectile every 10 min. The final asymptotic resistance with injecting projectiles from the beginning of operation (case ii) was similar to the asymptotic resistance in case of injecting projectiles at the end of the induction time (case iii), i.e. 0.00027 m^2K/W but the induction time has been prolonged from 2.05 h in case i to 2.8 h in case iii, and decreased to 0.65 h in case ii, as can be seen in Figure 4-33. It can be concluded that the induction time has increased by 36 % in case of injecting projectiles at the end of the induction time (2.05 h) and decreased by 68.3 % in case of injecting the projectile from the beginning of operation. Injecting projectiles at the end of the induction time delays the increase of fouling in the process, and injecting projectiles from the beginning of operation fastens the fouling process.

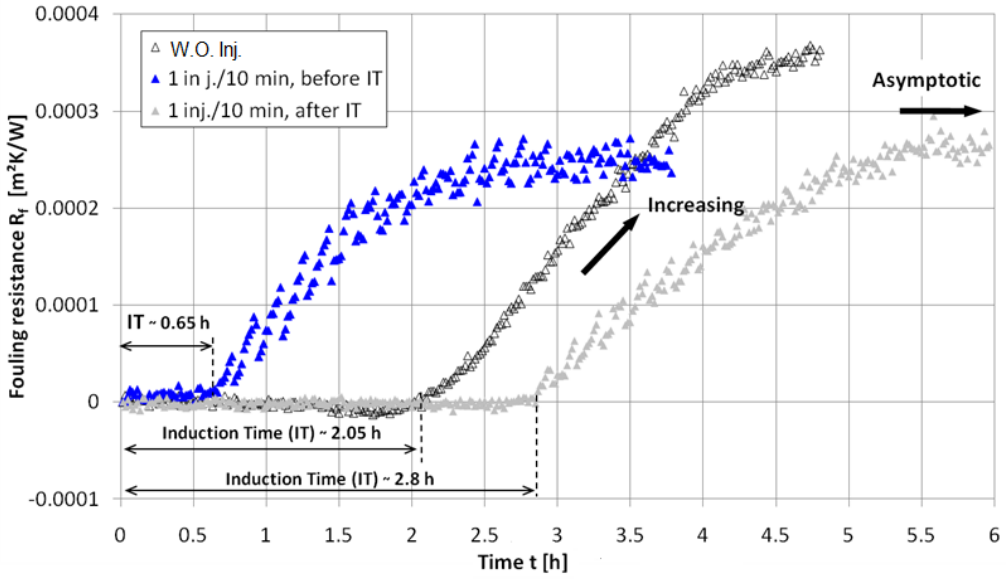

Figure 4-33 Fouling resistance versus time for various operating scenarios
The bulk concentration 4.6 g/L, bulk temperature 40°C, surface temperature 71°C, flow velocity 2.2 m/s, injection intervals every 10 min, projectile P12

4.4.2 Influence of multiple injections on the induction time

Another set of experiments has been performed in which the injection interval is varied at a given flow velocity of 1.3 m/s. This is intended to get insight into the influence of the injection interval on the induction time for multiple injections. The injection interval has been varied between one and three injections every 10 minutes, with results being shown in Figure 4-34. With 3 inj./10 min, the three injections were injected successively one after the other every 10 minutes. The whole injection time for the three injections takes about one minute. The fouling resistance increases with time in case of 1 inj./10 min. But in case of 3 inj./10 min it has changed from a continuous increase to an asymptotic behavior in less than 6 h. The asymptotic fouling resistance, R_f^*, with 3 inj./10 min is 0.0002 m^2K/W, which is less than R_f^* for 1 inj./10 min after 6 h of operation, i.e. 0.00033 m^2K/W. Changing from single to triple injection has hence decreased the fouling resistance by 40% after 6 h of operation. It was also expected that the asymptote with a single injection will be significantly larger than that of triple injection. However it was not possible to continue the fouling run with 1 inj./10 min till the asymptotic behavior is approached, as the tube wall temperature exceeded the set limit.

The induction time in case of 1 inj./10 min is approximately 0.65 h, while for 3 inj./10 min is only about 0.3 h, as can be seen in Figure 4-34(a) indicating a reduction of up to 54%. The induction time without injection is 1.3 h, as shown in Figure 4-32, which indicates up to 50% reduction with 1 inj./10 min and 77% for 3 inj./10 min. Thus multiple injection decreases the induction time. The reasons will be explained in section 4.4.3 and 5.3.1 in detail.

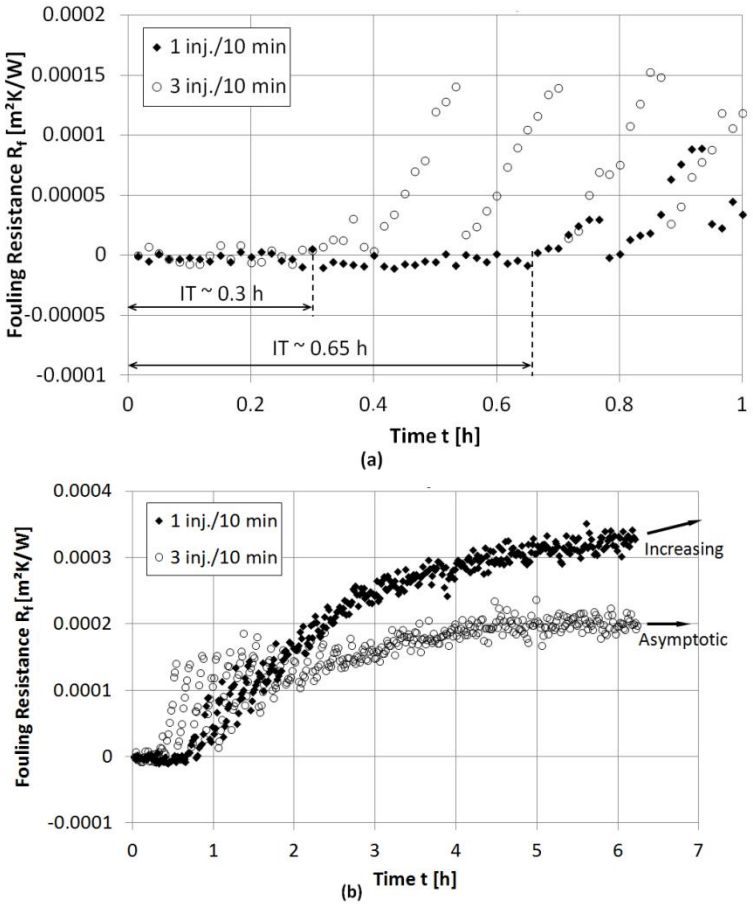

Figure 4-34 Fouling resistance versus time as a function of the injection interval
Bulk concentration 4.6 g/L, bulk temperature 40°C, surface temperature 71°C, flow velocity is 1.3 m/s, projectile P12

4.4.3 Visualization of injected projectiles through the transparent glass tube

The reduction in the induction time, i.e. the untimely beginning of the fouling process, due to injecting a projectile is an important phenomenon that should be studied in more detail, because it could have a profound impact on the overall fouling process. A visualization experiment has been performed to explore the influence of projectiles on the fouling process. The same experimental setup was used but with a transparent glass tube. No heating has been supplied during the visualization experiment thus no $CaSO_4$ has been used, i.e. the experiment was performed with demineralised water at room temperature. The flow has been recorded using a high speed camera, SpeedCam Visario 1500, with a maximum recording rate of 10,000 frames per second. The camera was positioned in front of the glass tube. Lighting of the set-up was obtained via a light source from the back side of the glass tube, in order to prevent disturbing scattering of the light in the camera due to the smooth surface of the tube. The measuring technique used is known as the shadow-graph technique (Settles, 2001), where the moving object to be tracked becomes dark and the surroundings becomes white. A single projectile (P01) was injected with a flow

velocity of 0.8 m/s. The result of the visualization experiment is shown in Figure 4-35. The time indicated on the images is the one that has elapsed after injecting the projectile. The pictured part (visualized part) of the tube shown in Figure 4-35 is the middle section of the tube.

Injection of the projectile started at t = 0 s and the flow was steady, as can be seen in Figure 4-35(a). Lots of air bubbles started to appear in the tube after 100 ms from injecting the projectile, see Figure 4-35(b) and (c), however, the projectile did not yet reach the pictured part of the tube at that time. The projectile appeared in the pictured part of the tube at t=211 s, with lots of air bubbles moving together with the projectile and close to it, see Figure 4-35(d) and (e). It has been observed that many air bubbles have been entrapped between the projectile and the tube upper surface as indicated by the dotted circle in Figure 4-35(e). Not surprisingly, most of the bubbles are concentrated at the upper half of the tube, and almost no bubbles are at the bottom part of the tube due to buoyancy effects. The water flow became steady once more and free of air bubbles after 477 ms, see Figure 4-35(f). Thus the injected projectile has induced lots of small air bubbles into the tube, and once the cycle of the projectile is completed, i.e. the projectile returns back to its starting position, the air bubbles diminished and the systems turns to be free of bubbles again. It is very difficult to eliminate all air bubbles in the flow caused by each injection. Therefore, increasing the injection rate (number of injections per unit of time) increases the amount of air bubbles in the tube. While discussion in the open literature about the effect of air bubbles on fouling is limited, it nevertheless seems that the presence of air bubbles may be accounted for the shorter induction time with multiple injections as will be proven in section 4.4.4. Another reason for shorter induction time is the scratched surface and the resettlement of particles detached by the projectiles on the heat transfer surface and acting as nuclei (Bansal et al. 1997). This also was proven by a series of experiments that will be discussed in section 5.3.1.

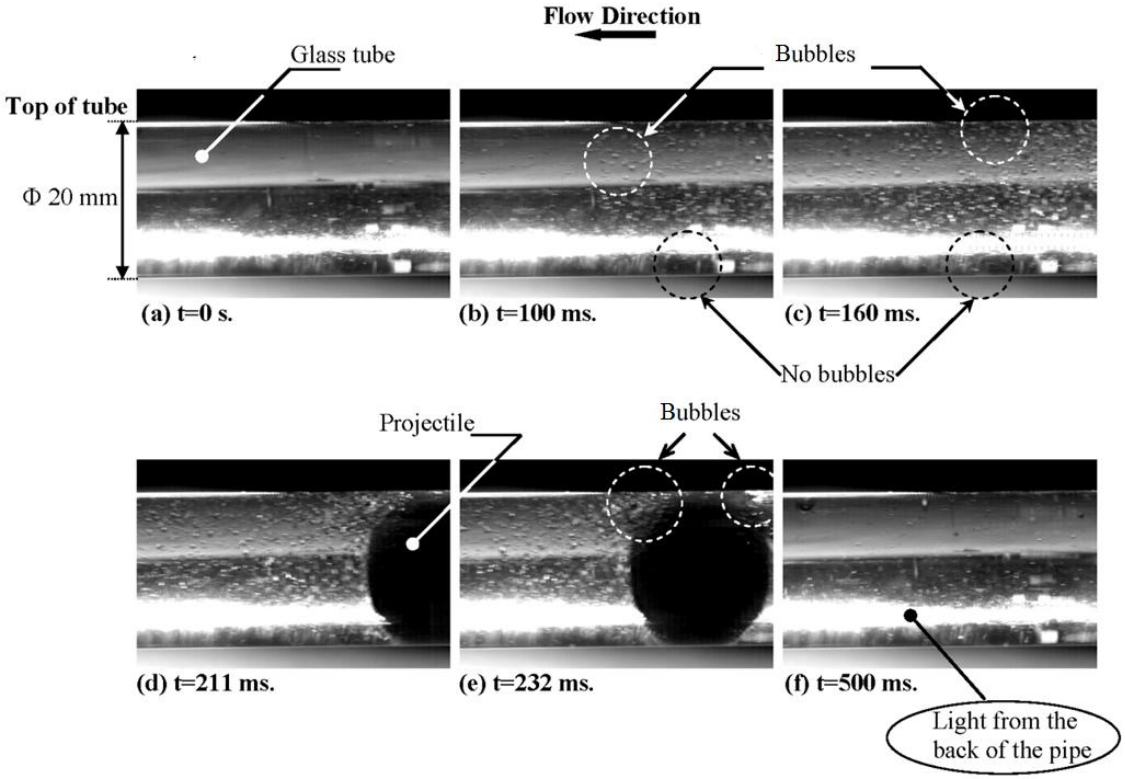

Figure 4-35 Visualization of the injected projectile (P01) passing through a transparent glass tube Flow velocity 0.8 m/s, the tube is installed horizontally

A cross-sectional picture of the tube after a fouling run in which a projectile (P12) was injected every 10 min is presented in Figure 4-36. Note that the behavior of this fouling run has already been shown in Figure 4-31(b). Figure 4-36 illustrates that the fouling layer is thicker at the top of the tube, i.e. the upper half of the tube, than at the bottom of the tube. The thickness of the fouling layer at the bottom of the tube is 0.3 mm, while at the top it is 0.78 mm. This implies that fouling with injecting projectiles is more likely to occur at the top of the tube than at the bottom. This could probably be due to the high concentration of air bubbles at the top of the tube compared to the bottom of the tube during an injection as has been found from the visualization experiments. Providing another picture like Figure 4-36 but without projectile was impossible due to the cost of the special techniques for tube construction.

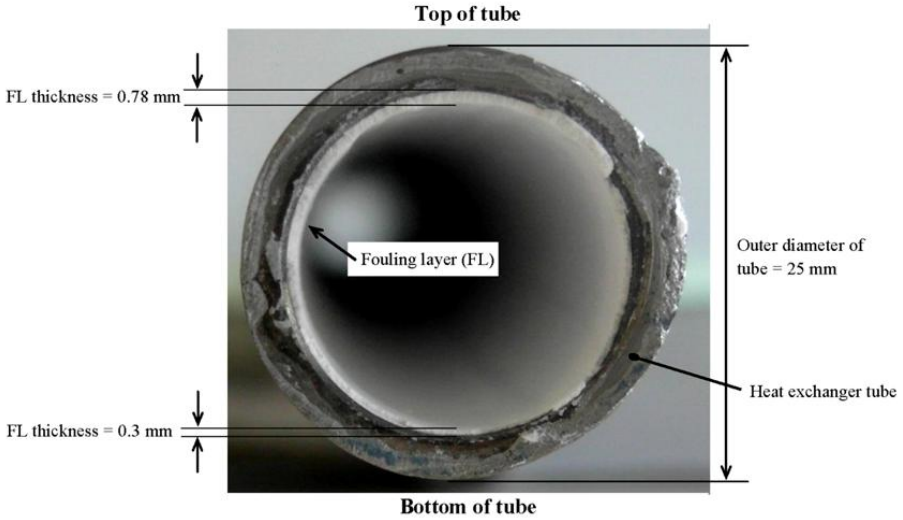

Figure 4-36 Cross section of the heated tube after a fouling experiment P12 injection every 10 min, flow velocity 1.3 m/s, concentration 4.6 g/L

4.4.4 Influence of injected air on the induction time

To further examine the impact of air bubbles, two additional fouling experiments were performed in which only air was injected. Air is injected every 10 minutes via the projectile insert tube, but no projectiles are injected. It has been tried during the experiments to inject the same amount of air as for the above-referenced run with the glass tube. The flow velocity varied from 2.2 m/s to 3 m/s. The fouling resistances at a flow velocity of 3 m/s in case of i) no injection, ii) injecting a projectile and iii) air injection are shown in Figure 4-37(a). The induction time has been reduced from 3 h in case of no injection to 1.65 h due to air injection, and to 0.75 h due to injecting a projectile. Similar behavior has been observed at 2.2 m/s, as can be seen in Figure 4-37(b). The induction time has been decreased from 2.05 h in case of no injection to 1.55 h with air injection, and to 0.65 h when injecting a projectile. The fouling rate, dR_f/dt, is illustrated in the upper left corner of Figure 4-37 which confirms that injecting air increases the fouling rate. It can be concluded that injecting air decreases the induction time and increases the fouling rate, i.e. enhances fouling. This conclusion is in agreement with the work of Yang et al. (2000). They found that the presence of dissolved air bubbles on the modified low-energy surfaces enhances the fouling process, and that the fouling rate is depressed when the modified low-energy surfaces are free from air bubbles. Thus they used degassed solution to prevent enhancement of bubbles on the heat transfer surface. Hasson and Zahavi (1970) also found anomalous results due to adhering air bubbles on the exchanger surface in a study of calcium sulfate scale.

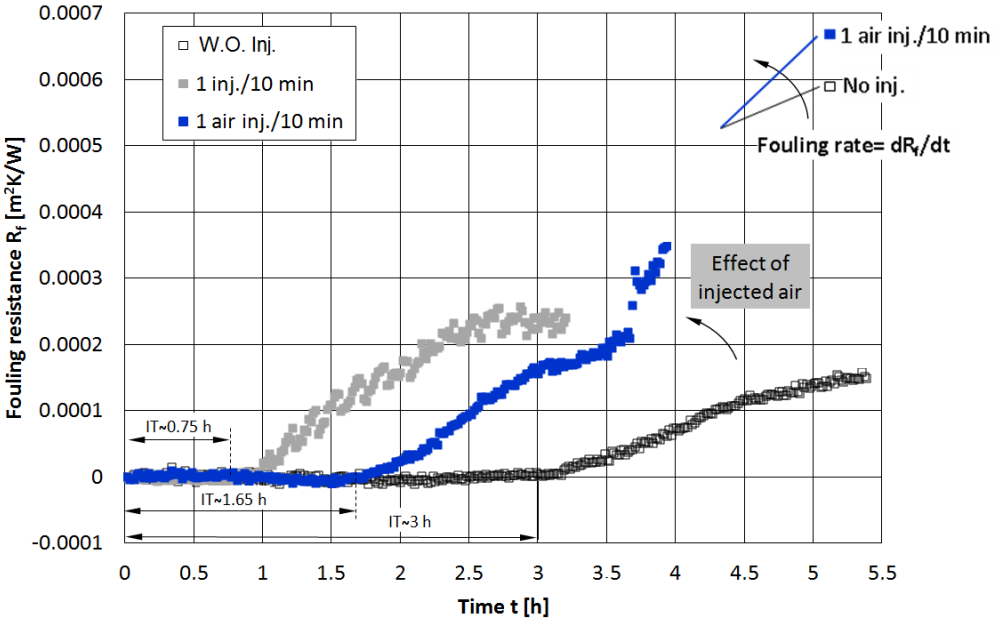

(a)

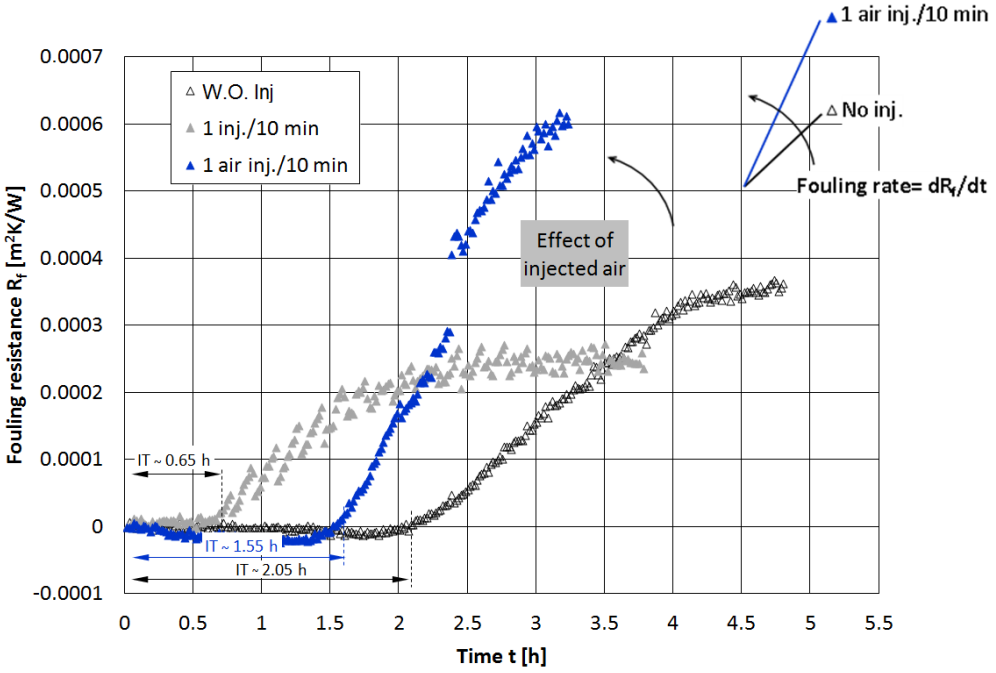

(b)

Figure 4-37 Fouling resistance versus time at a flow velocity of (a) 3 m/s and (b) 2.2 m/s
Air at an injection interval of 1 inj./10 min, bulk concentration 4.6 g/L, bulk temperature 40°C, surface temperature 71°C

Najibi et al. (1997) investigated fouling during subcooled flow boiling of pure calcium sulfate and calcium carbonate. They considered the effect of bubble nucleation on heat transfer surfaces and presented the nucleate boiling fraction, NBF. It may be interpreted as a measure of the fraction of the heat transfer area affected by bubble growth mechanisms.

Helalizadeh et al. 2005 calculated the value of this parameter for different flow velocities and heat fluxes. Peyghambarzadeh et al. (2012) also found that bubble generation on the heat transfer surface promotes scale formation due to crystallization and that rapid deposition occurred under subcooled flow boiling conditions in comparison with forced convection. The difference is the result of bubble activity. Yang et al. (2000) investigated the influence of desorbed air bubbles on the fouling of a modified copper surface with low surface energy, and it was observed that a ring of precipitates was left on the heat transfer surface after the release of each bubble. This fouling ring was observed by many researchers including Gill and Nancollas (1980) and Gunn (1980). Scale formation under nucleate boiling occurs at the triple interface of the steam bubble with the scale producing solution and the heating surface, forming fouling rings as have been found by Freeborn and Lewis (1962). Partridge (1929) and White (1929) explained that the origin of rings is due to the local increase in heat transfer surface temperature at the base of the steam bubble, i.e. the triple interface as can be seen in Figure 4-38(a), causing supersaturation conditions in the thin film surrounding the gas-liquid interface leaving rings of crystals at the base of the bubble. Thus the frequency and density of bubbles determines the fouling rate as have been correlated by Jamialahmadi et al. (1989).

Technical data about the effect of air bubbles on fouling in the literature are scarce. Maybe the induced air bubbles that stick to the heat transfer surface produce a similar effect on crystallization fouling but not as severe as generated steam bubbles during nucleate boiling, see Figure 4-38(b). This would be attributed to the fact that the presence of desorbed air bubbles enhances the fouling process during convective heat transfer by increasing the possibility of supersaturation which would facilitate crystallization. Contrariwise, the fouling process is minimized when the flow is free from air bubbles, as it has been shown in the air injection experiments already presented. It was found that the injected projectiles induce air bubbles into the flow during the time of injection. Therefore, increasing the injection interval increases the amount of air bubbles in the flow that consequently enhance the fouling process. However this is not the only reason for faster starting up the fouling process and reducing the induction time. More explanations will be discussed in section 5.3.1.

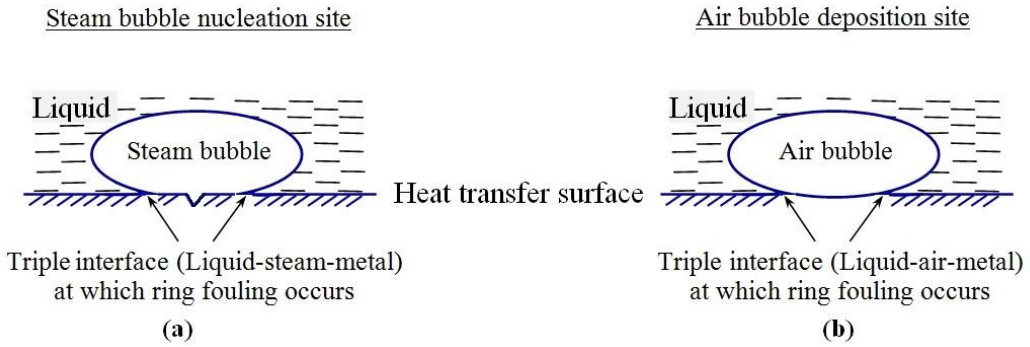

Figure 4-38 Bubble and ring fouling occurring at the triple interface
(a) nucleate boiling adopted from (Jamialahmadi et al. 1993) (b) Air bubble because of projectile injection

4.5 Technical Problems in Using Projectile

In the course of this experimental study, several technical problems occurred that need to be highlighted as they may happen in practical applications, as well.

4.5.1 Thermal shock due to cleaning by projectiles

It occurred several times that the surface temperature increased rapidly as soon as a projectile got stuck in the tube. This, in turn, causes differential thermal expansion forcing the deposit to spall off from the surface. For instance, two thermal shocks with double injections each 15 min removed deposition completely (experiment #072 with P12; velocity 1.3 m/s, surface temperature 71°C, concentration 4.6 g/L). Apart from this, operating any projectile which is likely to get stuck is risky and projectiles should be selected carefully with a save margin to sticking.

4.5.2 Metal projectiles

4.5.2.1 Brush Projectile (EX04)

The projectile consists of two parts: the front part in a bullet shape with responsibility for maintaining direction and preventing any vertical rotation in the tube. The rear part is a brush consisting of fine steel strings which are fixed by a round steel plate to the bottom (see Figure 4-39). The brush should wipe out the formed deposit while passing though the tubes. The diameter of the brush is exactly the diameter of the tube (20 mm). This metal projectile was intended for high temperature conditions. The tests of cleaning efficiency and appropriate flow velocity were selected as follows.

Before testing the projectile at fouling conditions, it was tried at ambient temperature in order to figure out the appropriate flow velocity that is required to avoid getting stuck in the tube. It was injected 35 times at 3.0 m/s but it then got stuck at the last injection. It was found that this kind of projectile tends to stick in the reducer where the diameter of the pipe reduces from 25 mm to 20 mm in the entrance area of the heated zone. This could also happen in the tube-sheet of a real heat exchanger. Figure 4-40 sketches the projectile getting stuck as it passes through the reducer. The reducer was modified from a sharp reduction to a slight slope, as shown in Figure 4-41, to make passage more probable, even though not 100%. Figure 4-42 shows the side arrangement of the projectile in the reducer before (left) and after (right) modification.

Figure 4-39 View of the brush projectile from the top side (EX04)

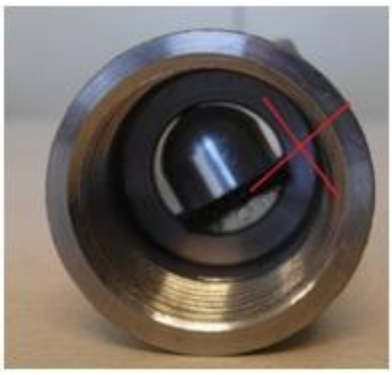

Figure 4-40 Projectile gets stuck while trying to pass horizontally through the reducer

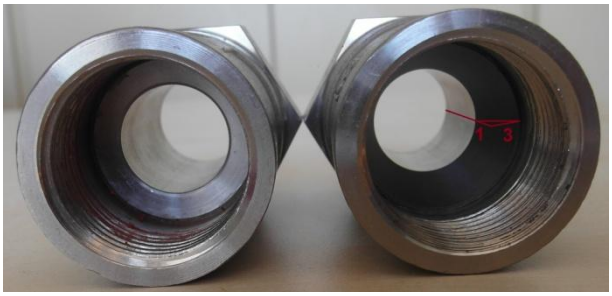

Figure 4-41 Reducers before (left) and after (right) modification

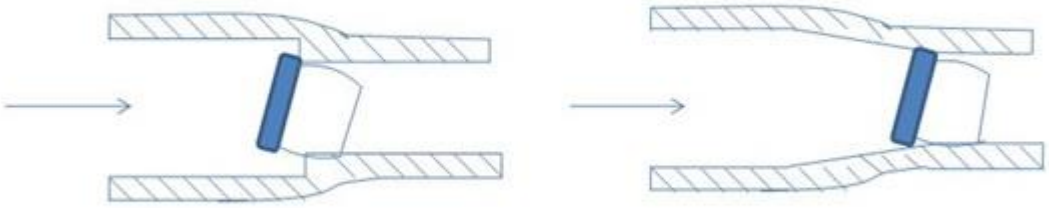

Figure 4-42 Sketch of projectile, EX04, in the reducer before (left) and after (right) modification

Then a hot experiment was carried out with injection of the projectiles every 10 minutes with a velocity of 3.0 m/s and compared with results without injection at the same velocity, in order to determine the cleaning impact. This test had to be terminated at 3h10´, only half an hour after the deposit formation had started (Figure 4-43). By testing the metal projectile with velocity 2.2 m/s, the sticking happened again at 2h30´. Figure 4-43 and

Figure 4-44 confirm that there is no variation after each injection and the tendency of deposit formation stays the same. Therefore, this projectile has no effect on deposit removal. Instead, it even worsened the deposit formation problem.

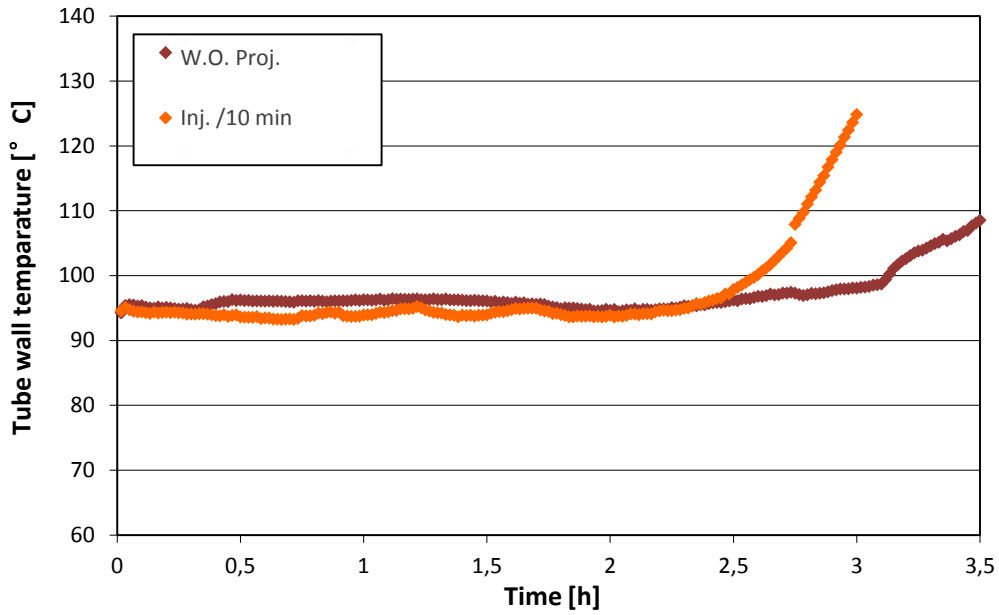

Figure 4-43 Tube wall temperature vs. time at a flow velocity 3.0 m/s
Bulk temperature 40°C, surface temperature 71°C, concentration 4.6 g/L, projectile EX04

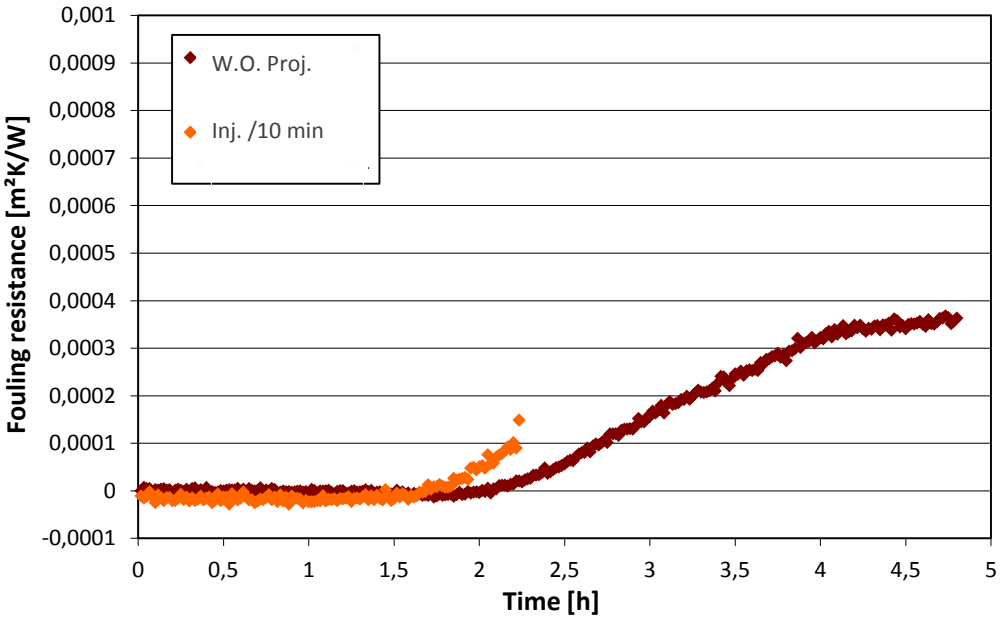

Figure 4-44 Fouling resistance vs. time at a flow velocity 2.2 m/s
Bulk temperature 40°C, surface temperature 71°C, concentration 4.6 g/L, projectile EX04

The intent of using these metal projectiles was to sustain at high temperature. Nevertheless, ever for the present conditions of using demineralized water at a bulk temperature of 40°C, the projectile got rusty and the brush bended towards the center after only 20 injections. This shows a very short lifetime (Figure 4-45) with no practicable use.

Figure 4-45 Projectile EX04 before (left) and after (right) one day of experiment

4.5.2.2 Open Spring Projectile (EX05)

The spring projectile (EX05) had a diameter of 20 mm. The potential problem of this spiral projectile was whether it can flow smoothly in the test rig. Therefore, it was tested at ambient temperature at 2.2 m/s in a straight tube. In the first injection, the projectile got stuck in the tube and then a soft projectile was injected to push it out. Instead they both got stuck together in the tube. After disassembling the piping, they were found in the middle of the pipe even though there was no groove or deposit. They were subsequently pushed out using a metal stick. The released projectile was severely twisted as shown in Figure 4-46.

Figure 4-46 Spring projectile (EX05) at different conditions
Before injection (left), sticking with the soft projectile (middle) and after removal from pipe (right)

4.6 Development of a Criterion to Compare Cleaning Performance of Various Projectiles under Fouling Conditions

A parameter is required to allow rigorous comparison of results when different projectiles are used to mitigate deposit formation. Through the observation of the experimental fouling resistances versus time only the overall quality of projectile cleaning could be obtained, but there is no quantitative value to express how much better a

projectile is when compared to others. The cleaning action of projectiles normally depends on their type in terms of size, stiffness, texture and the injection interval. Thus the cleaning efficiency is defined to quantify the performance of various projectiles. It is based on the average fouling resistance of the tube with and without (w/o) injection. Considering a given time of the experiment, the efficiency would be the relative difference of the areas with and without (w/o) projectiles in the two related curves of fouling resistance vs. time (see Figure 4-47).

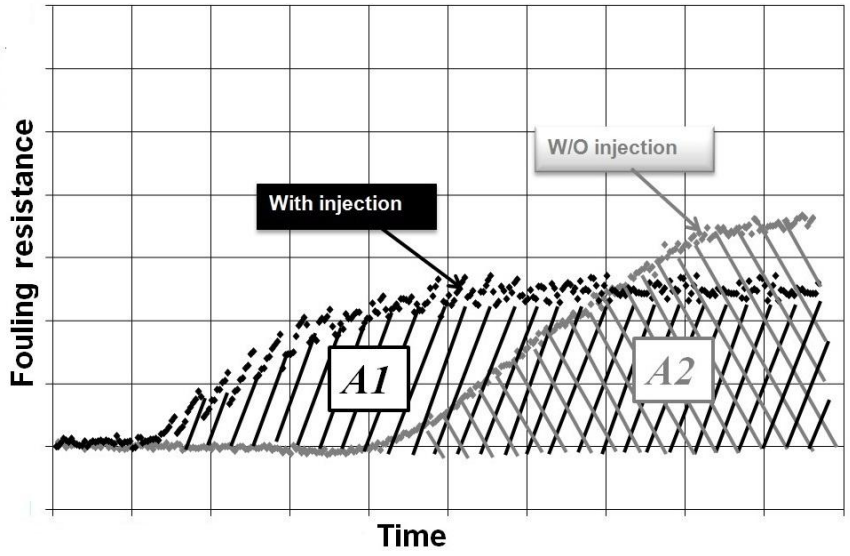

Figure 4-47 Overall efficiency (OE) of projectile cleaning, (1-A1/A2)×100

The overall efficiency (OE) can be defined as:

$$OE = \left(1 - \frac{A1}{A2}\right) \times 100 \tag{4.1}$$

where A1 is the area below the curve of fouling resistance vs. time when the projectile is injected and A2 is the area when it is not injected.

$$A1 = \int_a^b R_{f,w}\,(t)dt \tag{4.2}$$

$$A2 = \int_a^b R_{f,wo}\,(t)dt \tag{4.3}$$

Here $R_{f,w}$ and $R_{f,wo}$ are fouling resistances which can be determined from Eq. 3.1. The tube wall temperature T_w is taken where the thermocouples are embedded. The surface temperature T_s is calculated by the Wilson Plot Method (Briggs et al. 1969). Considering the Eq. 3.1 and Eq. 3.2:

$$R_f = \frac{A_i[(T_{s,f} - T_{bb}) - (T_{s,c} - T_{bb})]}{\dot{Q}} \tag{4.4}$$

$$\frac{dR_f}{dt} = \frac{A_i}{\dot{Q}} \times \frac{d(T_{s,f} - T_{s,c})}{dt} \tag{4.5}$$

This implies that the difference of surface temperature under fouling and clean condition is linearly proportional to the fouling resistance. Then:

$$\frac{dR_f}{dt} \sim \frac{d(T_{s,f} - T_{s,c})}{dt} \tag{4.6}$$

A_i and Q are constant for a series of experiments and only $T_{s,f}$ varies, thus:

$$OE = \left(1 - \frac{\sum_{i=0}^{n}(T_{s,f,w,i} - T_{s,c})}{\sum_{i=0}^{n}(T_{s,f,wo,i} - T_{s,c})}\right) \times 100 \tag{4.7}$$

where $T_{s,c}$ and $T_{s,f,w}$ denote the surface temperatures at clean and fouling conditions with injection and $T_{s,f,wo}$ is the surface temperature for fouling conditions w/o injection. Moreover "i" counts the number of recorded data during the experiment. If *OE* = 100%, then it corresponds to perfect cleaning of the surface by the projectile. For good cleaning this value should be close to 100%. However, for values far from this, one should not consider using projectiles as injection would only intensify fouling nucleation and make the induction time much shorter. This implies that mitigation should be profound at the early stage of the fouling process; otherwise the action of projectiles would be counterproductive resulting in an intensified deposition as proven before. Furthermore sometimes the efficiency could be negative, even less than -200%. This mainly occurs for loose projectiles and the ones with the exact size of the tube inside diameter. The induction time has a direct effect on areas *A1* and *A2* and the efficiency is calculated from these two areas. If the initial period is long in an experiment with projectiles it makes the efficiency close to 100%. It is also very important to note that the reported values of *OE* in section 4.8 are limited to the present test rig and the investigated operating conditions.

4.7 Tribological Analysis of Various Projectiles

As shown before the stiffness and size of projectiles, i.e. physical properties are important in asserting whether a projectile is effective or not. Thus several projectiles of spherical shape with various sizes and stiffness were investigated as specified in Table 4-3. The stiffer and larger projectiles show better cleaning as long as they could be propelled through the tube. Accordingly, the diameter of the projectile has been selected carefully to

cover a wide range of operating conditions. The largest, P10, was 15% bigger than the inner diameter of the tube but soft enough to pass through the tube. The reported contact areas were simply measured in a transparent tube with similar inner diameter to that of the metal tube (20.0 mm) which is used in the fouling experiments. This contact area here is called dynamic contact area as will be explained later. In order to select a suitable projectile among various with different stiffness, two distinctive but interrelated shear forces are required i.e. dynamic and hydrodynamic. In combination with stiffness measurements, they would imply whether a projectile is suitable or not. In this study, force, shear and contact area with subscript "dynamic" represent the dynamic movement of projectiles in the tube under a mechanical force with a tensometer. Parameters with subscript "hydrodynamic" correspond to the movement of projectiles in the tube under the force of flow. In what follows, we first define soft and hard projectiles based on stiffness measurements then dynamic and hydrodynamic shear will be measured.

Table 4-3 Specifications of investigated projectiles for stiffness measurements

Projectile ID	Diameter mm	Dynamic force, F_{dyn} wet, N	Dynamic contact area, A_{dyn} mm^2	Dynamic shear force τ_{dyn} pa
P01 	21.0	1.9	132.1	14,199
P02 	22.0	20.8	277.3	75,010
P09 	22.0	14.1	277.3	21,637
P10 	23.0	15.8	436.4	36,208
P11 	20.0	negligible	negligible	negligible
P12 	20.2	23.7	25.4	932,313

4.7.1 Dynamic shear force test

The dynamic force was measured when a projectile was mechanically pulled through a tube by a tensometer as shown in Figure 4-48. Shear forces at wet conditions, i.e. when water was present inside the tube, were measured by the tensometer with a constant dragging velocity. Wet condition provides environments similar to actual practice of injecting projectiles in a heat exchanger. A cap was placed in the back of the projectile to apply consistent and uniform loads as it is shown in Figure 4-48(a). A string was used which passed through the projectile and is connected to the cap on one side while the other side is connected to the tensometer as illustrated in Figure 4-48(b). The string was flexible enough to dampen any peak force if the operator pulled it abruptly. The test was carried out for different velocities but except for the minimum velocity required for the initial

motion, the tensometer always showed similar values. They imply that the required force was independent of velocity when the projectile moves inside the tube. The measured force was called "dynamic" because as it represents the dynamic movement in the tube by a mechanical force. Thereafter the shear force can be calculated according to Eq. 4.8, which is the standard calculation of force over contact area.

$$\tau_{dyn} = \frac{F_{dyn}}{A_{dyn}} \tag{4.8}$$

where F_{dyn} denotes the mechanical force obtained by the tensometer and A_{dyn} was the measured contact area found by putting the projectile in a transparent tube with the size of the metal tube. The results of the dynamic tests are given in Table 4-3. As expected larger and harder projectiles would require more dynamic forces to be pulled through the tube and thus would produce larger shear. As it can be seen in Table 4-3, the surface contact area for P02 is approximately 100% larger than for P01. Furthermore, as P02 is harder and bigger compared to P01, it can produce a shear which at least 500% higher than that of P01. While P12 has a relatively small diameter but is characterized by the largest stiffness it still exerts the largest dynamic shear. Larger projectiles which would have larger contact area are presently under investigation. It should be pointed out that there is no limit to using larger projectiles as long as operating conditions, i.e. the pressure drop across the exchanger, allow the proper operation.

Figure 4-48 Tensometer to measure the required force to pull the projectile through the tube

4.7.2 Hydrodynamic force test

An experimental setup is constructed as schematically shown in Figure 4-49. A long tube with inner diameter of 20.0 mm was equipped with a pressure transducer, a flow-meter for measuring velocity and also a facility for injecting the projectiles into the tube. The pressure transducer was model DPX101 Series of Omega, which was sensitive to read the pressure every 1 μs, even though it was only recorded every 0.5 s because of limitations of the data acquisition program. The maximum error associated with the

pressure transducer occurs close to absolute vacuum and is ±50 Pa. The normal frequencies of the pressure signal for flow were ±70 Pa. The flow was pumped into the system and then discharged to the ambient in order to avoid long piping with many connections and fittings that would otherwise influence the measured pressure. Fewer piping provides lower pressure losses, and thus the propulsion of projectiles at lower velocities is possible. This allowed that even hard projectiles could be shot at small velocities through the devise. The effective length of the tube is 2250 mm. The projectile is shot through the tube by the flow while the pressures behind the projectile and the respective flow velocity are recorded. Considering the cross-section of the tube, the gage pressure behind the projectile represents the required force for pushing it by the flow if the head loss of the tube is ignored (pressure loss is 700 Pa for the tube length 2250 mm and flow velocity 0.4 m/s). If this hydrodynamic force is divided by the contact area between projectile and tube then the respective shear force can be determined as:

$$\tau_{hyd} = \frac{F_{hyd}}{A_{hyd}} = \frac{p_g A_c}{A_{hyd}} \tag{4.9}$$

where 'p_g' is the gage pressure behind the projectile when the projectile passes through the tube and it could be calculated from the logged absolute pressure 'p' by pressure transducer. A_c is the cross-section of the tube and A_{hyd} is the contact area between projectile and tube under the force of the flow. A_{hyd} cannot be measured directly like A_{dyn} as it has to be measured while the projectile is moving and the flow is unstable.

To obtain reliable and consistent experimental results only projectiles that can move with similar minimum velocity have been chosen. For this reason, P01 was not selected as it was soft and required a much lower velocity than the others. Accordingly, the minimum flow velocity is adjusted at 0.4 m/s for the propulsion of projectiles P12, P02 and P10 without the risk of getting stuck inside the tube. Under normal operation with further piping and fittings, hard projectiles would need higher flow velocity. Nevertheless due to a small head loss for this particular experimental setup, even the hard projectiles can move at a velocity of 0.4 m/s.

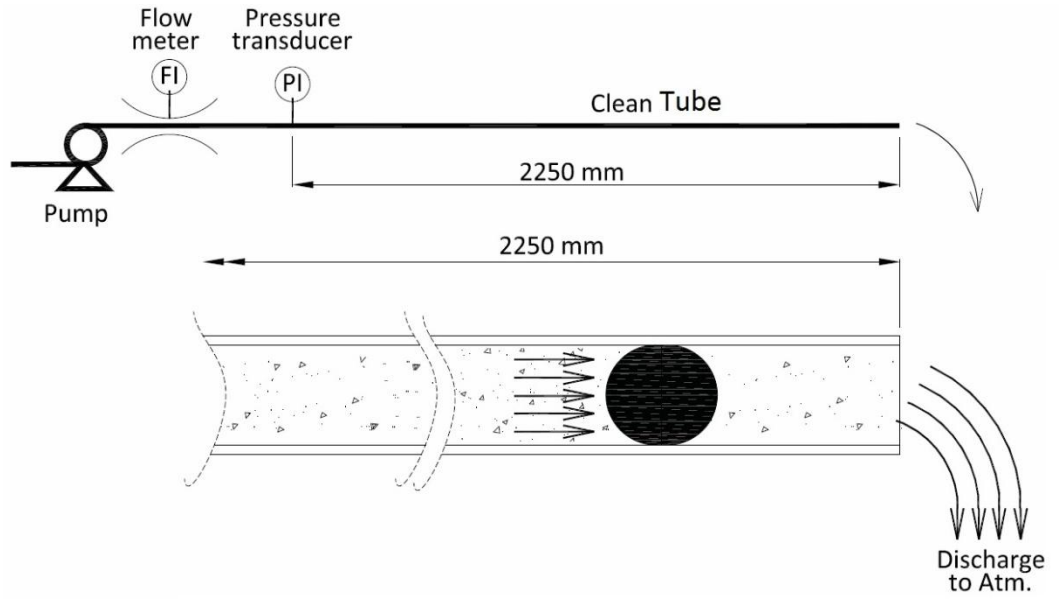

Figure 4-49 Sketch of the rig to measure hydrodynamic shear stress.

In the second set of experiments, the projectiles were propelled through the tube as explained before with a flow velocity of 0.4 m/s while the pressure is being logged. Due to the fast movement of projectiles at higher velocities, visualization would be difficult, and thus experiments at higher velocities were not attempted. The recorded pressure was the atmospheric pressure plus the head loss of 2250 mm tube plus the required pressure to overcome the friction between the tube and the projectile. The head loss for the tube and the atmospheric pressure were constant for the investigated projectiles. If the head loss of tube is ignored, the gage pressure behind the projectile represented the required force for propulsion of each projectile which was expected to vary based on stiffness.

Figure 4-50 shows the variation of the recorded absolute pressure and flow velocity vs. time for P02, P10 and P12 for the minimum flow velocity of 0.4 m/s. The projectiles were tested several times showing a repeatability of about 90%. Moreover, the velocity was quite stable. In this figure, the pressure fluctuations for P12 are greater than for P02. The large fluctuations for P12 imply high stiffness and poor contact area with the tube. Although P12 is characterized by the larger stiffness, it does not have continuous contact with the tube. The pressure results seem to indicate that P12 sometimes slides without any effective contact. The same experiment is repeated for P10. As it is much softer, no noticeable fluctuation in pressure is observed. The average absolute pressure to push projectile P02 is 1.36 bar while for P10 it is 1.18 bar. The pressure cannot be averaged for P12 due to the large fluctuations and was hence not reported here.

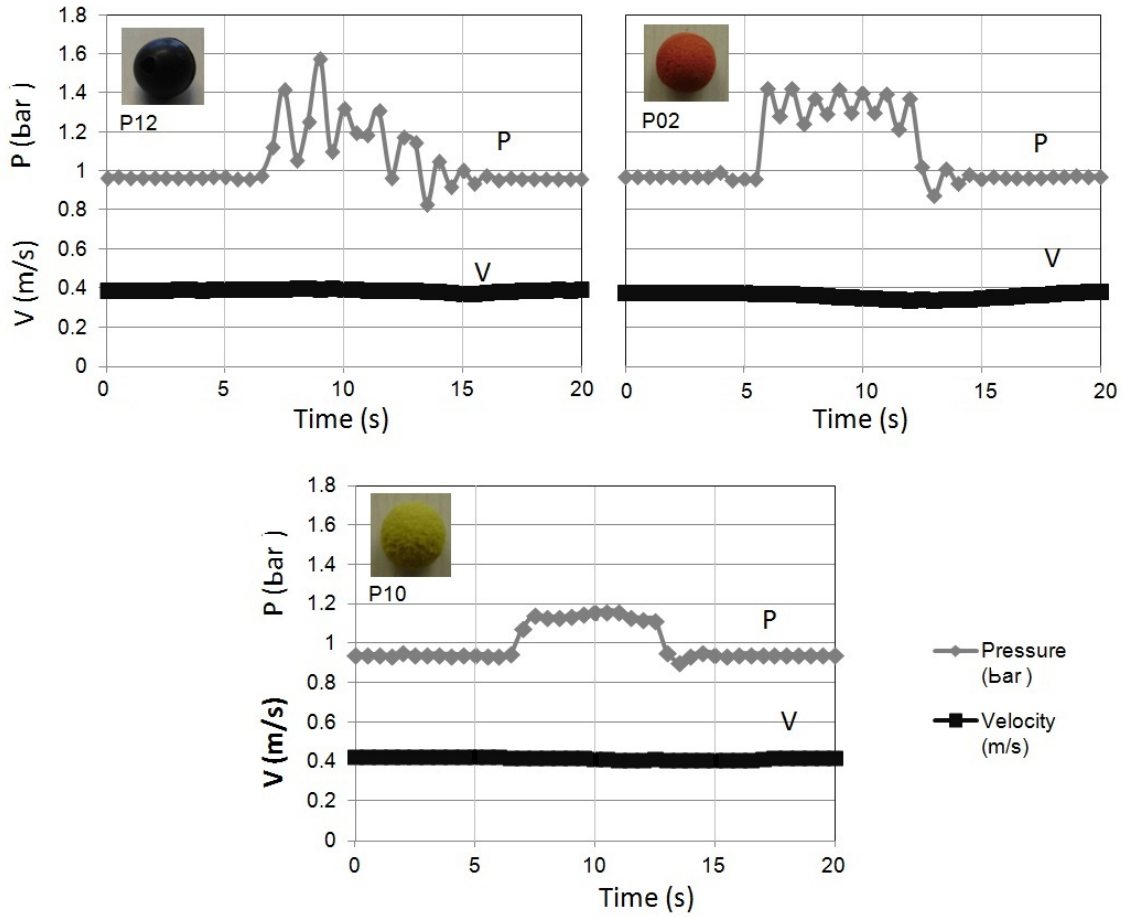

Figure 4-50 Fluctuation of absolute pressure (*p*) behind the projectiles and fluid velocity for P02, P10 and P12.

4.7.3 Ideal projectiles and contact stability (Z factor)

The softer the projectile, the lower would be the pressure fluctuation, as demonstrated in Figure 4-50. To combine the tribological results, a new parameter "surface contact stability" was defined which will simply be referred to as "Z factor" hereafter. The ratio of hydrodynamic and dynamic forces is:

$$\frac{F_{hyd}}{F_{dyn}} = \frac{p_g A_c}{\tau_{dyn}.A_{dyn}} \tag{4.10}$$

$$\frac{F_{hyd}}{F_{dyn}} = c\frac{p_g}{\tau_{dyn}} = c \times Z \tag{4.11}$$

Where:

$$c = \frac{A_c}{A_{dyn}} \tag{4.12}$$

Once A_c and A_{dyn} are known then c will be constant for each specific projectile. It is a parameter representing the geometrical features of the projectile with respect to the tube. The values of p_g and τ_{dyn} can be measured as explained before. Figure 4-51 compares these two values both quantitatively and qualitatively. These two values are closer together and p_g fluctuates less for softer projectiles. In addition, the resulting τ_{dyn} for P12 is almost 8-times larger than p_g while it is only 20% higher for P10. Eq. 4.11 shows that Z is proportional to the ratio of hydrodynamic and dynamic forces.

τ_{dyn} is a reference for the amount of exerted shear force in the ideal case, but p_g shows how stable the projectile moves in the tube with flow. Large fluctuations indicate that the projectile does not have a uniform contact with the tube and hence cannot exert a uniform shear force. Thus the ratio of these two parameters (p_g and τ_{dyn}) characterizes the contact stability. Based on what has been discussed above, an ideal projectile can be introduced as one where p_g is closer to τ_{dyn}, or $Z \rightarrow 1$, because this means that the projectile has the maximum contact area with the tube. As already discussed in section 4.3.1.2 before, contact area is a main parameter for the cleaning performance. Figure 4-51 shows that these two values differ to a great extent for P12 which underlines two facts, i.e. i) the pressure under the force of the flow fluctuates more for stiffer projectiles and ii) for softer projectiles the difference between the dynamic and hydrodynamic forces is small. This would, in turn, explain why the cleaning performance of hard projectiles is not better than of soft ones. The results indicate that the loss of contact with the surface while moving is the principal reason for the poor cleaning action of the hard projectiles.

Visualization of projectile movement inside a transparent tube confirms that P12 moves, then momentarily stops, before slipping over the surface for a short distance. This phenomenon repeats itself and explains the high pressure fluctuations in Figure 4-51. Listed below are various hypotheses as to why this should occur, which require further research:

- Leakage of fluid around the projectile while it is moving: For P12 the contact between tube and projectile is very pointed and thus leading to by-pass flow through the conjunction. A soft/big projectile has a flatter contact area, and consequently reduces the probability of flow between tube and projectile.
- Compression toward the projectile center; it is also probable that the pressure of flow reduces the volume of the projectile or deforms it longitudinally, so it passes easier through the tube. Pressure in the tube is higher than atmospheric pressure and this compresses the projectile anyway.

- Porosity of projectile; for porous projectiles the deviance is less, because flow passes through the projectiles and not through its contact with the tube, and also it avoids more compression.

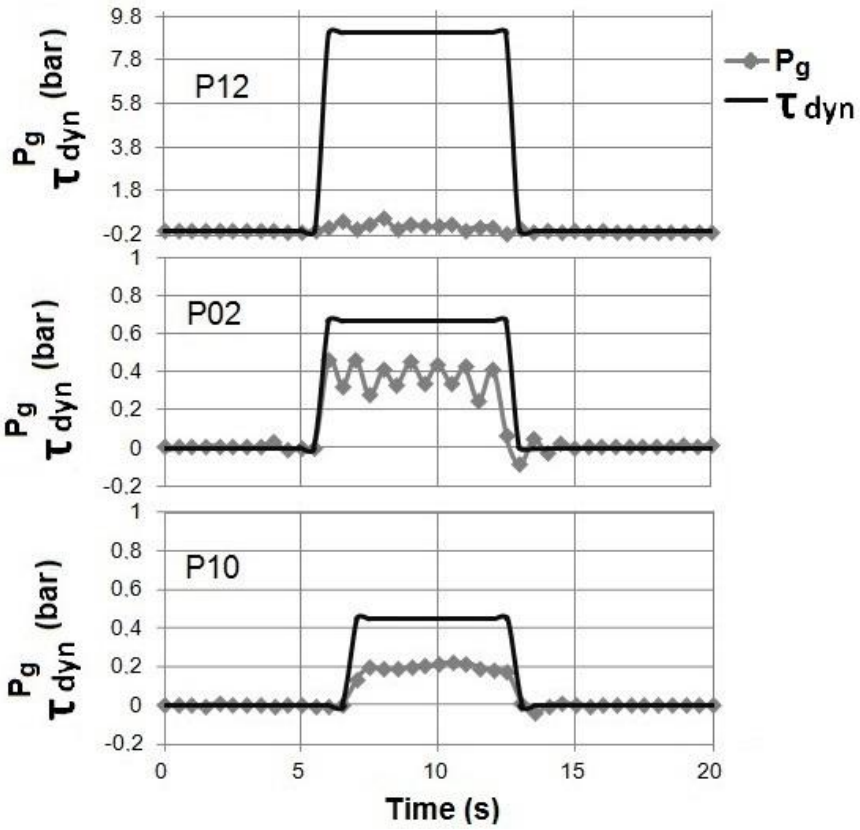

Figure 4-51 Results of p_g and τ_{dyn} for 3 projectiles (P02, P10 and P12)

Figure 4-51 exemplifies how to calculate the Z factor as the ratio of p_g/τ_{dyn}. For example it could be 0.85 for P10. After repeating the experiment to prove repeatability it turned out to be 0.9. It is still a question which parameters influence the Z factor. The velocity of flow would be a potential parameter that may influence this factor. However, the repeated experiments show that the dynamic force is independent of the velocity at which the projectile is pulled through the tube by the tensometer. Nevertheless, there has been no experimental proof if the pressure fluctuations are independent of velocity or not. This would require a large laboratory which can accommodate long piping so that the movement of the projectiles can be tested at higher velocities. The results presented here are, nonetheless, for the minimum velocity that is required to propel the investigated projectiles P02, P10 and P12 in the tube without the risk of getting stuck, as otherwise the results would not have been comparable. As the Z factor mostly presents a physical characteristic of the projectile which indicates how effective the exerted force on the tube is, it is recommended that a standard procedure for measuring this parameter should follow.

The Z factor explains to some extent what would occur at the tube/projectile interface when the projectile passes through the tube. P12 exerts a dynamic force which is about 12 times larger than the hydrodynamic force while it is only 1% larger than the tube inside diameter. This means that stiffness has a direct effect on applying shear under dynamic movement even when its contact with the tube is small, because stiffer projectiles are pushed more strongly at the surface of the tube and cause more intense contact and hence require more shear force for pushing. For movement by flow (hydrodynamic pushing), it is completely different. A reason for this difference is the uniform force by the flow behind the projectile and flow by-pass escaping from the gap between tube and projectile, which reduces the contact. This contact under propulsion force of flow (hydrodynamic pushing) is instable and it is considerably smaller than mechanical pushing (dynamic pushing).

4.7.4 Effect of stiffness on contact stability

A selected number of projectiles were examined at the Institute of Polymer Technology (IKT) in the University of Stuttgart to measure their stiffness. Based on standard test procedures for such measurement, five samples of each P02, P10 and P12 having different stiffness and sizes are selected for the tests as listed in Table 4-4. P01 is soft with a diameter 5% larger than the tube. P02 is harder, but not as much as P12, with a diameter 10% larger than the tube. P12 was the hardest, thus its size could not be larger than +1% of the inner tube diameter. P01 and P02 are referred as soft and P12 as hard projectiles. They are tested by a Zwick universal stiffness testing machine (model ZPM 1455). For the stiffness test procedure which is recommended by IKT, stiffness would be independent of diameter in the range of ±10% of projectile sizes.

The tests are conducted such that the projectiles are clamped and then loaded from above with a plate (see Figure 4-52). This is carried out for conditions listed in Table 4-4. The percentage of deformation of the initial diameter is plotted versus the applied force for each projectile. Then the applied force for 50% of deformation is reported as a measure to characterize the stiffness.

The parameter α represents the relation of force and deformation based on Hooke's law:

$$\alpha = \frac{x}{\varepsilon} \tag{4.13}$$

with:

x = Average force of each attempt on projectile [N]

ε = Deformation [%]

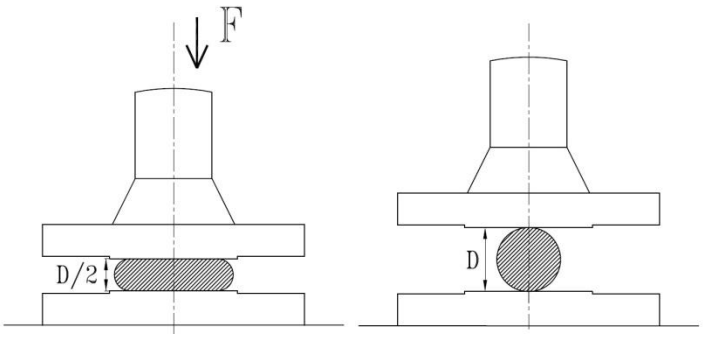

Figure 4-52 The arrangement to measure the hardness

Table 4-4 Parameter settings compression test

Parameter	Setting
Test standard	DIN EN ISO 3386-1
Climate	DIN EN ISO 291-23/50-2
Sample pretreatment	Storage in standard atmosphere DIN EN ISO 291-23/50-2
Force transducer	1 kN
Transducer	Traverse
Sample holder	plates
Test speed	100 mm/min
preload	0.5 N

The results show that for the same force exerted, P12 has the smallest deformation while P01 has the most severe deformation. In comparison with the tube inner diameter (20 mm) the maximum deformation during the fouling experiments can be as much as 15% ($D_{proj.}/D_{tube}$), which shows that the testing range of 50% ($D_{proj.}/2$) is definitely in the range of practical application.

The stiffness tests were intended to provide information on how deformation takes place when curves for load versus deformation are plotted. Projectiles were loaded until a compression of 50% is reached, meaning the projectiles retained 50% of their initial diameter at the end. The force exerted on the projectile over deformation has an approximately linear shape, as shown in Figure 4-53. As five samples of each projectile are tested, each plot contains five curves.

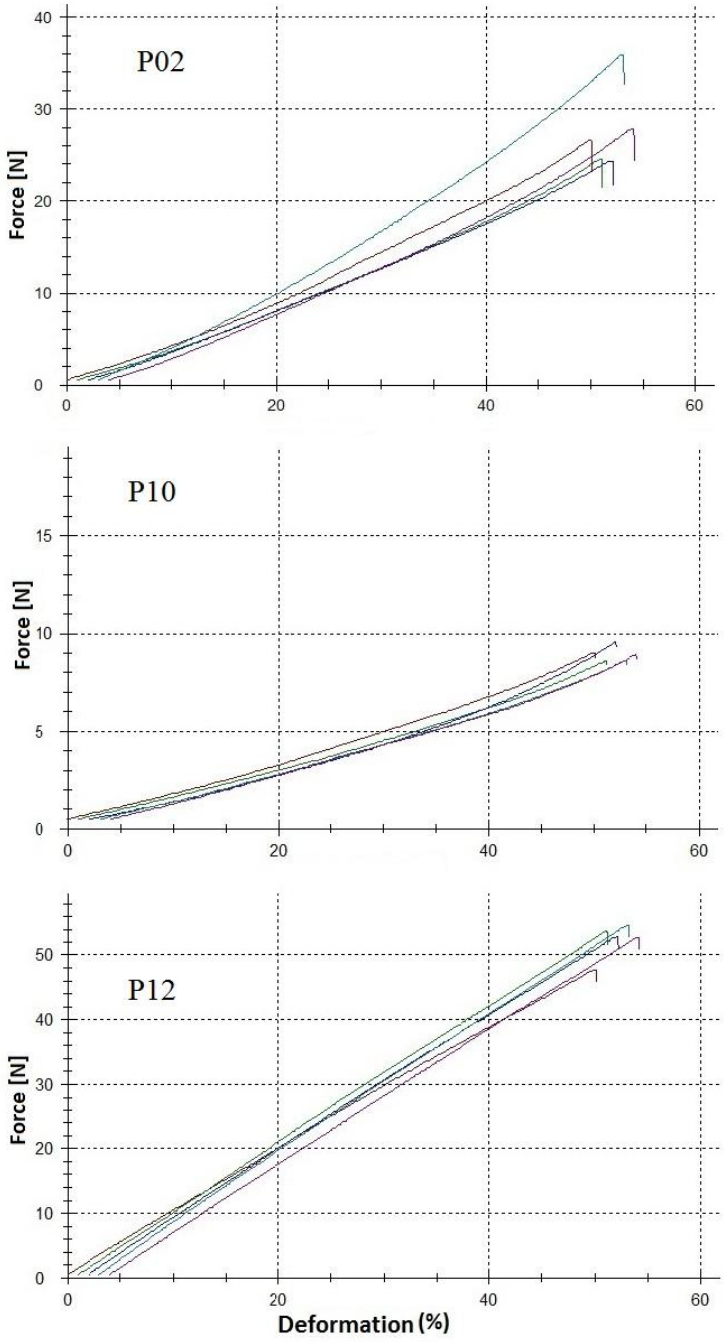

Figure 4-53 Diagram of compression test for P02, P10 and P12

The graphs are close to linear. 50% deformation fully covers the range of deforming that practically happens for a projectile during injections. The percentage of deformation in the linear range is a good criterion to compare the stiffness of different projectiles. This linear range mostly appears in the first 50% deformation as the standard method of experiment is also set. In Table 4-5 the statistics of the stiffness tests for P02, P10 and P12 are listed.

Table 4-5 Statistics test series of P02, P10 and P12

Projectile	P02		P10		P12	
	force F by ε 50%	ε	force F by ε 50%	ε	force F by ε 50%	ε
	N	%	N	%	N	%
x (mean)	27.9	49.98	8.9	50.01	52.3	50.04
s (standard deviation)	4.7	0.06	0.4	0.10	2.7	0.04
v (variation coefficient)	16.97	0.12	4.68	0.20	5.09	0.07

Assuming linearity it can be calculated from this data, how much force in average is required to deform the projectile by 1%., i.e. for projectile P02 it is:

$$\alpha_{P02} = \frac{x}{\varepsilon} = \frac{27.9\ N}{50\%} = 0.558\ \frac{N}{1\%\ deformation}$$

4.7.4.1 Comparison of stiffness test results

In Figure 4-53, the gradual increase in loaded force to 50% deformation reflects the projectile stiffness. For rubber projectile P12, forces are ranging from 48 to 54 N. Soft sponge projectile P01 has the weakest stiffness, as forces range from 6 to 10 N. Sponge ball P02 is the intermediate among the three investigated projectiles with forces of 22 N to 24 N. The loaded force stops compressing the projectile further when deformation is beyond 50%. This results in small abrupt drops at the end of the curves. The average deformation results of each 5 samples are listed in Table 4-6. The table shows that P02 and P12 are 3.1 and 5.8 times harder than P01 while P12 is only 1.9 harder than P02. Some other data such as contact area, porosity and stiffness for these three projectiles are indicated in Table 4-7, as well.

Table 4-6 Stiffness factors (α) for different projectiles

Stiffness factor (α)	Value [$\frac{N}{1\%\ deformation}$]	Relative magnitude
α_{P01} and α_{P10}	0.178	1
α_{P02}	0.558	3.135 * α_{P01}
α_{P12}	1.040	5.843 * α_{P01} 1.864 * α_{P02}

Table 4-7 Physical features, contact area, porosity and stiffness for P12, P02 and P10

Proj. ID	Diameter mm	Dynamic Drive Force (wet) N	Contact Area mm²	τ wet pa	Porosity %	Stiffness N/[1% Def.]
P12	20.2	23.7	25.4	932,313	0.9	1.04
P02	22.0	20.8	277.3	75,010	7.9	0.558
P10	23.0	14.1	436.4	36,208	18.4	0.178

Returning to Figure 4-51 it can be found that contact stability is lower for stiffer projectile. Figure 4-54 indicates that more contact stability is associated with the softer projectile.

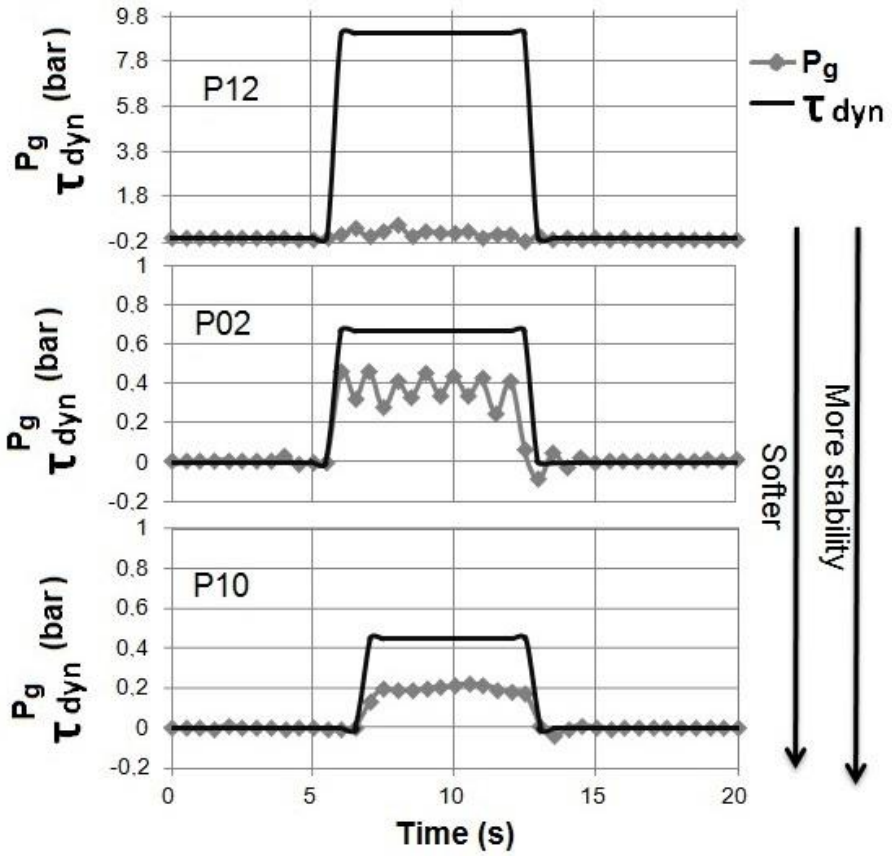

Figure 4-54 Contact stability with tube for 3 projectiles (P02, P10 and P12) with different stiffness

Figure 4-55 shows the variation of *Z* factor vs. stiffness. This figure indicates that for a range of stiffness between 0.2-0.5N per 1% of deformation, the contact stability is constant in the order of 0.9, while for stiffer projectiles it decreases sharply. Thus, if the projectile is stiffer than 1.0 N per 1% of deformation, the stability would be even less than 10%. It is important to note that the tested projectiles were not of identical size but in a size to be passed at a minimum velocity of 0.4 m/s. Due to the short length of the tube, passing hard projectiles was possible if the flow is discharged into the atmosphere.

Based on Figure 4-55, a force of 0.5 N per 1% of deformation is taken as the threshold to distinguish between soft and hard projectiles when the *Z* factor is less than 0.8. For a secure passage of projectiles with a normal velocity like 1.3 m/s, a projectile as hard as P12 is just 1% larger than the inner diameter of the tube. As discussed in section 4.3.1.2, it has the potenciality of sticking. However, soft projectiles may be even more than 5% larger than the inner diameter of tube. It is recommended not to produce any projectile

between these two ranges, as i) they do not have sufficient contact area or ii) they do not exert enough shear or iii) they cannot pass through the tube. Hard projectiles need more force of flow to avoid getting stuck if fouling occurs.

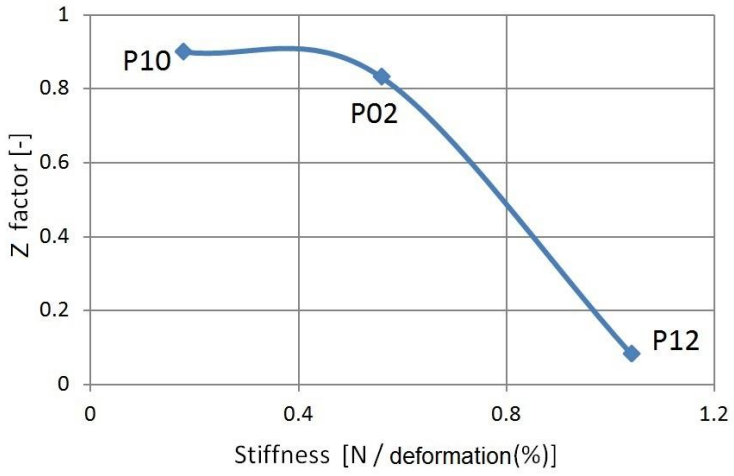

Figure 4-55 Z factor vs. stiffness

Figure 4-56 shows the variation of the ratio of projectile compression with respect to the minimum flow velocity that is required for secure passage. Soft projectiles can be compressed more than hard ones but require lower velocity for propulsion. Contrariwise, a hard projectile compresses less but requires higher velocity. In other regions identified with "non applicable", the utilization of projectiles may be problematic as they either get stuck or can move but with low exerted shear on the tube surface. Moreover, the hard projectiles produce high shear but with lower surface contact stability whereas the soft projectiles produce low shear but with high contact stability. In Figure 4-56 areas of soft/hard projectiles based on the diameter and minimum required velocity of flow for propelling the projectile inside the tube are identified, considering a safe margin for sticking. P11 and P04 are located in the non-applicable area.

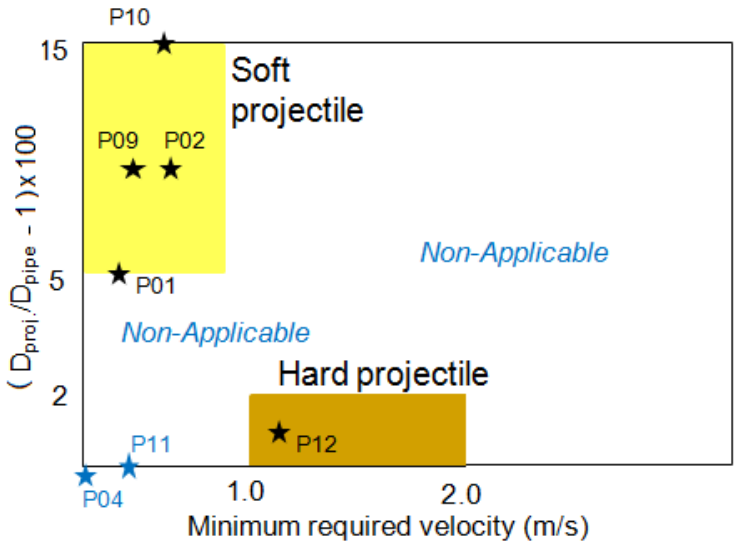

Figure 4-56 Applicability of soft/hard projectiles based on the diameter and minimum required velocity

4.8 Criterion for the Selection of Efficient Projectiles

15 experiments with projectiles of different stiffness and sizes were carried out under fouling conditions. Different injection intervals have also been attempted to find out the optimum diameter and stiffness which corresponds to the best cleaning performance. The summary of the findings is given in Table 4-8.

Table 4-8 Efficiency of various projectiles for different injection intervals

Proj. Code	Diameter mm	Drive Force (wet) N	Contact area mm²	τ wet pa	OE% inj/5 min	OE% inj/10 min	OE% inj/15 min
P01	21.0	1.9	132.1	14,199	40 v=0.8		
P02	22.0	20.8	277.3	75,010	80 v=0.8 m/s	60 v=0.8 m/s	10 v=0.8 m/s
P04	19.8	loose	loose	0	-60 v=1.3 m/s	-300 (Stuck)	
P05	24.0		609.9		Projectile was torn after 29 injections		
P11	20.0	negligible	negligible	negligible	0.0 v=1.3 m/s	-210 (Stuck)	
P12	20.2	23.7	25.4	932,313	60 v=1.3 m/s	-60 v=1.3 m/s	-220 v=1.3 m/s

As can be seen, P02 has the best efficiency. The hard projectiles P04, P11 and P12 from the same material but with different sizes of 19.8, 20.0 and 20.2 mm were also examined. Only P12, which has a small contact area with the tube, had a better efficiency among them. The loose projectiles as well as those having a similar size as the tube inner diameter are not expected to clean in an appreciable manner. This also means that they may even intensify deposit formation and that they are liable to get stuck in the tube. P05 is a soft projectile and 20% larger than the tube inner diameter, but its life time was short because of severe deformation while passing through the tube. This indicates that getting stuck is

not as much of a problem for soft projectiles as they are 20% larger than the inner tube diameter. It was observed that criteria such as head of flow, pressure loss in piping, length and roughness of tube, and also velocity of flow have an impact on sticking. Also, soft projectiles have a wider margin in size to stick than hard projectiles. In other words they are less likely to stick in case of decreasing flow velocity, increasing tube roughness due to deposit or even deposit build-up. The threshold before sticking is important and it should be wide enough, because the surface of a new tube is smooth and projectiles may passes easily, but problems may occur when the deposit forms, resulting in a roughened surface and a reduced cleaning efficiency.

The experimental results for P01, P02 and P12 are also presented in Figure 4-57 in terms of efficiency versus exerted shear force. The figure shows that applying a higher shear force does not always mean that the projectile has a better cleaning performance. Quite opposite, it is the projectile size that may have a much stronger impact. Size implies the extent of contact area between the projectile and the tube. In Figure 4-57, the positions of three projectiles based on size or efficiency versus applied shear force are specified. These three projectiles represented soft (P01), medium (P02) and hard (P12) balls, respectively. As can be seen the most efficient projectile is P02. The optimum efficiency is represented by the dashed curve relating to the "efficiency axis" on the left side. The optimum size is also depicted by the solid curve to the right axis to show how much the projectile is bigger than then tube.

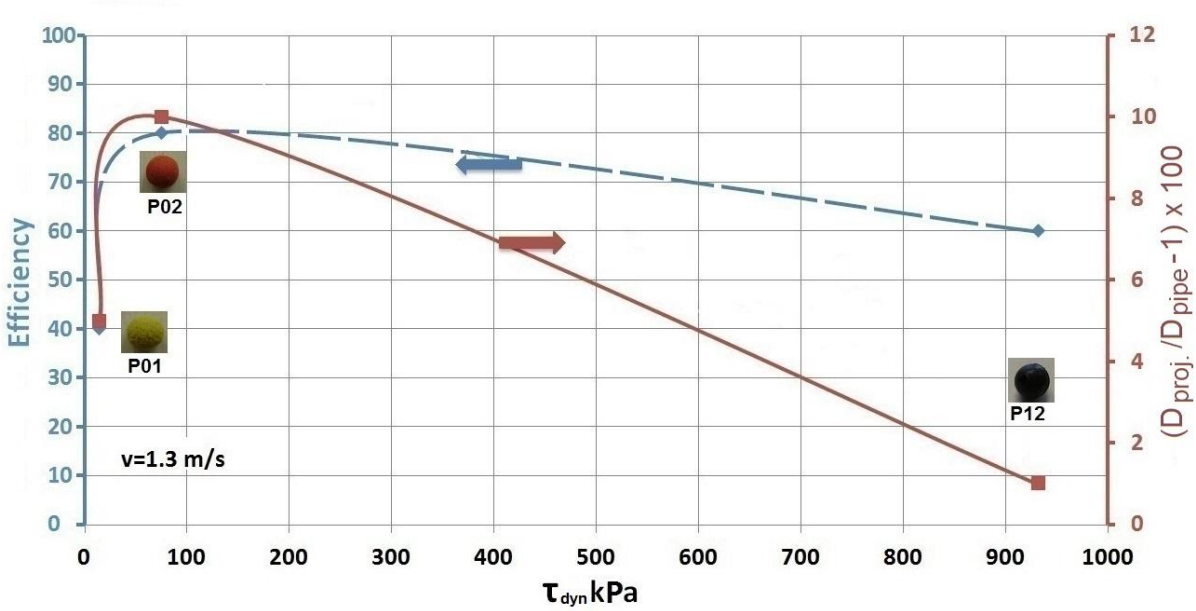

Figure 4-57 Efficiency based on the exerted dynamic shear and contact area, results from Table 4-8

As shown in Table 4-8, hard projectiles exert much higher shear forces even 12 times higher than soft projectiles though their cleaning efficiency is not much better than for the softer ones. It is already proven that the reason is the instability of the contact with the tube. Hard projectiles exert much higher shear forces on the surface during mechanical

pushing, but under the propulsion force of flow there is no remarkable shear due to less and unstable contact between projectiles and tube. This can be represented by the contact stability factor, *Z*, which is less than 0.1 for hard projectiles like P12 and between 0.8 – 1.0 for soft projectiles like P01 and P02 as it is indicated in Figure 4-55. It has also been shown that the *Z* factor is a function of stiffness. A disadvantage of hard projectiles is their possibility to get stuck in the tube which is more likely than for soft projectiles. At the same time, projectiles should not be too soft either, since then they cannot exert enough shear for cleaning. This means there is an optimum stiffness for the best cleaning efficiency.

Apart from stiffness, another parameter which plays an important role for cleaning is the projectile size. The results in Table 4-8 demonstrate that projectiles with more contact area have better cleaning efficiencies. When the projectile is large, it will have more contact with the tube, and thus better cleaning is expected. Nonetheless, there are also some limitations in size too, i.e. sticking probability and the life time of projectiles under continuous deformation. This implies that there is an optimum area for projectile size as well. Attempts were consequently made to develop a graph to select the most efficient projectiles based on stiffness and size. Since the exerted shear force by projectiles is directly related to the stiffness, the horizontal axis in Figure 4-57 was substituted by the stiffness. This makes more sense from the experimental point of view.

Figure 4-58 shows the optimum size and stiffness for the best cleaning performance. The specified box of ABCD signifies the optimum size and stiffness. It means that projectiles 10% bigger than the tube could be the most efficient even if they are hard enough as to deform just 1% under an average 0.6 N force. In general, this figure shows that using soft projectiles is more advantageous.

Another criterion to discern how efficient a projectile is, is the ratio of fouling resistance with and without projectile injection in the asymptotic region ($R^*_{f,w}/R^*_{f,wo}$). In this investigation, the tube diameter, heat flux, flow velocity and size of projectiles are similar to industrial application. For example cases where this ratio is less than 0.2 could be considered a good efficient cleaning in industry and enormously reduce the costs (see Table A-1 in Appendix A). It is predicted that this ratio is depended upon the mechanism of deposit formation, flow velocity and rate of injection, so it can be extended to industrial scale. An equation (Eq. 5.20) is presented in Chapter 5 to express this ratio. Fouling resistances for various fluid streams are reported in heat exchanger books e.g. CRC Handbook of Energy Efficiency (Kreith, F. et al. 1996). The most common compilation of fouling resistances as a design factor, for a variety of fluids in various applications, is supplied by the Tubular Exchanger Manufacturers Association (TEMA) 9th Edition (2007), section 10, part RGP-T-2.4. These values can, to some extent, determine the size and construction cost of heat exchangers. Thus $R^*_{f,w}/R^*_{f,wo}$ can give a better guidance to heat exchanger engineers.

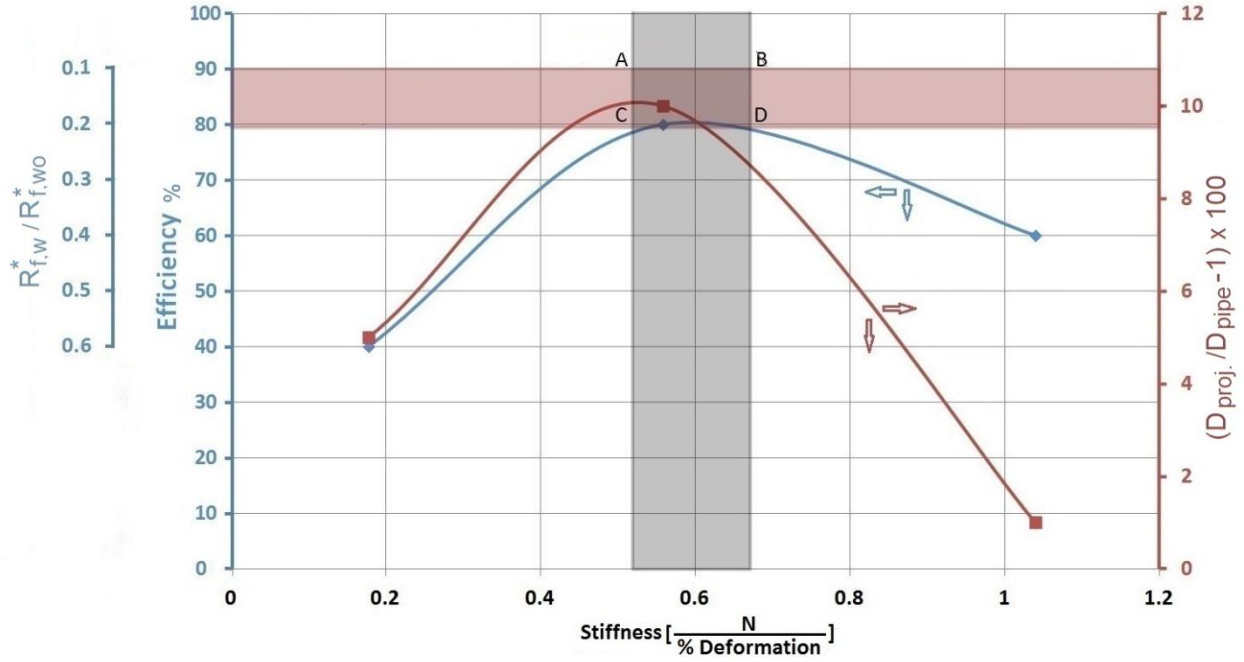

Figure 4-58 Efficiency, ratio of asymptotic fouling resistances with and w/o injections and contact area as function of stiffness

5 THEORETICAL STUDY

Chapter 4 presented experimental results on the performance of various projectiles for mitigating fouling. The experimental findings highlighted that due to projectile injection the asymptotic region was reached quicker compared to the case with no injection. Thus its prediction is imperative from a practical point of view. There is also no model available in the open literature. In this chapter a new model will be proposed to predict the asymptotic fouling resistance when the projectiles are injected. The development of a model to cover other regions i.e. induction and transition is even more complex. This, though, was not attempted as the present study was part of a European project and industrially-oriented. Thus, the focus was on the region where fouling may last for a long time i.e. the asymptotic region.

5.1 Kern and Seaton Model (1958)

Kern and Seaton (1958) proposed a model that describes the process of fouling as function of time. They observed that after an initial period the fouling resistance tends to reach an asymptote. Crystallization fouling of calcium sulfate dehydrate, which is investigated in the present study, also has a feature in which after an initial period of fouling build-up, the fouling resistance tends to remain constant. Since the highest possible wall temperature of the investigated tube was T_w=300°C (see section 3.1.3), fouling curves without projectile injection in this study did not reach to a complete asymptote.

The same fouling propensity at elevated wall temperature was also observed by Bohnet et al. (1997). They performed some experiments with calcium sulfate solutions for a surface temperature of 75°C using an annular test section and showed at a velocity of more than 0.2 m/s the asymptotic fouling resistance. Mori et al. (1996) reported that asymptotic fouling resistance and deposition rate decrease with increasing velocity. They used an electrically heated annular heat exchanger and calcium sulfate dihydrate as solution. Mwaba et al. (2001) also investigated the influence of surface temperature and fluid velocity for calcium sulfate scaling on a heated plate. They provided a table for the asymptotic fouling resistance at different velocities (maximum 0.6 m/s). Middis et al. (1998) performed several experiments with the same solution at a surface temperature of 55°C and a concentration of 3.6 g/L for different velocities between 0.4 m/s – 0.8 m/s. They have provided a graph indicating that the fouling resistance becomes asymptotic within 3 days for 0.6 m/s, and 6 days for 0.8 m/s.

The asymptotic fouling propensity is also observed when projectiles are injected (see for instance Figure 4-21). It has also been shown that in case of projectile injection the asymptotic behavior can be approached faster. For the purpose of predicting the asymptotic fouling resistance when injecting projectiles, the original Kern and Seaton model can be

modified to include the delay or induction time with and without injection (t' and t''). At first for the case without injection, the fouling resistance can be expressed as:

$$R_{f,wo} = 0 \qquad \text{m}^2\text{K/W} \qquad \text{if} \quad t < t' \tag{5.1}$$

$$R_{f,wo} = R^*_{f,wo}(1 - e^{-\theta'(t-t')}) \qquad \text{if} \quad t > t' \tag{5.2}$$

where $R^*_{f,wo}$ is the asymptotic fouling resistance when time tends to infinity and θ' is a coefficient representing the inverse of a relaxation time. Kern and Seaton (1958) also considered that fouling is a trade-off between simultaneous deposition and removal processes.

With projectile injection, the experimental results showed a fouling curve with the same trend, only with different asymptotic fouling resistances and relaxation times. This is schematically illustrated in Figure 5-1. Accordingly, for projectile injection, the model can be rewritten as below, if the fluctuations due to the injections in the transition stage are ignored:

$$R_{f,w} = 0 \qquad \text{m}^2\text{K/W} \qquad \text{if} \quad t < t'' \tag{5.3}$$

$$R_{f,w} = R^*_{f,w}(1 - e^{-\theta''(t-t'')}) \qquad \text{if} \quad t > t'' \tag{5.4}$$

where similarly $R^*_{f,w}$ is the asymptotic fouling resistance when time tends to infinity and θ'' is a coefficient representing the inverse of a relaxation time. t' and t'' are induction times without and with projectiles. It has already been demonstrated experimentally in section 4.4 (Figure 4-32) that t' is linearly proportional to the flow velocity in case of no injection and t'' is independent of the flow velocity as long as the injection interval is kept constant. The values for $R^*_{f,wo}$, θ', $R^*_{f,w}$ and θ'' will be evaluated in the followings sections.

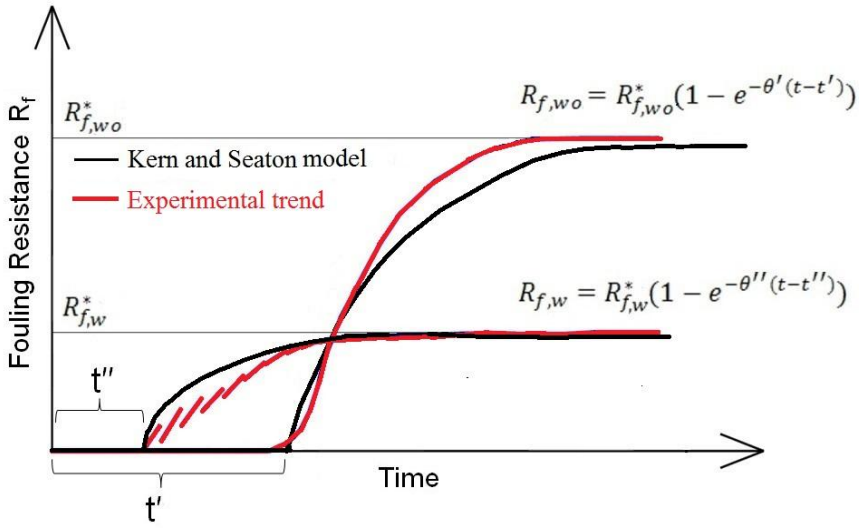

Figure 5-1 Fouling resistance vs. time with and w/o injecting projectiles using the Kern and Seaton model

5.2 Model for Prediction of Fouling Resistance without Projectile Injection

Based on the fouling model proposed by Kern and Seaton, the net rate of fouling is equal to the deposition rate $\dot{m}_d$ minus the removal rate $\dot{m}_r$:

$$\frac{dm_f}{dt} = \dot{m}_d - \dot{m}_r \tag{5.5}$$

Based on Taborek (1972), the removal rate $\dot{m}_r$ is directly proportional to the shear stress of flow (τ_{flow}) and inversely proportional to the deposit strength *(φ)*:

$$\dot{m}_r = k\frac{\tau_{flow}}{\varphi} \tag{5.6}$$

Taborek (1972) also assumed that the deposit strength *(φ)* is inversely proportional to the deposit thickness *(x_d)*:

$$\frac{1}{\varphi} \propto x_d \tag{5.7}$$

Also,

$$R_{f,wo} = \frac{x_d}{\lambda_d} \tag{5.8}$$

Thus Eq. 5.5 can be rearranged as:

$$\frac{dR_{f,wo}}{dt}\lambda_d\rho_d = \dot{m}_d - k_2\tau_{flow}R_{f,wo}\lambda_d \tag{5.9}$$

where k_2 is a proportionality constant for Eq. 5.7. Eq. 5.9 can also be expressed as:

$$\frac{(\lambda_d\rho_d)dR_{f,wo}}{\dot{m}_d - k_2\tau_{flow}R_{f,wo}\lambda_d} = dt \tag{5.10}$$

After integration from time t' to t

$$\int_0^{R_{f,wo}} \frac{(\lambda_d\rho_d)dR_{f,wo}}{\dot{m}_d - k_2\tau_{flow}R_{f,wo}\lambda_d} = \int_{t'}^{t} dt \tag{5.11}$$

Eq. 5.11 yields:

$$ln\left[\frac{\dot{m}_d - k_2\tau_{flow}R_{f,wo}\lambda_d}{\dot{m}_d}\right] = -\frac{k_2\tau_{flow}}{\rho_d}(t-t') \tag{5.12}$$

Then $R_{f,wo}$ can be obtained as:

$$R_{f,wo} = \frac{\dot{m}_d}{\lambda_d k_2\tau_{flow}}(1 - e^{-\frac{k_2\tau_{flow}}{\rho_d}(t-t')}) \tag{5.13}$$

The deposition rate $\dot{m}_d$ can be calculated based on a second order chemical reaction extended in form of the Arrhenius term. Although several expressions have been proposed for kinetics of calcium sulfate crystallization, Smith and Sweett (1971) suggested that the following equation, given by Nancollas (1968) and Konak (1974), describes calcium sulfate deposition best (Fahiminia, 2007):

$$\dot{m}_d = k_0 e^{-E/RT_s}(C_b - C_s)^2 \tag{5.14}$$

T_s (in Kelvin) is the surface temperature where deposit forms, k_0 the reaction rate constant, E the activation energy, and R the universal gas constant. C_b is the bulk concentration and C_s the saturation concentration at the respective surface temperature. Therefore, from Eq. 5.13 and Eq. 5.14 one can deduce that:

$$R_{f,wo} = \frac{k_0 e^{-E/RT_s}(C_b - C_s)^2}{\lambda_d k_2\tau_{flow}}(1 - e^{-\frac{k_2\tau_{flow}}{\rho_d}(t-t')}) \tag{5.15}$$

Eq. 5.15 resembles Eq. 5.2 which explains the relations of θ' and $R^*_{f,wo}$ including the other dominant physical properties. In this case, the asymptotic fouling resistance $R^*_{f,wo}$ can be obtained as:

$$R^*_{f,wo} = \frac{k_0 e^{-E/RT_s}(C_b - C_s)^2}{\lambda_d k_2 \tau_{flow}} \tag{5.16}$$

and also θ', the reverse of the relaxation time as:

$$\theta' = \frac{k_2 \tau_{flow}}{\rho_d} \tag{5.17}$$

Eq. 5.16 indicates that $R^*_{f,wo}$ is a function of the Arrhenius term. It means that the temperature at the surface of reaction and also the activation energy are two main parameters to evaluate the asymptotic fouling resistance. Meanwhile, $R^*_{f,wo}$ can be determined from experimental data for given values of surface temperature T_s and bulk concentration of C_b.

5.3 Model for Prediction of Fouling Resistance with Projectile Injection

The mechanisms of fouling with projectile injection differ from those without projectiles in many ways. Injection of projectiles is not continuous, so a non-continuity factor η needs to be introduced to correct the value of the exerted shear force. The non-continuity factor is a correction factor to convert the momentary exerted shear force by the projectile, to an equivalent value that represents a continuous shear force with the same effect on the surface in the model. It is also only a function of the injection rate, because for more frequent injections the shear force becomes more prominent. Furthermore, the contact stability factor, Z, as a function of stiffness should be included in the model because Eq. 4.11 showed that Z is directly related to the ratio of hydrodynamic and dynamic forces. Thus it is used to represent the hydrodynamic shear force on the surface. The measured dynamic and hydrodynamic shear forces, τ_{dyn} and τ_{hyd} were described in section 4.7. τ_{dyn} is the momentary shear force under dynamic pushing to be used in the model to indicate the amount of actually exerted shear on the surface. Momentary dynamic shear can be measured by a force meter as explained in section 4.7.1. The continuous hydrodynamic shear force ($\tau_{c,hyd}$) can be presented as a function of momentary dynamic shear force (τ_{dyn}), contact stability factor (Z) and non-continuity factor (η) as

$$\tau_{c,hyd} = Z\eta\tau_{dyn} \tag{5.18}$$

Given all these considerations, then Eq. 5.16 can be extended for the projectile injection. The overall shear force is assumed to be the summation of the projectile hydrodynamic shear plus the shear of flow. To calculate the fouling resistance with projectiles $R^*_{f,w}$, Eq. 5.16 may be rewritten as:

$$R^*_{f,w} = [\frac{k_0 e^{-E/RT}(C_b - C_s)^2}{k_2 \lambda_d (\tau_{c,hyd} + \tau_{flow})}]_w \tag{5.19}$$

If Eq. 5.19 is divided by Eq. 5.16 and with the assumption that τ_{flow} is negligible (approximately 10^2 Pa for v_{max}=3.0 m/s) compared to $\tau_{c,hyd}$ (larger than 10^4 Pa as shown in Table 4-3), leads to:

$$\frac{R^*_{f,w}}{R^*_{f,wo}} = \frac{[k_2 \lambda_d]_{wo}}{[k_2 \lambda_d]_w} \times \frac{\tau_{flow}}{\tau_{c,hyd}} \times \frac{[k_0 e^{-E/RT_s}(C_b - C_s)^2]_w}{[k_0 e^{-E/RT_s}(C_b - C_s)^2]_{wo}} \tag{5.20}$$

Eq. 5.20 presents a ratio of the asymptotic fouling resistance with and without injection. According to Eq. 5.20 the asymptotic fouling resistances are proportional to the reaction constant (Arrhenius term) and inversely proportional to shear stresses (τ_{flow} and $\tau_{c,hyd}$) and also directly proportional to the squared difference between bulk and saturation concentrations. The term $(C_b - C_s)$ is the driving force for transferring mass from the bulk of the flow to the surface. The saturation concentration C_s of calcium sulfate dihydrate is at the interface between deposit and solution. The solubility of calcium sulfate is a strong function of temperature.

Eq. 5.20 also indicates that the asymptotic fouling resistance with and without injection depends linearly on the reaction constants. The Arrhenius terms are not identical with and without injections, because the deposition process without projectiles is surface crystallization and with projectiles it is a combination of surface and seeded bulk crystallization. Changes in the induction time strengthen the hypothesis that reaction is influenced by injection. The projectile may alter the surface of reaction or the activation energy for crystallization; hence the reaction constants are not the same with and without injection. The decreasing induction time with injection is an indication that the Arrhenius term in case of injection is greater than without injection.

5.3.1 Representative saturation concentration

The saturation concentration, C_s in Eq. 5.20, is a function of temperature at the interface between the solution and the growing deposit and could be affected by the presence of other ions. The temperature at the surface of the deposit depends on deposit compactness, its thermal conductivity and thickness which all are unknown. Nevertheless, a series of

tests at the end of the experiments, i.e. #087, #088 and #089 were performed to substitute C_s by another parameter which is introduced as "representative saturation concentration" and could be measured by titration. The "representative saturation concentration" is the minimum concentration above which no more crystallization would take place.

As mentioned in section 3.2.2 the concentration of $CaSO_4$ during the fouling experiments was determined by titration every 30 min and controlled by the addition of the respective solutions to be adjusted to a set point. To maintain the concentration of $CaSO_4$, the two highly concentrated solutions of calcium nitrate and sodium sulfate were added to the supply tank.

For these series of experiments, the bulk temperature was 40°C and velocity, surface temperature and bulk concentration (C_b) were 1.3 m/s, 71°C, 4.6 g/L. To measure the "representative saturation concentration" the tests were continued till the asymptotic period was reached but thereafter C_b was not kept constant so no chemicals were added to the solution. Results indicated that the bulk concentration was reduced to a lower value before it became constant again. R_f^* was monitored to trace any possible changes since any alteration of this parameter indicates a variation of the deposit physical structure. As the concentration decreases, the mass deposition rate becomes less than the removal rate; $\dot{m}_d < \dot{m}_r$. But the fouling layer in the asymptotic region is sintered and very hard, so no reduction in $R_{f,w}^*$ and $R_{f,wo}^*$ was observed at least during the investigated times. The minimum bulk concentrations without and with injection are reported as C^* and C^{**} in Table 5-1. C^{**} was measured when projectiles were injected every 5 minutes. The experiments were repeated several times for different surface temperatures and their repeatability was confirmed. The results were surprising as different values with and without injection were observed. Values are lower when projectiles were injected.

The observation of the above mentioned phenomenon was important and the explanation for these results is that possibly many crystals are broken from the surface after every injection. These detached crystals could provide seeding in the supersaturated solution at the surface. The presence of suspended particles in solutions significantly affects the crystallization rate (Bansal et al, 1997). The solution at the temperature of the deposit surface is supersaturated; but crystallization takes place at lower supersaturation when the solution is in contact with a broken surface or small crystals are present. Furthermore, the crystals can settle on the heat transfer surface and act as nucleation sites (Bansal et al. 1997). Bansal et al. (1997) found that the availability of additional nucleation sites increases the crystallization rate significantly. They also proposed using a filter for a remarkable reduction of the crystallization fouling rate. Such a filter was used in the current test facility, but it seems that the settling of crystals happen even before they left the heated section and could be caught by the filter.

It is hard to say that the results given in Table 5-1 are saturation concentrations at the surface of the deposit. Saturation concentration thermodynamically is a function of temperature and is independent of any nucleation or seeding phenomena. However the results prove that the concentration at the surface of the deposit is supersaturated as it is affected by the presence of crystals broken by the projectiles. What happens here is probably a kind of seeding in the solution that causes crystallization to occur at lower supersaturation.

Figure 5-2 schematically illustrates the concentration profile at the surface of the deposit with and without projectile injection. Since the rate of heating up is very fast (the residence time of flow in the heated section is a fraction of a second), this short period of time is not enough for full development of crystallization. Thus there is an area near to the surface of the deposit where the solution is supersaturated. It seems, in case of injection, detached crystals and broken surface accelerate the crystallization rate and reduce the of bulk concentration, such as seeding in a supersaturated solution. Thus C^* and C^{**} are not essentially the saturation concentration at the surface, but representative values when no more crystallization would be observed at the deposit surface. Since these parameters naturally play the role of saturation concentration, they are a strong function of surface temperature as shown in Table 5-1 and also of the presence of crystalline particles. It is predicted that they are almost independent of parameters like velocity.

A tentative assumption could be that C^* and C^{**} approach to C_s and will become identical after a long flow circulation when no make-up chemicals are added. It should be pointed out that after heating up the flow, it cools down again in the supply tank and then it has a residence time for more than two minutes (150 seconds for 1.3 m/s) before it passes through the filter. Thus, at the end, there is a balance between what is deposited on the hot surface and what is dissolved in the supply tank or even in the filter drum. As mentioned, experiments proved that these concentrations are different with and without projectile injection. Table 5-1 shows that not only C^{**} is lower than C^*, but also that this gap is more noticeable at higher surface temperatures.

Table 5-1 *C and *C*** for different surface temperatures**

Surface Temp. of tube (T_s) °C	C_b (g/L)	C^* (g/L)	C^{**} (g/L)	C_b-C^* (g/L)	C_b-C^{**} (g/L)
63°C	4.6	4.3	4.1	0.3	0.5
71°C	4.6	4.1	3.9	0.5	0.7
76°C	4.6	3.6	3.2	1.0	1.4

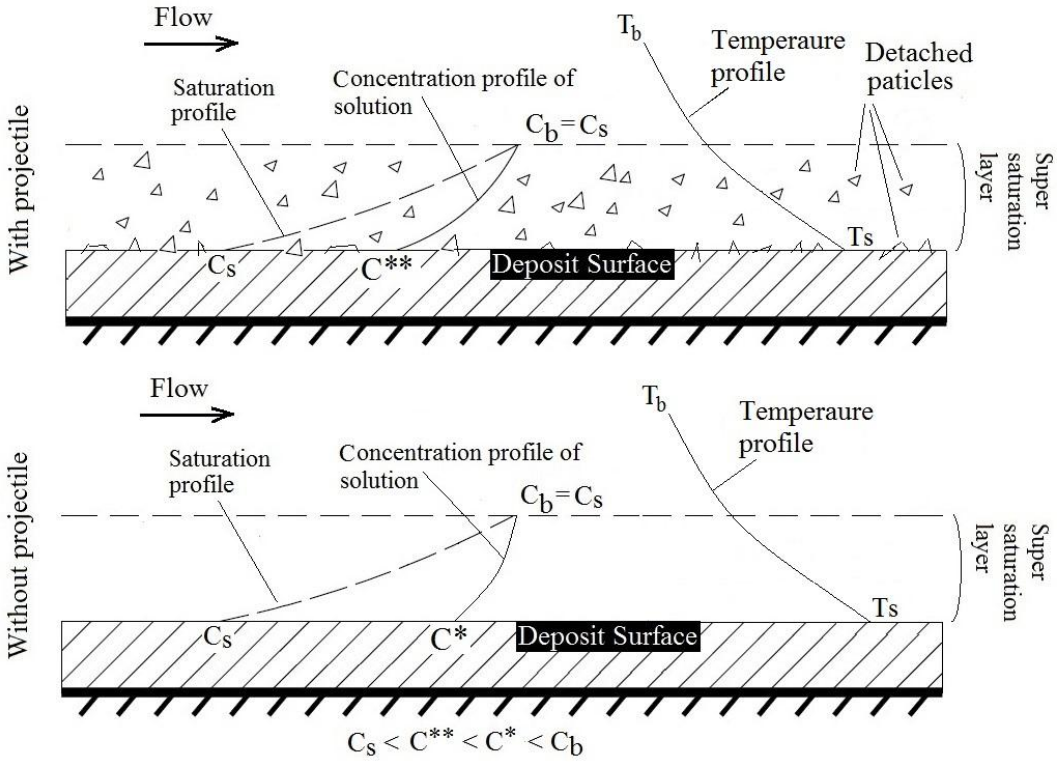

Figure 5-2 Concentration profile at the surface of deposit with and w/o injections

Thus Eq. 5.21 can be rewritten as:

$$\frac{R^*_{f,w}}{R^*_{f,wo}} = \frac{[k_2\lambda_d]_{wo}\tau_{flow}[k_0 e^{-E/RT_s}]_w(C_b - C^{**})^2}{[k_2\lambda_d]_w\tau_{c,hyd}[k_0 e^{-E/RT_s}]_{wo}(C_b - C^*)^2} \tag{5.21}$$

Figure 5-2 and Table 5-1illustrate that the difference in case of injection is larger than without injection, or C_b-C^*<C_b-C^{**}. Existing nuclei and roughened surface made by projectiles support the crystal growth at lower supersaturation. This possibly is another reason for the shorter induction time when projectiles are injected. The impact of surface properties like roughness on the rate of deposition has intensively been investigated before. Herz et al. (2008) proved that the heat transfer coefficient of very rough stainless steel surfaces during crystallization fouling of an aqueous solution decreases more rapidly than for smoother surfaces. They suggested several reasons for this behavior 1) increase of primary heterogeneous nucleation rate on the surfaces; (2) reduction of local shear stress in the valleys and (3) reduced removal rate of the crystals from the surfaces where the roughness elements protrude out of the viscous sub-layer.

5.3.2 Asymptotic fouling resistance as a function of injection interval

The integration of Eq. 5.18 into Eq. 5.19 considering that τ_{flow} is negligible compared to $\tau_{c,hyd}$ Eq. 5.22 yields to:

$$R^*_{f,w} = \left(\frac{k_0 e^{-E/RT_s}}{k_2 \lambda_d}\right)_w \times \frac{(C_b - C^{**})^2}{\eta \cdot \tau_{dyn} \cdot Z} \tag{5.22}$$

The extended model for the injection is based on an equivalent continuous shear force on the inner surface of the tube ($\tau_{c,hyd}$) which is, in turn, a function of the momentary dynamic shear force (τ_{dyn}), non-continuity (η) and contact stability (Z). In Eq. 5.18 the non-continuity was introduced. Here it is extended as it is inversely proportional to the injection rate with a power of p

$$R^*_{f,w} \propto \frac{1}{n^p} \tag{5.23}$$

In this equation, n is the number of injections per time or injection rate (e.g. #/min) and p is called "injection interval factor". To calculate p, based on Eq. 5.23, a correlation was developed for the asymptotic fouling resistance ($R^*_{f,w}$) vs. injection rate (n) from the experimental results at similar operating conditions but different injection intervals. For the soft projectiles, p = 0.6 and for the hard ones p = 0.4 were calculated. This means that soft projectiles show better results for long injection intervals. Considering this, Eq. 5.22 may be rewritten as:

$$R^*_{f,w} = \left(\frac{k_A}{k_2 \lambda_d}\right)_w \times \frac{(C_b - C^{**})^2}{n^p \tau_{dyn} Z} \tag{5.24}$$

This equation simply shows that the asymptotic fouling resistance is directly proportional to the reaction constant, k_A, which is introduced as Arrhenius equation ($k_A = k_0 e^{-E/RT_s}$) and it is a function of temperature and activation energy. By increasing the temperature, the fouling resistance will be shifted to a higher level. The asymptotic fouling resistance is also inversely proportional to the shear force of the projectile and the contact stability. The accuracy of this model will be discussed in section 5.3.5. The denominator of Eq. 5.24 is the dynamic shear stress multiplied with the contact stability and the non-continuity. It is equal to the continuous hydrodynamic shear force by the projectiles and directly related to the cleaning potential of the projectile or $\tau_{dyn}Z$ and the injection rate. Generally speaking, Eq. 5.24 indicates that:

$$R_{f,w}^{*} \propto \frac{deposition\ rate}{injection\ rate \times \text{ projectile cleaning potential}} \tag{5.25}$$

Eq. 5.24 is rewritten as:

$$R_{f,w}^{*} = \frac{k}{\lambda_d} \times \frac{k_A (C_b - C^{**})^2}{n^p \times \tau_{dyn} Z} \tag{5.26}$$

$k_A(C_b\text{-}C^{**})^2$ is the deposition rate, n^p the injection rate and $\tau_{dyn}Z$ the projectile cleaning potential. k is the overall constant for the model which could be evaluated from the experiment data.

Eq. 5.26 is independent of velocity and hence consistent with the experimental results in section 4.4 (see Figure 4-31b).

5.3.3 Reaction constant of the Arrhenius equation

In order to obtain $R_{f,w}^{*}$ in Eq. 5.26, the values of the Arrhenius equation ($k_A = k_0 e^{-E/RT_s}$) must be known. k_A is a function of activation energy and reaction temperature. Bansal et al. (2005) proved that the activation energy changes during the three steps of nucleation, nucleation/growth and growth individually for calcium sulfate crystallization on a surface. All studies before that were focused on bulk calcium sulfate crystallization (Fahiminia 2007). Bansal et al. (2005) reported that for each fouling experiment three different regions exist after the induction time is elapsed. The first region has a low rate, which is probably associated with nuclei formation. The second region corresponds to an intermediate rate, which is presumably related to both nuclei formation and crystal growth. The third region shows the highest rate, in which the crystal growth is dominant. Bansal et al. (2005) observed the same trends for all the experiments. For each experiment, three different reaction rate constants were evaluated: k_l for the low rate region, k_{int} for the intermediate rate region, and k_h for the high rate region. This means that considering a single value for the whole experiment is not realistic.

Fahiminia (2007) also presented activation energies for the three regions. The data cover a range from 193 to 249 kJ/mol for all regions and for two different initial concentrations. These values overlap at the high end of the range 105 - 219 kJ/mol reported by Bansal et al. (2005), and are higher than the values reported by other researchers (Fahiminia, 2007). The differences between values of the activation energy reported in the literatures may be justified by determining the operating conditions under which the concentration is monitored (Fahiminia, 2007). For bulk crystallization, most of the researchers have focused on the seeded crystallization technique, where the initial total surface area of the crystals is known, and the main assumption is that no further nucleation

occurs during the experiment (Fahiminia, 2007). Fahminia (2007) obtained several values of k_A for different regions in a temperature range between 60-84°C (333-357 K).

Undoubtedly, considering a value as k_A is even more complicated in case of projectile injection, due to a combination of seeded bulk and surface crystallizations. Nevertheless the introduction of the equivalent saturation concentration (C^{**}) in section 5.3.1 simplifies the method for the asymptotic region. It is a parameter that represents the impact of additional particles, which are broken by the projectiles from the surface. Since the modeling is done for the asymptotic region, using a constant value as k_A is a plausible assumption.

As injecting projectiles produces particles in the system and the presence of particles impacts on the results, the results of Fahiminia (2007) were used to evaluate k_A.

5.3.4 Constant value of developed model (*k*)

In Eq. 5.26, the value of *k* could be obtained from the experimental results when $R^*_{f,w}$ is plotted against $\frac{k_A(C_b-C^{**})^2}{\lambda_d n^p \tau_{dyn} Z}$. The experimental $R^*_{f,w}$ values for various projectiles at different injection intervals are provided in Table 5-2. The surface temperature is assumed to be equal to the set point surface temperature and also assumed to be fixed during the test, i.e. T_s=71°C (344 K). Furthermore the activation energy, *E*, equal to 226 kJ/mol (see section 5.3.3) and the Arrhenius coefficient, k_A, 0.0018 m^4/kg·s were considered (Fahimina 2007). A thermal conductivity of sintered calcium sulfate dehydrate, λ_d, 0.47±10% W/m·K was used (ČSN 72 2301). In Table 5-2 the results for the term $\frac{k_A(C_b-C^{**})^2}{\lambda_d n^p \tau_{dyn} Z}$ are presented.

Table 5-2 Inserting the values of the parameters in Eq. 5-26 from the experimental results

Proj. No.	$R^*_{f,w}$ (Experimental) m²K/W	C_b g/L	C^{**} g/L	P	n (#/min)	Z	τ_{dyn} kPa	$\frac{k_A(C_b - C^{**})^2}{\lambda_d n^p \tau_{dyn} Z}$ K·s/W
P02	0.00010	4.6	4.1	0.6	0.5	0.8	75	**0.024**
P02	0.00014	4.6	4.1	0.6	0.2	0.8	75	**0.042**
P02	0.00021	4.6	4.1	0.6	0.1	0.8	75	**0.064**
P02	0.00030	4.6	4.1	0.6	0.067	0.8	75	**0.081**
P12	0.00011	4.6	4.1	0.4	0.5	0.085	932	**0.016**
P12	0.00017	4.6	4.1	0.4	0.2	0.085	932	**0.023**
P12	0.00022	4.6	4.1	0.4	0.1	0.085	932	**0.030**
P12	0.00025	4.6	4.1	0.4	0.067	0.085	932	**0.036**
P09	0.00031	4.6	4.1	0.6	0.5	0.9	50	**0.032**
P09	0.00042	4.6	4.1	0.6	0.2	0.9	50	**0.056**
P09	0.00055	4.6	4.1	0.6	0.1	0.9	50	**0.085**
P06	0.00013	4.6	4.1	0.6	0.5	0.8	95	**0.019**
P06	0.00012	4.6	4.1	0.6	0.2	0.8	95	**0.033**
P06	0.00022	4.6	4.1	0.6	0.1	0.8	95	**0.050**
P06	0.00027	4.6	4.1	0.6	0.067	0.8	95	**0.064**
P10	0.00035	4.6	4.1	0.6	0.5	0.9	36	**0.045**
P10	0.00046	4.6	4.1	0.6	0.2	0.9	36	**0.078**
P10	0.00062	4.6	4.1	0.6	0.1	0.9	36	**0.118**

These results are illustrated in Figure 5-3. The linear trend line has a slope of 5.36×10^3 m^2/s for the data presented in Table 5-2.

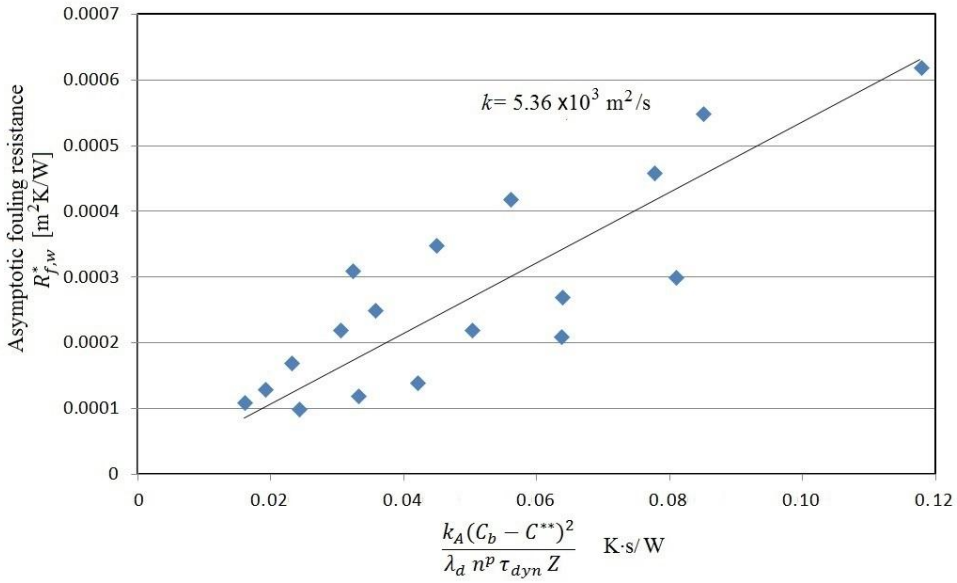

Figure 5-3 Calculated *k* value for the developed model

Thus the proposed model is:

$$R^*_{f,w} = 5.36 \times 10^3 \frac{k_A (C_b - C^{**})^2}{\lambda_d \, n^p . \tau_{dyn} Z} \tag{5.27}$$

It seems that the model provides a predictive tool in most cases to estimate asymptotic fouling resistances over an acceptable range of injection intervals and operating conditions i.e. surface temperature, velocity and concentration.

Table 5-3 presents the experimental results of $R^*_{f,w}$ and the calculated ones from the proposed model with an average error of 30.4% that seems to be acceptable for a complicated fouling process as in the present experiments.

Table 5-3 Calculated errors for the model

$R^*_{f,w}$ (Experimental) m²K/W	$R^*_{f,w}$ (Model) m²K/W	**Error %**
0.00010	**0.00013**	**29.6**
0.00014	**0.00022**	**60.5**
0.00021	**0.00034**	**62.1**
0.00030	**0.00043**	**44.3**
0.00011	**0.00009**	**22.3**
0.00017	**0.00012**	**27.5**
0.00022	**0.00016**	**26.0**
0.00025	**0.00019**	**23.6**
0.00031	**0.00017**	**44.2**
0.00042	**0.00030**	**28.7**
0.00055	**0.00045**	**17.5**
0.00013	**0.00010**	**21.3**
0.00012	**0.00018**	**47.8**
0.00022	**0.00027**	**22.2**
0.00027	**0.00034**	**26.6**
0.00035	**0.00024**	**31.4**
0.00046	**0.00042**	**9.6**
0.00062	**0.00063**	**1.7**
Average of error (%)		**30.4**

6 CONCLUSIONS AND FUTURE WORK

6.1 Conclusions

In this study a test facility was designed and constructed to simulate the conditions for the crystallization fouling of $CaSO_4$ which can occur in thermal water services. It included an online cleaning system with injection of projectiles for different time intervals. A comprehensive set of experimental runs was carried out with and without projectiles. Fouling runs were performed at accelerated conditions to rigorously characterize the impact of projectile cleaning in terms of injection intervals and various types of projectiles. Moreover a model has also been developed to predict the asymptotic fouling resistance when a projectile is injected. From the experimental and theoretical studies, the following conclusions can be drawn:

- At clean conditions, injection of projectiles, even at the smallest injection intervals did not have an appreciable impact on the heat transfer coefficient

- The projectiles were capable of removing parts of the fouling layer at the early stage of the fouling process. Nevertheless, the cleaning efficiency decreased as the fouling layer built up such that the projectiles were not effective when the asymptotic fouling was approached. Faster projectile injections accelerated approaching the asymptotic fouling resistance. Sintering of the fouling layer also hindered the cleaning action of projectiles.

- Projectiles decreased the induction time and the asymptotic fouling resistance. The asymptotic fouling resistance can be approached much quicker compared to that of no injection.

- Soft sponge balls were more efficient than the hard rubber ones. Between soft projectiles, larger and stiffer sponge balls are more effective than smaller and softer types as long as they can be propelled inside the tube. Hard balls with exact diameter of the tube may even worsen the deposition process due to the lack of contact with the tube and as they may compact the deposit on the inner wall. For both types of projectiles (soft and hard) the initial deposition of crystallization was faster due to scratches on the surface and the presence of air bubbles when projectiles were injected.

- The induction time was linearly proportional to the flow velocity in case of no injection, and it is independent of the flow velocity in case of projectile injection as long as the injection interval was kept constant. Faster projectile

injection reduced fouling, due to the increased removal of the deposits from the fouling layer, and decreases the induction time.

- Presence of air decreases the induction time and increases the fouling rate. Injecting projectiles induced air bubbles into the heated section that promoted fouling to occur and consequently reduced the induction time. Thus, air must be avoided as much as possible to enter the system during projectile injection.

- As an alternative, it is recommended to inject projectiles only after the induction time, to make use of the fouling free operation during the induction time.

- Double projectile injections accelerated the initiation of the fouling process such that the asymptotic behavior was approached quickly compared to single injection and no injection. Double injection also reduced the asymptotic fouling dramatically compared to single injection. Shorter injection intervals reduce the fouling process, but it is possible to reach the same effect using longer injection intervals together with multiple injections.

- Contact area between projectiles and the inner tube surface, and their stiffness are the most important parameters determining the extent of projectile cleaning. The stiffness produces mainly shear force and the size sufficient contact area. To have the best cleaning performance, there is an optimum value for projectile size and stiffness. The best size would be 10% bigger than the tube and the optimum stiffness is 1% deformation under an average 0.6 N force. Using projectiles outside range may be problematic. Bigger and softer projectiles cannot stand longtime injections as their life-expectancy would be reduced. Contrariwise, harder projectiles are more likely to get stuck. $R^*_{f,w}/R^*_{f,wo}$ (the ratio of asymptotic fouling resistance with and without injection) can give a better meaning for cleaning the heat exchanger and could be decreased by 80% if a suitable projectile of the right size and stiffness was selected.

- Generally speaking, the size of hard projectiles does not exceed the tube diameter by more than 2% and the minimum required velocity to push them in to the tube is more than 1 m/s. On the contrary soft projectiles can be bigger by as much as 5% and can move even for velocities less than 1 m/s. The important point to distinguish between the two groups is their action in contact with the tube. In a mechanical test, hard projectiles exerted much higher shear force than soft projectiles but under propulsion force of flow there is no remarkable shear due to less and unstable contact between projectiles and tube. Thus their cleaning performance is not as efficient as far softer ones. Accordingly a new term called contact stability factor, *Z*, was proposed which was less than 0.2 for

hard projectiles and between 0.8 – 1.0 for soft projectiles. The *Z* factor is a function of stiffness and is about 0.9 for a wide range of soft projectiles. The *Z* factor mainly represents the physical features of a projectile in contact with the tube.

- Scratching the surface of deposit and the detachment of particles after injections facilitate nucleation at the surface of deposit and accelerate the crystallization rate.

- A model is proposed to predict the asymptotic fouling resistance in case of projectile injection. In the developed model, the asymptotic fouling resistance is proportional to the deposition rate and inversely proportional to the exerted shear stress by the projectiles and also to the injection rate. The *Z* factor as contact stability between projectile/tube is used in the model. The model includes three main terms; the deposition rate $k_A(C_b-C^{**})^2$, the injection rate n^p and the projectile cleaning potential $\tau_{dyn}Z$.

6.2 Future Work

The experimental and theoretical results of this study highlighted the potential advantages of using projectiles to mitigate fouling, as well as challenges that require further investigation. Some general remarks and suggestions for future work are as follows:

- Concerning the mechanical properties of the projectiles, only compactness ratio and stiffness have been considered as two main parameters for the cleaning process of the projectiles. Nevertheless, other mechanical properties of projectiles, e.g. elasticity and Poisson's ratio, may also account for the cleaning performance of projectiles as well as their deformation and lifetime.

- Another interesting point is the influence of the surface texture of projectiles on the cleaning performance. This has not been investigated in the present work and should be considered as an important aspect.

- The present work has dealt only with crystallization fouling where $CaSO_4$ was used as foulant. The results have showed that, under some circumstances, the injection of projectiles may intensify the fouling of calcium sulfate. Similar investigations are suggested for other fouling mechanisms i.e. crude oil and biofouling as potential industry for the utilization of projectiles.

- As for the geometrical aspects of projectiles, only symmetrical projectiles, i.e. sponge balls, rubber, bullet and spring types, have been investigated in the present work. However, asymmetrical projectiles need to be studied.

- All experiments of this study were carried out below 80°C tube surface temperature and low pressures (less than 3 bar). Projectiles which are resistant against high temperature and pressure, which are common in industriy need to be developed.

References

Ainslie, E.A., Quarini, G.L., Ash, D.G., Deans, T.J., Herbert, M., and Rhys, T.D.L., Heat Exchanger Cleaning Using Ice Pigging, *Proceedings of 6th International Conference on Heat Exchanger Fouling and Cleaning—Challenges and Opportunities*, Editors: Müller-Steinhagen, H., Malayeri, M.R., and Watkinson, A.P., Schladming, Austria, June 14–19, pp. 433–438, 2009.

Al-Bakeri, F. and El Hares, H., Optimization of Sponge Ball Cleaning System Operation and Design in MSF Plants, *Desalination*, vol. 92, pp. 353-375, 1993.

Albert, F., Augustin, W. and Scholl, S., Enhancement of Heat Transfer in Crystallization Fouling due to Surface Roughness, *Proceedings of the Eurotherm International Conference on Heat Exchanger Fouling and Cleaning VIII*, Editors: Müller-Steinhagen, H., Malayeri, M.R., and Paul Watkinson, A., Schladming, Austria, pp. 303-310, June 14 - 19, 2009.

Al-Janabi, A., Malayeri, M.R., Müller-Steinhagen, H. and Badran, O.O., Precipitation on Various Austentic Alloys, Proceedings of the *Eurotherm International Conference on Heat Exchanger Fouling and Cleaning VIII*, Editors: Müller-Steinhagen, H., Malayeri, M.R., and Watkinson, A.P. , Schladming, Austria, pp. 332-339, June 14 - 19, 2009.

Al-Janabi, A., Esawy, M., Malayeri, M.R. and Müller-Steinhagen, H., Consideration of Dynamic Uncertainty in Fouling Experimentation, Proceedings of the *Eurotherm International Conference on Heat Exchanger Fouling and Cleaning VIII*, Editors: Müller-Steinhagen, H., Malayeri, M.R., and Watkinson, A.P., Schladming, Austria, pp. 217-220, June 14 - 19, 2009.

Al-Otoom, A.Y., Bryant, G.W., Elliott, L.K., Skrifvars, B.J., Hupa, M. and Wall, T.F., Experimental Options for Determining the Temperature for the Onset of Sintering of Coal Ash, *Energy Fuels*, vol. 14, pp. 227–233, 2000.

Alfa Aesar, A Johnson Matthey Company, http://www.alfa.com, 16/7/2012.

Al-Sofi, M. A., Khalaf, S., and Al-Omran, A., Practical Experience in Scale Control, *Desalination*, 73, 313-325, 1989.

Andritsos, N. and Karabelas, A.J., Calcium Carbonate Scaling in a Plate Heat Exchanger in the Presence of Particles, *International Journal of Heat and Mass Transfer*, vol. 46(24), pp. 4613–4627, 2003.

Aschoff, A.F., Rose, M.D., and Sopocy, D.M., Performance of Mechanical System for Condenser Cleaning, ReportCS 5032, Research Project 2300-11, EPRI, Palo Alto, 1987.

ASME Boiler & Pressure Vessel Code - Section II & VIII (Division 1), 2010 Edition with Addenda, *ASME*, 2010.

Awad, M.M., Fouling of Heat Transfer Surfaces, *Heat Transfer - Theoretical Analysis, Experimental Investigations and Industrial Systems*, Prof. Aziz Belmiloudi (Ed.), 2011.

Azimi, G., Papangelakis V.G., J.E., and Dutrizac J.E., Modelling of Calcium Sulphate Solubility in Concentrated Multi-Component Sulphate Solutions, *Fluid Phase Equilibria*, pp.300–315, 2007.

Bansal, B., Müller-Steinhagen, H., and Chen, X. D., Effect of Suspended Particles on Crystallization Fouling in Plate Heat Exchangers, *J. Heat Transfer* 119(3), 568-574, 1997.

Bansal, B., Chen, X. and Müller-Steinhagen, H., Deposition and Removal Mechanisms during Calcium Sulfate Fouling in Heat Exchangers, *International Journal of Transport Phenomena* 7 (1), pp. 1-22, 2005.

Bansal, B., Chen, X. and Müller-Steinhagen, H., Analysis of 'Classical' Deposition Rate Law for Crystallization Fouling, *Chemical Engineering and Processing*, vol. 47, pp. 1201–1210, 2008.

Betz Laboratories Inc, Handbook of Industries Water Conditioning. 7th Edition. Betz Trevose Pa 19047, USA, 1976.

Bott, T.R., Crystallisation Fouling – Basic science and models, in: Melo, L.F., Bott, T.R., and Bernardo, C.A. eds., *Fouling Science and Technology*, Kluwer Academic Publisher, Dordrecth, 1988.

Bohmer, H., On-load Tube Cleaning Systems and Debris Filters for Avoidance of Micro- and Macro-Fouling in MSF Desalination Plants, *Desalination*, 93, 171, 1993.

Bohnet, M., Augustin, W., Hirsch, H., Influence of Fouling Layer Shear Strength on Removal Behavior, *Proceeding of an international conference on Understanding Heat Exchanger Fouling and its Mitigation*, Müller-Steinhagen, H., Watkinson, A.P., Malayeri, M.R., eds., II Ciocco Conference Center, Castelvecchio Pascoli, Italy, May 1997, pp. 201-208, 1997.

Bott, T.R., Fouling Notebook Inst. Chem. Engrs., Rugby, 1990.

Bott, T. R., Fouling of Heat Exchangers, Elsevier, 1995.

Briggs, D.E. and Young, E.H., Modified Wilson Plot Techniques for Obtaining Heat Transfer Correlations for Shell and Tube Heat Exchangers, *Chemical Engineering Progress Symposium Series*, No. 92, vol. 65, pp. 35-45, 1969.

Chemical Information Review Document for Synthetic and Natural Mined Gypsum (Calcium Sulphate Dehydrate), *Integrated Laboratory Systems, Inc.*, Contract no. N01-ES-35515, 2006.

CQM: http://www.cqm-tech.com/products_atcs.html, 11.11.2011.

Crittenden, B.D. and Aldermann, N.J., Negative fouling resistance: Effect of Surface Roughness, *Chemical Engineering Science*, vol. 43(4), pp. 829-838, 1988.

ČSN 72 2301 Gypsum binding materials, Czech standard (in Czech), Vydavatelství Úřadu pro normalizaci s měření, Praha 1979.

Eimer, K., Recommendations for the optimum cleaning frequency of the Taprogge tube cleaning system. Technical Report 85 - 26, *Taprogge Gesellschatt mbH*, Wetter, 1985.

Esawy, M., Abd-Elhady, M.S., Malayeri and M.R., Müller-Steinhagen, H., Influence of Sintering on Deposit Formation during Pool Boiling of Calcium Sulfate Solutions, *Experimental Thermal and Fluid Science*, vol. 34, pp. 1439-1447, 2010.

Esawy, M., Malayeri, M. R. and Müller-Steinhagen, H., Crystallization Fouling of Finned Tubes During Pool Boiling: Effect of Fin Density, *J. Heat and Mass Transfer*, vol. 46, pp. 1167–1176, 2010.

Esawy, M., Fouling of Structured Surfaces during Pool Boiling of Aqueous Solutions, *Ph.D. thesis*, University of Stuttgart, Germany, September 2011.

Evangelidou, M., Crystallization Fouling of Structured Tubes During Pool Boiling Heat Transfer, *Diploma thesis*, University of Stuttgart, Stuttgart, Germany, 2010.

Fahiminia, F., Watkinson, A.P. and Epstein, N., Calcium Sulfate Scaling Delay Times under Sensible Heating Conditions, in: *Proceedings of 6th International Conference on Heat Exchanger Fouling and Cleaning - Challenges and Opportunities*, Editors H. Müller-Steinhagen, M. R. Malayeri, and A. P. Watkinson, Kloster Irsee, Germany, June 5 - 10, pp. 310-315, 2005.

Fahiminia, F., Initial Fouling Rate and Delay Time Studies of Aqueous Calcium Sulphate Scaling under Sensible Heating Conditions, Ph.D. thesis, The University of British Columbia, Canada, March 2007.

Figliola, R.S., Beasly, D.E., Theory and Design for Mechanical Measurement, *John Wiley and Sons*, New York, 1991.

Fritz, J.S. and Schenk, G.H., *Quantitative Analytical Chemistry*, 5th edition, Allyn and Bacon Inc., USA, 1987.

Freeborn, J. and Lewis, D., Initiation of Boiler Scale Formation, *International Journal of Mechanical Sciences*, vol. 4, pp. 46-52, 1962.

Geddert, T., Bialuch, I., Augustin, W. and Scholl, S., Extending the Induction Period of Crystallization Fouling Through Surface Coating, *Heat Transfer Engineering*, vol. 30(10-11), pp. 868-875, 2009.

Ghulam, M. M., Osman, A. H., Khalid, B., and Hamed, A. W., Performance Evaluation of Technos Cleaning Balls in RDC MSF Pilot, Al-Jubail Phase II, and Jeddah Phase III Plants, Saline Water Conversion Corporation P.O.Box 8328, Al-Jubail-31951, Saudi Arabia, *Issued as Technical Report No. TR-3808/EVP 95010*, December 2001.

Gill, J.S. and Nancollas, G.H., Kinetics of Growth of Calcium Sulfate Crystals at Heated Metal Surfaces, *Journal of Crystal Growth*, vol. 48, pp. 34-40, 1980.

Griffin, C.M., Tube Cleaner, *U.S. Patent No. 1,814,752*, July 14, 1931.

Griffin, C.M., Tube Cleaner, *U.S. Patent No. 2,170,997*, August 29, 1939.

Griffin, C.M., *U.S. Patent No. 2,418,509*, 1947.

Griffin, C.M., Tube Cleaner, *U.S. Patent No. 2,734,208*, February 14, 1956.

Gunn, D.J., Effect of Surface Roughness on the Nucleation and Growth of Calcium Sulfate on Metal Surfaces, *Journal of Crystal Growth*, vol. 50, pp. 533-537, 1980.

Hamed, O.A., Mardouf, K.B. and Al-Omran, A., Impact of Interruption of Antiscalant Dosing or Cleaning Balls Circulation during MSF Plant Operation, *Desalination*, vol. 208, pp. 192–203, 2007.

Hasson D., Zahavi J., Mechanism of Calcium Sulfate Scale Deposition on Heat Transfer Surface, *Ind. Eng. Chem. Fundamentals*, vol. 9, pp 1-10, 1970.

Heat exchanger: *A Global Strategic Business Report, Global Industry Analysts*, Inc., San Jose, CA, USA, 2008.

Helalizadeh, A., (2002), Mixed Salt Crystallisation Fouling, *Ph.D thesis*, University of Surrey, UK.

Helalizadeh, A., Müller-Steinhagen, H., and Jamialahmadi, M., Crystallisation Fouling Of Mixed Salts during Convective Heat Transfer and Sub-Cooled Flow Boiling Conditions *Chemical Engineering Science* vol. 60 issue 18 September, p. 5078-5088, 2005.

Herz, A., Malayeri, M.R., and Müller-Steinhagen, H., Fouling of roughened stainless steel surfaces during convective heat transfer to aqueous solutions, *Energy Conversion and Management*, Vol. 49, pp. 3381-3386, 2008.

Holvand, A.W., Rankin, D.A., and Saxon, E.G., Heat Exchanger Tube Wear by Mechanical Cleaners, *Proc. Power Generation Conf.*, Philadelphia, 25- 29 Sept. 1988.

Incropera, F.P., DeWitt , D.P., Bergman, T.L., Lavine, A.S. Fundamentals of Heat and Mass Transfer, John Wiley & Sons; 6th edition, 2006.

Jamialahmadi, M. and Müller-Steinhagen, H., Scale Formation during Nucleate Boiling – A review, *Corrosion Reviews*, vol. 11, pp. 25-54, 1993.

Jamialahmadi, M., and Müller-Steinhagen, H., A New Model for the Effect of Calcium Sulphate Scale Formation on Pool Boiling Heat Transfer, *Journal of Heat Transfer*, vol. 126, pp. 507-517, 2004.

Jamialahmadi, M., Blöchl, R. and Müller-Steinhagen, H., Bubble Dynamics and Scale Formation during Boiling of Aqueous Calcium Sulfate Solutions, *Chemical Engineering and Processing*, vol. 26, pp. 15-26, 1989.

KALVO VOGLER GmbH web page, www.kalvo.de: Automatisches Reinigungssystem für Kondensatoren und Röhrenwärmetauscher.

Konak, A.R., A New Model for Surface Reaction Controlled Growth of Crystals from Solution, *Chemical Engineering Science*, vol. 29, pp. 1537-1543, 1974.

Kern, D.Q. and Seaton, R.E., A Theoretical Analysis of Thermal Surface Fouling, *Chemical Engineering Progress*, vol. 4, pp. 258-262, 1959.

Kim, W.T., Bai, C. and Cho, Y.I., A study of $CaCO_3$ Fouling with a Microscopic Imaging Technique, *International Journal of Heat and Mass Transfer*, vol. 45(3), pp. 597-607, 2002.

Kreith, F., West, R.E., CRC Handbook of Energy Efficiency, CRC Press, 1996.

Kuczynski, G.C., Self-Diffusion in Sintering of Metallic Particles, *Trans. Am. Inst. Min. Metal*, vol. 185, pp. 169–178, 1949.

Longstaff, D.C. and Palen, J.W., Fouling Data for Six Crude Oils, *F-10, Heat Transfer Research, Inc., College Station,* TX, 2001.

Lu, H., Fouling Mitigation Using Various Projectiles, Master thesis No. 2012-14, University of Stuttgart, Germany, 2012.

Malayeri, M.R., Müller-Steinhagen, H. and Bartlett, T.H., Fouling of Tube Bundles under Pool Boiling Conditions, *Chemical Engineering Science*, vol. 60, pp. 1503 – 1513, 2005.

Malayeri, M.R. and Müller-Steinhagen, H., Initiation of $CaSO_4$ Scale Formation on Heat Transfer Surface under Pool Boiling Conditions, *Heat Transfer Engineering,* vol. 28, pp. 240-247, 2007.

Marshall, W.L., Slusher , R. and Jones, E.V., Aqueous Systems at High Temperatures XIV. Solubility and Thermodynamic relationships for $CaSO_4$ in NaCl-H_2O solutions from 40° to 200°C, 0 to 4 Molal NaCl, *Journal of Chemical and Engineering Data,* vol. 9(2), pp. 187-191, 1964.

Middis, J., Müller-Steinhagen, H., Paul, S.T., Duffy, G. G., Reduction of Heat Transfer Fouling by the Addition of Wood Pulp Fibbers", *Heat Transfer Engineering*, 19, pp. 36-44, 1998.

Moshe, P., System for Cleaning the Inside of Tubing, Cooling Quality Management Ltd, Patent Genius No. 5388636, 1995.

Mori, H., Nakamura, M.,Toyama, S., Crystallization Fouling of Calcium Sulfate Dihydrate on Heat Transfer Surfaces, *Journal of Chemical Engineering of Japan*, 29, pp.166-173, 1996.

Müller-Steinhagen, H. and Malayeri, M.R., Watkinson, A.P., Heat Exchanger Fouling: Mitigation and Cleaning Strategies, *Heat Transfer Engineering*, vol. 32, pp. 189-196, 2011.

Müller-Steinhagen, H., Heat Transfer Fouling: 50 Years After the Kern and Seaton Model, *Heat Transfer Engineering*, vol. 32(1), pp. 1–13, 2011.

Müller-Steinhagen, H.; Heat Exchanger Fouling - Fundamental Approaches and Technical Solution, Publico Publication, Essen, 2002.

Müller-Steinhagen, H.; Heat Exchanger Fouling - Mitigation and Cleaning Technologies, Publico Publication, Essen, 2000.

Muñoz Sellarès, M., Utilisation of Various Projectiles to Mitigate Fouling in Tubular Heat Exchanger, *Master Thesis No. 2010-27*, University of Stuttgart, Germany, 2011.

Mwaba, M.G., Rindt, C.C.M., Vorstman, M.A.G., Van Steenhoven, A.A., Calcium Sulfate Deposition and Removal Characteristics on a Heated Plate, *Proceedings of an Engineering Foundation Conference on Heat Exchanger Fouling: Fundamental Approaches & Technical Solutions*, Müller-Steinhagen, H. Watkinson, A.P., Malayeri, M.R. eds., Davos, Switzerland, July 2001, pp. 57-63, 2001.

Najibi, S.H., Heat Transfer and Heat Transfer Fouling during Subcooled Flow Boiling for Electrolyte Solutions, *Ph.D. Thesis*, The University of Surrey, UK, 1997.

Najibi, S. H., Müller-Steinhagen, H. and Jamialahmadi, M., Calcium Sulphate Scale Formation duringSubcooled Flow Boiling, *Chem. Eng. Sci.*, 52, pp. 1265-1284, 1997.

Najibi, S. H., Müller-Steinhagen, H. and Jamialahmadi, M., Calcium Carbonate Scale Formation during Sub-cooled Flow Boiling, Trans. *ASME J. of Heat Transfer*, 119, pp. 1-9, 1997.

Nancollas, G. H., "Kinetics of Crystal Growth from Solution", *Journal of Crystal Growth*, 3-4, pp. 335-339, 1968.

Partridge, E.P. and White, A.H., Mechanism of Formation of Calcium Sulfate Boiler Scale, *Industrial and Engineering Chemistry*, vol. 21(9), pp. 834-838, 1929.

Partridge, E.P. and White, A.H., Thermal Effects of Boiler Scale, *Industrial and Engineering Chemistry*, vol. 21(9), pp. 839-844, 1929.

Production Sintering Practices, *ASM Handbook vol. 7: Powder Metal Technologies and Applications*, pp. 468-503, 1998.

Peyghambarzadeh, S.M., Vatani, A., Jamialahmadi, M., Influences of Bubble Formation on Different Types of Heat Exchanger Fouling, *Applied Thermal Engineering*, vol. 50(1), pp. 848–856, 2012.

Preimesser, R., Experimental Study of Fouling Mitigation Using Various Projectiles, *Master Thesis No. 2162904*, University of Stuttgart, Germany, 2011.

Ristic, M.M., *Sintering - New Developments, Elsevier Scientific Publisher Company*, Amsterdam, 1979.

Rizzo, G., Induction Time during Crystallisation Fouling on Ion-Implanted Heat Exchanger Surfaces, *Ph.D. thesis*, University of Stuttgart, Germany, 2008.

Settles, G.S., Schlieren and Shadowgraph Techniques — Visualizing Phenomena in Transparent Media, Springer Verlag, Heidelberg, Germany, 2001.

Skrifvars, B.J. and Hupa, M., Sintering of Ash During Fluidized Bed Combustion, *Ind. Eng. Chem. Res.*, vol. 31, pp. 1026–1030, 1992.

Smith, B.R., Sweett, F., "The Crystallisation of Calcium Sulfate Dihydrate", *Journal of Colloid and Interface Science*, 37(3), pp. 612-618, 1971

Solano, J. P; Garcia, A; Vicente, P. G and Viedma, A., Performance Evaluation ZeroFouling Reciprocating Scraped Surface Heat Exchanger, Proceedings of International Conference on Heat Exchanger Fouling and Cleaning VIII, June 14-19, 2009, Schladming, Austria. Pp. 392-398, 2009.

Steinhagen, R., Müller-Steinhagen, H. and Maani, K., Problems and Costs due to Heat Exchanger Fouling in New Zealand Industries, *Heat Transfer Engineering*, vol.14 (1), pp. 19–30, 1993.

Taborek, J., Aoki, T., Ritter, R.B., Palen, J.W. and Knudsen, J.G., Predictive Methods for Fouling Behavior. Chem. Eng. Prog. 68, No. 7, 69 – 78, 1972.

Technos Co.: http://www.technos.fr/index.php, 12.02.2012.

Thome, J. R., Engineering Data Book, Wolverine Tube Heat Transfer Data Book, Wolverine Tube Inc., PP. 50-53. 2010.

TEMA, *Tubular Exchanger Manufacturers Associations*, 9th Ed., New York, 2007.

Yang, M., Young, A., Niyetkaliyev, A. and Crittenden, B., Modeling Fouling Induction Periods, *International Journal of Thermal Sciences*, vol. 51, pp. 175-183, 2012.

Yang, C.F., Xu, D.Q., & Shen and Z.Q., A Theoretical Analysis and Experimental Study of the Induction Period of Calcium Carbonate Scaling, *Journal of Chemical Industry and Engineering*, vol. 45, pp. 199–205, 1994.

Yang, Q. F., Ding, J. and Shen, Z. Q., Investigation of Calcium Carbonate Scaling on ELP Surface, *Journal of Chemical Engineering of Japan*, vol. 33, pp. 591–596, 2000.

Yang, Q., Liu, Y., Gu, A., Ding, J. and Shen, Z., Investigation of Induction Period and Morphology of $CaCO_3$ Fouling on Heated Surface, *Chemical Engineering Science*, vol.57 pp. 921 – 931, 2002.

Yang, Q., Ding, J. and Shen, Z., Investigation on Fouling Behaviors of Low-Energy Surface and Fouling Fractal Characteristics, *Chemical Engineering Science*, vol. 55, pp. 797-805, 2000.

Appendix A – Weight Estimation of Heat Exchangers

Designed by Aspen B-JAC Software

Weight estimation of a typical water service shell and tube heat exchanger, based on different fouling resistances:

Main Input Data:		
TEMA Type:	BEU	
TEMA class	B	
Fluid Type:	Water/Water	
Fluid quantity:	20000/30000	kg/h
Shell side temperature (input/output):	95/70	°C
Tube side Temperature (input/output):	35/-	°C
Pressure (shell/tube):	5/15	bar
Allowable pressure drop:	0.5/0.1	bar
Shell/Tube side fouling resistance:	0/different	m2K/W
Tube diameter	19.05	mm
Tube thickness	2.11	mm
Tube Pattern:	90	°C
Tube pitch:	25.4	mm

Output: See Figure A-1 till Figure A-7

Table A-1 Size and weight of typical heat exchanger designs with different fouling resistances on the tube side

Fouling resistance on tube side m^2K/W	TEMA size mm×mm	No. of tubes	Length of tube mm	Heat transfer coefficient (Service) $W/(m^2K)$	Heat transfer coefficient (Dirty) $W/(m^2K)$	Heat transfer coefficient (Clean) $W/(m^2K)$	Weight of designed heat exchanger kg
0.0000	307-1800	42U	1800	1799	2235	2522	401
0.0001	307-2000	42U	2000	1583	1924	2556	479
0.0002	307-2500	42U	2500	1263	1558	2598	557
0.0003	307-2500	42U	2500	1263	1300	2604	557
0.0004	307-3000	42U	3000	1050	1119	2630	636
0.0005	307-3000	42U	3000	899	982	2661	714
0.0006	339-3500	52U	3500	727	830	2309	820
0.0007	339-3500	52U	3500	727	751	2311	820

Heat Exchanger Specification Sheet

1									
2									
3									
4									
5									
6	Size	307--2000	mm	Type	BEU	hor	Connected in	1 parallel	1 series
7	Surf/unit(eff.)	9.9	m²	Shells/unit	1		Surf/shell (eff.)	9.9	m²
8	**PERFORMANCE OF ONE UNIT**								
9	Fluid allocation			Shell Side			Tube Side		
10	Fluid name								
11	Fluid quantity, Total		kg/h	20000			30000		
12	Vapor (In/Out)		kg/h						
13	Liquid		kg/h	20000	20000		30000	30000	
14	Noncondensable		kg/h						
15									
16	Temperature (In/Out)		°C	95	70		35	51.67	
17	Dew / Bubble point		°C						
18	Density		kg/m³	962.67	979.82		996	989.7	
19	Viscosity		mPa s	0.296	0.4107		0.7196	0.5371	
20	Molecular wt, Vap								
21	Molecular wt, NC								
22	Specific heat		kJ/(kg K)	4.193	4.186		4.189	4.186	
23	Thermal conductivity		W/(m K)	0.6742	0.6535		0.6135	0.6339	
24	Latent heat		kJ/kg						
25	Pressure		bar	5			15		
26	Velocity		m/s	0.62			1.16		
27	Pressure drop, allow./calc.		bar	0.5	0.22676		0.1	0.06258	
28	Fouling resist. (min)		m² K/W				0.0001		
29	Heat exchanged	581.7	kW				MTD corrected	37.16	°C
30	Transfer rate, Service	1583.4		Dirty	1924.2		Clean	2555.9	W/(m² K)
31	**CONSTRUCTION OF ONE SHELL**							**Sketch**	
32				Shell Side		Tube Side			
33	Design/Test pressure		bar	5.17107/	/Code	15.85794/	/Code		
34	Design temperature		°C	132.22		87.78			
35	Number passes per shell			1		2			
36	Corrosion allowance		mm	1.59		1.59			
37	Connections	In		76.2/150 ANSI		101.6/150 ANSI			
38	Size/rating	Out		76.2/150 ANSI		101.6/150 ANSI			
39	mm/	Intermediate		/150 ANSI		/150 ANSI			
40	Tube No. 42Us	OD	19.05	Tks-avg	2.11	mm	Length	2000	mm Pitch 25.4 mm
41	Tube type Plain			Material	CS			Tube pattern	90
42	Shell CS	ID		OD	323.85	mm	Shell cover	CS	
43	Channel or bonnet	CS					Channel cover		
44	Tubesheet-stationary	CS					Tubesheet-floating		
45	Floating head cover						Impingement protection	None	
46	Baffle-crossing	CS		Type	single seg		Cut(%d)	24 hor	Spacing: c/c 60.96 mm
47	Baffle-long			Seal type				Inlet	179.26 mm
48	Supports-tube			U-bend			Type		
49	Bypass seal			Tube-tubesheet joint			groove/expand		
50	Expansion joint			Type					
51	RhoV2-Inlet nozzle	1543		Bundle entrance	395		Bundle exit	276	kg/(m s²)
52	Gaskets - Shell side			Tube Side					
53	Floating head								
54	Code requirements	ASME Code Sec VIII Div 1					TEMA class	B	
55	Weight/Shell	478.4		Filled with water	634.8		Bundle	209.2	kg
56	Remarks								
57									
58									

Figure A-1 TEMA sheet of exchanger designed with a fouling resistance 0.0001 m^2K/W

6	Size	307 --2500	mm	Type	BEU	hor	Connected in	1 parallel	1 series	
7	Surf/unit(eff.)	12.4	m²	Shells/unit	1		Surf/shell (eff.)	12.4	m²	
8	**PERFORMANCE OF ONE UNIT**									
9	Fluid allocation			Shell Side			Tube Side			
10	Fluid name									
11	Fluid quantity, Total		kg/h	20000			30000			
12	Vapor (In/Out)		kg/h							
13	Liquid		kg/h	20000	20000		30000	30000		
14	Noncondensable		kg/h							
15										
16	Temperature (In/Out)		°C	95	70		35	51.67		
17	Dew / Bubble point		°C							
18	Density		kg/m³	962.67	979.82		996	989.7		
19	Viscosity		mPa s	0.296	0.4107		0.7196	0.5371		
20	Molecular wt, Vap									
21	Molecular wt, NC									
22	Specific heat		kJ/(kg K)	4.193	4.186		4.189	4.186		
23	Thermal conductivity		W/(m K)	0.6742	0.6535		0.6135	0.6339		
24	Latent heat		kJ/kg							
25	Pressure		bar	5			15			
26	Velocity		m/s	0.62			1.16			
27	Pressure drop, allow./calc.		bar	0.5	0.28917		0.1	0.07269		
28	Fouling resist. (min)		m² K/W				0.0002			
29	Heat exchanged	581.7	kW				MTD corrected	37.16	°C	
30	Transfer rate, Service	1262.4		Dirty	1557.8		Clean	2597.2	W/(m² K)	
31	**CONSTRUCTION OF ONE SHELL**							**Sketch**		
32				Shell Side		Tube Side				
33	Design/Test pressure		bar	5.17107 /	/Code	15.85794 /	/Code			
34	Design temperature		°C	132.22		87.78				
35	Number passes per shell			1		2				
36	Corrosion allowance		mm	1.59		1.59				
37	Connections	In		76.2 / 150 ANSI		101.6 / 150 ANSI				
38	Size/rating	Out		76.2 / 150 ANSI		101.6 / 150 ANSI				
39	mm /	Intermediate		/ 150 ANSI		/ 150 ANSI				
40	Tube No. 42Us	OD	19.05	Tks-avg	2.11	mm	Length	2500	mm	Pitch 25.4 mm
41	Tube type Plain			Material	CS				Tube pattern	90
42	Shell CS	ID		OD	323.85	mm	Shell cover	CS		
43	Channel or bonnet	CS					Channel cover			
44	Tubesheet-stationary	CS					Tubesheet-floating			
45	Floating head cover						Impingement protection	None		
46	Baffle-crossing CS			Type	single seg		Cut(%d)	24	hor Spacing: c/c	60.96 mm
47	Baffle-long			Seal type					Inlet	185.42 mm
48	Supports-tube			U-bend			Type			
49	Bypass seal			Tube-tubesheet joint			groove/expand			
50	Expansion joint			Type						
51	RhoV2-Inlet nozzle	1543		Bundle entrance	369		Bundle exit	261	kg/(m s²)	
52	Gaskets - Shell side			Tube Side						
53	Floating head									
54	Code requirements	ASME Code Sec VIII Div 1					TEMA class	B		
55	Weight/Shell	556.8		Filled with water	744.5		Bundle	255.9	kg	
56	Remarks									

Figure A-2 TEMA sheet of exchanger designed with a fouling resistance 0.0002 m^2K/W

1										
2										
3										
4										
5										
6	Size	307 – 2500	mm	Type	BEU	hor	Connected in	1 parallel	1 series	
7	Surf/unit(eff.)	12.4	m²	Shells/unit	1		Surf/shell (eff.)	12.4	m²	
8	**PERFORMANCE OF ONE UNIT**									
9	Fluid allocation			Shell Side			Tube Side			
10	Fluid name									
11	Fluid quantity, Total		kg/h	20000			30000			
12	Vapor (In/Out)		kg/h							
13	Liquid		kg/h	20000	20000		30000	30000		
14	Noncondensable		kg/h							
15										
16	Temperature (In/Out)		°C	95	70		35	51.67		
17	Dew / Bubble point		°C							
18	Density		kg/m³	962.67	979.82		996	989.7		
19	Viscosity		mPa s	0.296	0.4107		0.7196	0.5371		
20	Molecular wt, Vap									
21	Molecular wt, NC									
22	Specific heat		kJ/(kg K)	4.193	4.186		4.189	4.186		
23	Thermal conductivity		W/(m K)	0.6742	0.6535		0.6135	0.6339		
24	Latent heat		kJ/kg							
25	Pressure		bar	5			15			
26	Velocity		m/s	0.62			1.16			
27	Pressure drop, allow./calc.		bar	0.5	0.28841		0.1	0.07249		
28	Fouling resist. (min)		m² K/W	0.0003						
29	Heat exchanged	581.7	kW				MTD corrected	37.16	°C	
30	Transfer rate, Service	1262.4		Dirty	1299.6		Clean	2603.4	W/(m² K)	
31	**CONSTRUCTION OF ONE SHELL**							**Sketch**		
32				Shell Side		Tube Side				
33	Design/Test pressure		bar	5.17107 /	/Code	15.85794 /	/Code			
34	Design temperature		°C	132.22		87.78				
35	Number passes per shell			1		2				
36	Corrosion allowance		mm	1.59		1.59				
37	Connections	In		76.2 / 150 ANSI		101.6 / 150 ANSI				
38	Size/rating	Out		76.2 / 150 ANSI		101.6 / 150 ANSI				
39	mm /	Intermediate		/ 150 ANSI		/ 150 ANSI				
40	Tube No. 42Us	OD 19.05		Tks-avg 2.11	mm	Length 2500	mm	Pitch 25.4	mm	
41	Tube type Plain			Material CS				Tube pattern 90		
42	Shell CS		ID	OD 323.85	mm	Shell cover	CS			
43	Channel or bonnet CS					Channel cover				
44	Tubesheet-stationary CS					Tubesheet-floating				
45	Floating head cover					Impingement protection	None			
46	Baffle-crossing CS			Type single seg		Cut(%d) 24	hor	Spacing: c/c 60.96	mm	
47	Baffle-long			Seal type				Inlet 185.42	mm	
48	Supports-tube		U-bend			Type				
49	Bypass seal			Tube-tubesheet joint		groove/expand				
50	Expansion joint			Type						
51	RhoV2-Inlet nozzle	1543		Bundle entrance 369			Bundle exit 261		kg/(m s²)	
52	Gaskets - Shell side			Tube Side						
53	Floating head									
54	Code requirements	ASME Code Sec VIII Div 1					TEMA class B			
55	Weight/Shell	556.8		Filled with water 744.5			Bundle 255.9		kg	
56	Remarks									
57										
58										

Figure A-3 TEMA sheet of exchanger designed with fouling a resistance 0.0003 m^2K/W

Heat Exchanger Specification Sheet

1								
2								
3								
4								
5								
6	Size	307--3000	mm	Type BEU	hor	Connected in	1 parallel	1 series
7	Surf/unit(eff.)	14.9	m²	Shells/unit 1		Surf/shell (eff.)	14.9	m²
8	**PERFORMANCE OF ONE UNIT**							
9	Fluid allocation			Shell Side		Tube Side		
10	Fluid name							
11	Fluid quantity, Total		kg/h	20000		30000		
12	Vapor (In/Out)		kg/h					
13	Liquid		kg/h	20000	20000	30000	30000	
14	Noncondensable		kg/h					
15								
16	Temperature (In/Out)		°C	95	70	35	51.67	
17	Dew / Bubble point		°C					
18	Density		kg/m³	962.67	979.82	996	989.7	
19	Viscosity		mPa s	0.296	0.4107	0.7196	0.5371	
20	Molecular wt, Vap							
21	Molecular wt, NC							
22	Specific heat		kJ/(kg K)	4.193	4.186	4.189	4.186	
23	Thermal conductivity		W/(m K)	0.6742	0.6535	0.6135	0.6339	
24	Latent heat		kJ/kg					
25	Pressure		bar	5		15		
26	Velocity		m/s	0.62		1.16		
27	Pressure drop, allow./calc.		bar	0.5	0.35089	0.1	0.08264	
28	Fouling resist. (min)		m² K/W			0.0004		
29	Heat exchanged	581.7	kW			MTD corrected	37.16	°C
30	Transfer rate, Service	1049.6		Dirty 1118.4		Clean 2629.1		W/(m² K)
31	**CONSTRUCTION OF ONE SHELL**					**Sketch**		
32				Shell Side		Tube Side		
33	Design/Test pressure		bar	5.17107/	/Code	15.85794/	/Code	
34	Design temperature		°C	132.22		87.78		
35	Number passes per shell			1		2		
36	Corrosion allowance		mm	1.59		1.59		
37	Connections	In		76.2/150 ANSI		101.6/150 ANSI		
38	Size/rating	Out		76.2/150 ANSI		101.6/150 ANSI		
39	mm/	Intermediate		/150 ANSI		/150 ANSI		
40	Tube No. 42Us	OD 19.05		Tks-avg 2.11	mm	Length 3000	mm Pitch 25.4	mm
41	Tube type Plain			Material CS			Tube pattern 90	
42	Shell CS	ID		OD 323.85	mm	Shell cover	CS	
43	Channel or bonnet CS					Channel cover		
44	Tubesheet-stationary CS					Tubesheet-floating		
45	Floating head cover					Impingement protection	None	
46	Baffle-crossing CS			Type single seg		Cut(%d) 24	hor Spacing: c/c 60.96	mm
47	Baffle-long			Seal type			Inlet 191.58	mm
48	Supports-tube			U-bend		Type		
49	Bypass seal			Tube-tubesheet joint		groove/expand		
50	Expansion joint			Type				
51	RhoV2-Inlet nozzle	1543		Bundle entrance 346		Bundle exit 247		kg/(m s²)
52	Gaskets - Shell side			Tube Side				
53	Floating head							
54	Code requirements	ASME Code Sec VIII Div 1				TEMA class B		
55	Weight/Shell	635.2		Filled with water 854.2		Bundle 302.7		kg
56	Remarks							
57								
58								

Figure A-4 TEMA sheet of exchanger designed with a fouling resistance 0.0004 m^2K/W

Heat Exchanger Specification Sheet

1									
2									
3									
4									
5									
6	Size	307--3500	mm	Type	BEU	hor	Connected in	1 parallel	1 series
7	Surf/unit(eff.)	17.4	m²	Shells/unit	1		Surf/shell (eff.)	17.4	m²
8	**PERFORMANCE OF ONE UNIT**								
9	Fluid allocation			Shell Side			Tube Side		
10	Fluid name								
11	Fluid quantity, Total		kg/h	20000			30000		
12	Vapor (In/Out)		kg/h						
13	Liquid		kg/h	20000	20000		30000	30000	
14	Noncondensable		kg/h						
15									
16	Temperature (In/Out)		°C	95	70		35	51.67	
17	Dew / Bubble point		°C						
18	Density		kg/m³	962.67	979.82		996	989.7	
19	Viscosity		mPa s	0.296	0.4107		0.7196	0.5371	
20	Molecular wt, Vap								
21	Molecular wt, NC								
22	Specific heat		kJ/(kg K)	4.193	4.186		4.189	4.186	
23	Thermal conductivity		W/(m K)	0.6742	0.6535		0.6135	0.6339	
24	Latent heat		kJ/kg						
25	Pressure		bar	5			15		
26	Velocity		m/s	0.62			1.16		
27	Pressure drop, allow./calc.		bar	0.5	0.40794		0.1	0.09277	
28	Fouling resist. (min)		m² K/W				0.0005		
29	Heat exchanged	581.7	kW				MTD corrected	37.16	°C
30	Transfer rate, Service	898.3		Dirty	982.3		Clean	2661	W/(m² K)
31	**CONSTRUCTION OF ONE SHELL**							**Sketch**	
32				Shell Side		Tube Side			
33	Design/Test pressure		bar	5.17107/	/Code	15.85794/	/Code		
34	Design temperature		°C	132.22		87.78			
35	Number passes per shell			1		2			
36	Corrosion allowance		mm	1.59		1.59			
37	Connections	In		76.2/150 ANSI		101.6/150 ANSI			
38	Size/rating	Out		76.2/150 ANSI		101.6/150 ANSI			
39	mm/	Intermediate		/150 ANSI		/150 ANSI			
40	Tube No. 42Us	OD	19.05	Tks-avg	2.11	mm	Length	3500	mm Pitch 25.4 mm
41	Tube type	Plain		Material	CS			Tube pattern	90
42	Shell	CS	ID	OD	323.85	mm	Shell cover	CS	
43	Channel or bonnet	CS					Channel cover		
44	Tubesheet-stationary	CS					Tubesheet-floating		
45	Floating head cover						Impingement protection	None	
46	Baffle-crossing	CS		Type	single seg		Cut(%d)	24 hor	Spacing: c/c 61.98 mm
47	Baffle-long			Seal type				Inlet	172.85 mm
48	Supports-tube		U-bend			Type			
49	Bypass seal			Tube-tubesheet joint		groove/expand			
50	Expansion joint			Type					
51	RhoV2-Inlet nozzle	1543		Bundle entrance	425		Bundle exit	294	kg/(m s²)
52	Gaskets - Shell side			Tube Side					
53	Floating head								
54	Code requirements	ASME Code Sec VIII Div 1					TEMA class	B	
55	Weight/Shell	713.6		Filled with water	963.8		Bundle	349.4	kg
56	Remarks								
57									
58									

Figure A-5 TEMA sheet of exchanger designed with a fouling resistance 0.0005 m^2K/W

Heat Exchanger Specification Sheet

1									
2									
3									
4									
5									
6	Size	339--3500	mm	Type BEU	hor	Connected in	1 parallel	1 series	
7	Surf/unit(eff.)	21.6	m²	Shells/unit 1		Surf/shell (eff.)	21.6	m²	
8	**PERFORMANCE OF ONE UNIT**								
9	Fluid allocation			Shell Side		Tube Side			
10	Fluid name								
11	Fluid quantity, Total		kg/h	20000		30000			
12	Vapor (In/Out)		kg/h						
13	Liquid		kg/h	20000	20000	30000	30000		
14	Noncondensable		kg/h						
15									
16	Temperature (In/Out)		°C	95	70	35	51.67		
17	Dew / Bubble point		°C						
18	Density		kg/m³	962.67	979.82	996	989.7		
19	Viscosity		mPa s	0.296	0.4107	0.7196	0.5371		
20	Molecular wt, Vap								
21	Molecular wt, NC								
22	Specific heat		kJ/(kg K)	4.193	4.186	4.189	4.186		
23	Thermal conductivity		W/(m K)	0.6742	0.6535	0.6135	0.6339		
24	Latent heat		kJ/kg						
25	Pressure		bar	5		15			
26	Velocity		m/s	0.49		0.93			
27	Pressure drop, allow./calc.		bar	0.5	0.26593	0.1	0.06504		
28	Fouling resist. (min)		m² K/W			0.0006			
29	Heat exchanged	581.7	kW			MTD corrected	37.16	°C	
30	Transfer rate, Service	726.2		Dirty 830.6		Clean 2308.5		W/(m² K)	
31	**CONSTRUCTION OF ONE SHELL**						**Sketch**		
32				Shell Side		Tube Side			
33	Design/Test pressure		bar	5.17107/	/Code	15.85794/	/Code		
34	Design temperature		°C	132.22		87.78			
35	Number passes per shell			1		2			
36	Corrosion allowance		mm	1.59		1.59			
37	Connections	In		76.2/150 ANSI		101.6/150 ANSI			
38	Size/rating	Out		76.2/150 ANSI		101.6/150 ANSI			
39	mm/	Intermediate		/150 ANSI		/150 ANSI			
40	Tube No. 52Us	OD 19.05		Tks-avg 2.11	mm	Length 3500	mm	Pitch 25.4	mm
41	Tube type Plain			Material CS			Tube pattern 90		
42	Shell CS		ID	OD 355.6	mm	Shell cover	CS		
43	Channel or bonnet	CS				Channel cover			
44	Tubesheet-stationary	CS				Tubesheet-floating			
45	Floating head cover					Impingement protection	None		
46	Baffle-crossing CS			Type single seg		Cut(%d) 26	hor Spacing: c/c 70.1	mm	
47	Baffle-long			Seal type			Inlet 180.85	mm	
48	Supports-tube		U-bend			Type			
49	Bypass seal			Tube-tubesheet joint		groove/expand			
50	Expansion joint			Type					
51	RhoV2-Inlet nozzle	1543		Bundle entrance 515		Bundle exit 350		kg/(m s²)	
52	Gaskets - Shell side			Tube Side					
53	Floating head								
54	Code requirements	ASME Code Sec VIII Div 1				TEMA class B			
55	Weight/Shell	819.7		Filled with water 1126		Bundle 422.5		kg	
56	Remarks								
57									
58									

Figure A-6 TEMA sheet of exchanger designed with a fouling resistance 0.0006 m^2K/W

Heat Exchanger Specification Sheet

1									
2									
3									
4									
5									
6	Size	339--3500	mm	Type	BEU	hor	Connected in	1 parallel	1 series
7	Surf/unit(eff.)	21.6	m²	Shells/unit	1		Surf/shell (eff.)	21.6	m²
8	**PERFORMANCE OF ONE UNIT**								
9	Fluid allocation			Shell Side			Tube Side		
10	Fluid name								
11	Fluid quantity, Total		kg/h	20000			30000		
12	Vapor (In/Out)		kg/h						
13	Liquid		kg/h	20000	20000		30000	30000	
14	Noncondensable		kg/h						
15									
16	Temperature (In/Out)		°C	95	70		35	51.67	
17	Dew / Bubble point		°C						
18	Density		kg/m³	962.67	979.82		996	989.7	
19	Viscosity		mPa s	0.296	0.4107		0.7196	0.5371	
20	Molecular wt, Vap								
21	Molecular wt, NC								
22	Specific heat		kJ/(kg K)	4.193	4.186		4.189	4.186	
23	Thermal conductivity		W/(m K)	0.6742	0.6535		0.6135	0.6339	
24	Latent heat		kJ/kg						
25	Pressure		bar	5			15		
26	Velocity		m/s	0.49			0.93		
27	Pressure drop, allow./calc.		bar	0.5	0.2657		0.1	0.06498	
28	Fouling resist. (min)		m² K/W				0.0007		
29	Heat exchanged	581.7	kW				MTD corrected	37.16	°C
30	Transfer rate, Service	726.2		Dirty	750.8		Clean	2310.9	W/(m² K)
31	**CONSTRUCTION OF ONE SHELL**							**Sketch**	
32				Shell Side		Tube Side			
33	Design/Test pressure		bar	5.17107/	/Code	15.85794/	/Code		
34	Design temperature		°C	132.22		87.78			
35	Number passes per shell			1		2			
36	Corrosion allowance		mm	1.59		1.59			
37	Connections	In		76.2/150 ANSI		101.6/150 ANSI			
38	Size/rating	Out		76.2/150 ANSI		101.6/150 ANSI			
39	mm/	Intermediate		/150 ANSI		/150 ANSI			
40	Tube No. 52Us	OD	19.05	Tks-avg	2.11	mm	Length	3500	mm Pitch 25.4 mm
41	Tube type Plain			Material	CS			Tube pattern	90
42	Shell CS	ID		OD	355.6	mm	Shell cover	CS	
43	Channel or bonnet	CS					Channel cover		
44	Tubesheet-stationary	CS					Tubesheet-floating		
45	Floating head cover						Impingement protection	None	
46	Baffle-crossing CS			Type	single seg		Cut(%d)	26	hor Spacing: c/c 70.1 mm
47	Baffle-long			Seal type				Inlet	180.85 mm
48	Supports-tube			U-bend			Type		
49	Bypass seal			Tube-tubesheet joint			groove/expand		
50	Expansion joint			Type					
51	RhoV2-Inlet nozzle	1543		Bundle entrance	515		Bundle exit	350	kg/(m s²)
52	Gaskets - Shell side			Tube Side					
53	Floating head								
54	Code requirements	ASME Code Sec VIII Div 1					TEMA class	B	
55	Weight/Shell	819.7		Filled with water	1126		Bundle	422.5	kg
56	Remarks								
57									
58									

Figure A-7 TEMA sheet of exchanger designed with a fouling resistance 0.0007 m^2K/W

Appendix B – Measurement of $CaSO_4$ Concentration

The concentration of calcium sulphate was determined by a complexometric ethylenediaminetetraacetic acid (EDTA) titration. EDTA forms stable 1:1 complexes with alkaline earth metal ions at pH=10, i.e. 1mol Ca^{2+} bonds 1mol EDTA. An ammonia buffer solution is used to achieve a pH value of 10. In the presence of magnesium, first the calcium-EDTA and then the magnesium-EDTA-complex are formed. For detecting the end of titration, a metal ion indicator such as eriochrome black T (EBT) is required, which builds a wine-red calcium-indicator-complex. During titration the indicator is replaced by EDTA and a stable calcium-EDTA-complex is formed. Thus, the blue coloured free indicator serves for determination of the equivalence point. The experimental procedure for the titration method is as follows:

- Take 10 ml of $CaSO_4$ test solution in a beaker
- Add 3 ml of ammonia buffer solution 10
- Add 3 ml of magnesium sulphate solution
- Add 4-5 drops of eriochrome black T
- Start titration with EDTA until equivalence point, i.e. color change from wine-red to blue, is confirmed

Due to the 1:1 complex built, the $CaSO_4$ concentration of the test solution can then be calculated from the following equation:

$$C_{CaSO_4} = \frac{\left(V_{EDTA} - V_{MgSO_4}\right) \times 0.01}{V_{CaSO_4}} . M_{CaSO_4} \qquad (6.1)$$

Appendix C – Wilson Plot Method

A Wilson plot was produced in order to precisely determine the exact position of the thermocouples situated in the inside of the tube wall. Because the temperature gradient inside the tube wall is very steep, the temperature can vary considerably over a fraction of a millimeter. To obtain precise temperatures of the tube wall, both thermocouples must be exactly situated. By knowing the exact position of these two thermocouples and the temperature gradient, the surface temperature can be obtained. The method consists of performing a steady-state energy balance at different conditions in order to obtain an experimental curve from which the distance between inner tube surface and thermocouple can be found. By analyzing Figure C-1, and performing a steady-state energy balance, Eq. C-1 can be developed.

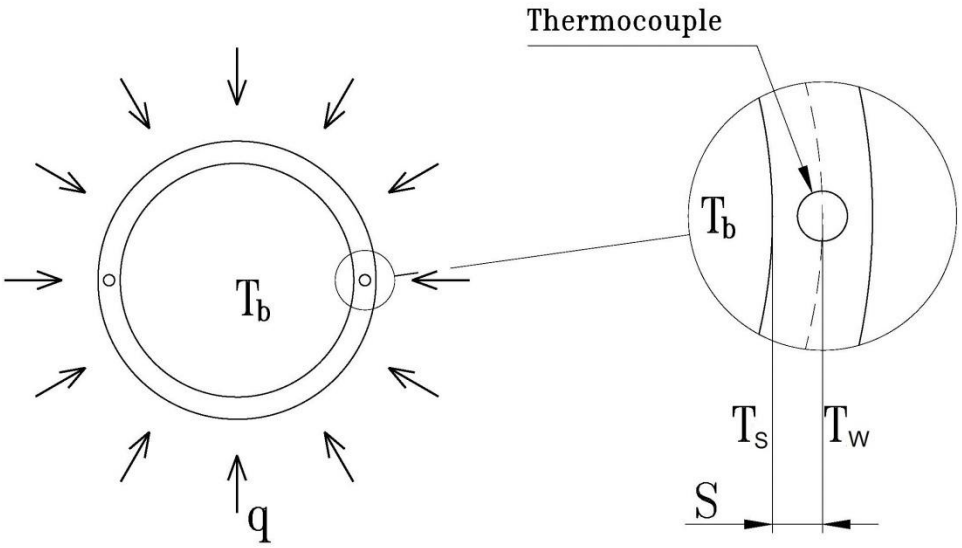

Figure C-1 Sketch of tube wall and of the embedded thermocouples

$$\frac{1}{U} = \frac{1}{\alpha} + \frac{S}{\lambda} \tag{C.1}$$

Where U is the overall heat transfer coefficient, S is the distance between the positions of thermocouple and inner surface of tube, λ is the thermal conductivity of the tube material and α is the convective heat transfer coefficient. Considering the two relations Eq. C.2 and Eq. C.3 then one yields that:

$$\alpha \propto f \cdot Re \tag{C.2}$$

$$f \propto \frac{1}{Re^{0.25}} \tag{C.3}$$

where f is the friction factor, the following equation is obtained:

$$\frac{1}{U} = \frac{C}{v^{0.75}} + \frac{S}{\lambda} \tag{C.4}$$

Eq. C.4 can be plotted as a straight line of $1/U$ vs. $1/v^{0.75}$ for each thermocouple where its intercept with the vertical axis gives the ratio of S/λ. Provided the tube is made of stainless steel, the distance S can easily be calculated. Figure C-2 is an example to show the variation of $1/U$ vs. $1/v^{0.75}$ for an embedded thermocouple in a tube which was used in this study. In this case the value of S/λ is 0.0598 m^2·K/kW and S would be 0.97 mm.

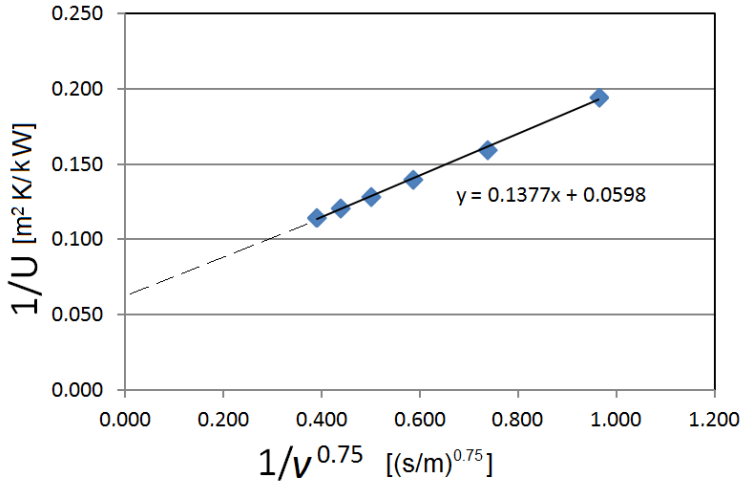

Figure C-2 Plot of $1/U$ vs. $1/v^{0.75}$ for determination of S/λ